DESIGN AND MODELLING OF MICROWAVE CIRCUITS USING OPTIMIZATION METHODS

S. Daijavad

SOS-86-3-T

June 1986

DESIGN AND MODELLING OF MICROWAVE CIRCUITS USING OPTIMIZATION METHODS

To my mother Camellia, and in loving

memory of my uncle Manouchehr.

DESIGN AND MODELLING OF MICROWAVE CIRCUITS USING OPTIMIZATION METHODS

By

SHAHROKH DAIJAVAD, B. Eng.

A Thesis

Submitted to the School of Graduate Studies

in Partial Fulfilment of the Requirements

for the Degree

Doctor of Philosophy

McMaster University

June 1986

DOCTOR OF PHILOSOPHY (1986)
(Electrical Engineering)

McMASTER UNIVERSITY
Hamilton, Ontario

TITLE: Design and Modelling of Microwave Circuits Using Optimization Methods

AUTHOR: Shahrokh Daijavad, B. Eng. (E.E.)
(McMaster University)

SUPERVISOR: J.W. Bandler, Professor, Department of Electrical and Computer Engineering
B.Sc. (Eng.), Ph.D., D.Sc. (Eng.) (University of London)
D.I.C., (Imperial College)
P.Eng. (Province of Ontario)
C.Eng., F.I.E.E. (United Kingdom)
Fellow, I.E.E.E.
Fellow, Royal Society of Canada

NUMBER OF PAGES: xiv, 179

ABSTRACT

This thesis addresses itself to the computer-aided design and modelling of microwave circuits using efficient minimax and ℓ_1 optimization techniques.

Recent algorithms for nonlinear minimax and ℓ_1 optimization are reviewed. The features of the ℓ_1 norm, its theoretical properties and the necessary conditions for optimality are discussed.

A comparative example with ℓ_2 optimization illustrates the robustness of ℓ_1 for the particular applications of this thesis. Efficient gradient approximation techniques, applicable to both minimax and ℓ_1 optimization, are presented.

A simplified and straightforward treatment of sensitivities for two-port networks, cascaded and branched cascaded structures is introduced. The objective is to calculate the sensitivities efficiently, without appealing to the adjoint network concept. A novel proof of a recent result in sensitivity analysis of lossless and reciprocal two-ports is presented.

Design of manifold type waveguide multiplexers has been considered as a major application for both minimax optimization and the theoretical work in branched cascaded network sensitivity analysis. Components of the multiplexer structure and nonideal effects such as dissipation and dispersion are discussed and a step-by-step implementation of an algorithm to calculate particular responses and sensitivities is presented. Examples of the design of 3-, 12- and 16-channel, 12 GHz multiplexers illustrate the practicality of the approach presented.

A new approach to modelling of microwave devices which exploits the theoretical properties of the ℓ_1 norm is presented. The concept of multi-circuit

measurements is introduced and its merits in obtaining unique and self-consistent parameters are discussed. The technique is applied to modelling of multi-coupled cavity filters and GaAs FET's. The application of efficient modelling techniques in developing algorithms for postproduction tuning and in establishing the relationship between physical parameters of a device and its equivalent circuit model parameters, is discussed.

ACKNOWLEDGEMENTS

The author wishes to express his appreciation to Dr. J.W. Bandler for his encouragement, expert guidance and supervision throughout the course of this work. He also thanks Dr. C.R. Carter and Dr. A.A. Smith, members of his supervisory committee, for their continuing interest.

The author acknowledges the opportunity given to him by Dr. J.W. Bandler to be involved in industrial projects developed by Optimization Systems Associates. Specifically, the author has benefitted from the industrial input and expertise provided by ComDev Ltd. of Cambridge, Ontario in the design of multiplexers and modelling of multi-coupled cavity filters. Useful technical discussions with R. Tong, L. Zaifman and H. AuYeung of the same company, and their assistance in preparing measurement data for filters are acknowledged.

It is the author's pleasure to acknowledge inspiring discussions with his colleagues S.H. Chen, Q.J. Zhang, M.L. Renault and Dr. W. Kellermann. Many suggestions by S.H. Chen have helped the author to develop, improve and test new ideas.

The assistance of S. Pan of McMaster University in running some of the problems in modelling is acknowledged.

The financial assistance provided by the Natural Sciences and Engineering Research Council of Canada through Grants A7239 and G1135 as well as a postgraduate scholarship, the Department of Electrical and Computer Engineering through a Teaching Assistantship and the Ministry of Colleges and Universities through an Ontario Graduate Scholarship is gratefully acknowledged.

Thanks go to the Engineering Word Processing Centre for their expert typing of this manuscript.

TABLE OF CONTENTS

TABLE OF CONTENTS (continued)

TABLE OF CONTENTS (continued)

TABLE OF CONTENTS (continued)

LIST OF FIGURES

LIST OF FIGURES (continued)

LIST OF FIGURES (continued)

LIST OF TABLES

1

INTRODUCTION

Over the past 20 years, computer-aided design (CAD) techniques have developed into an integral part of methods used for solving most engineering problems. In the past decade, the astonishing cost reduction in computer components and the availability of personal computers has generated further enthusiasm to use efficient and powerful CAD techniques. The use of highly interactive software systems and the capability of high resolution graphical displays has changed the image of CAD techniques from a topic understandable only by specialists to a powerful tool serving every practicing engineer.

Design of microwave filters using optimization methods is one of the earliest applications for CAD techniques in electrical engineering. In recent years, software systems for modelling and design of microwave circuits have been developed which are capable of handling most commonly used microwave devices. The application of such general purpose software systems to design problems requiring multiple objectives of cost reduction, design centering, tolerance optimization and post-production tuning, and modelling problems with complex and uncertain circuit equivalent topologies, necessitates the use of state-of-the-art optimization techniques. Unfortunately, while highly efficient optimization algorithms have been developed in the last decade, the algorithms used in most microwave software systems are the ones described by mathematicians 10-15 years ago. There are two major factors contributing to such a sizeable gap.

The first factor is that the implementation of nonlinear minimax and ℓ_1 algorithms, whose characteristic features can be exploited in many engineering problems and have been the subject of most recent advancements in optimization techniques, is generally complicated. This has led, for instance, to the use of the more straightforward least squares optimization with the limitation on linearity of constraints in most microwave software systems. It should be mentioned that a nonlinear programming problem with nonlinear constraints can be easily formulated as a minimax problem.

The second factor which has helped the use of rather old non-gradient optimization techniques (e.g., the random optimization in SUPER-COMPACT 1986 and TOUCHSTONE 1985) to continue, is the difficulties related to sensitivity analysis of many microwave circuits as required by the advanced gradient-based optimization methods. Deriving explicit sensitivity expressions is difficult or impossible in some microwave problems. On the other hand, using numerical differentiations to estimate the gradients at every iteration of an optimization procedure becomes prohibitively expensive when attempting to solve large problems.

This thesis addresses itself to modelling and design of microwave circuits using recent minimax and ℓ_1 optimization techniques. A major part of the thesis is concerned with a simplified treatment of sensitivity analysis applicable to general two-ports, cascaded and branched-cascaded structures frequently encountered in the microwave area. The sensitivities are directly used in conjunction with powerful minimax and ℓ_1 algorithms which will be described in some detail. We do not presume to be able to calculate exact sensitivities for all microwave structures. Therefore, efficient gradient approximation techniques will be described which enable

us to use minimax and ℓ_1 algorithms in problems in which exact gradient evaluation is not feasible.

The concepts described in design and modelling are applied to microwave devices such as multi-coupled cavity filters, waveguide manifold type multiplexers and GaAs FET's. These devices are all of current significant interest to researchers and engineers due to their application in satellite communication systems.

Chapter 2 deals with the use of minimax and ℓ_1 optimization techniques in computer-aided design. Problem formulations for both types of optimizations are given. The existing minimax algorithms are reviewed briefly and the Hald and Madsen algorithm (Hald and Madsen 1981) is described. For nonlinear ℓ_1 optimization, the Hald and Madsen algorithm (Hald and Madsen 1985) is reviewed and the features of the ℓ_1 norm are explained using necessary conditions for optimality. For problems in which exact gradient evaluation is not feasible, a recent method for efficient gradient approximations, as applied to both minimax and ℓ_1 optimizations, is described.

In Chapter 3, simple algebraic approaches are presented which reduce the networks described by their nodal admittance matrices to equivalent unterminated two-ports with simultaneous sensitivity analysis. The originality of the approach lies in the fact that there is no need to appeal to the adjoint network concept. Second-order sensitivities and computational effort are discussed. The original idea by Bandler, Rizk and Abdel-Malek (1978) in efficient simulation and sensitivity analysis of cascaded networks is extended to the branched cascaded structures with arbitrary junctions. The individual components of the structure, apart from the three-port junctions, are two-ports which may have been deduced by the reduction of complicated networks using the aforementioned algebraic approaches. A new proof for a recent

result in sensitivity analysis of lossless reciprocal two-ports is presented and a new and interesting result in sensitivity evaluation of branched cascaded networks is derived.

Chapter 4 covers the design of multiplexing networks using the minimax optimization in detail. This is one of the largest nonlinear optimization problems ever demonstrated in microwave circuit design. Models for individual components of the multiplexer with nonideal effects such as dissipation, dispersion and junction susceptances are presented. The branched cascaded sensitivity analysis is effectively used and 3-, 12- and 16-channel multiplexers are designed in reasonable computational times.

In Chapter 5, microwave device modelling techniques are considered. The existing techniques in typical commercially available software systems as well as more advanced techniques in modelling are reviewed. A new formulation for modelling using the concept of multi-circuit measurements is presented. We discuss the merits of this technique in obtaining unique and self-consistent models. The technique is applied to modelling of multi-coupled cavity filters and GaAs FET's. The application of efficient modelling techniques in developing algorithms for post-production tuning is briefly discussed.

We conclude in Chapter 6 with some suggestions for further research.

The author contributed substantially to the following original developments presented in this thesis:

(1) An integrated treatment of sensitivities for two-ports, cascaded and branched cascaded structures using simple algebraic approaches.

(2) A new proof of a result in sensitivity analysis of reciprocal lossless two-ports.

(3) A new result in sensitivity analysis of branched cascaded networks.

(4) Application of the theoretical results for branched cascaded network simulation and sensitivity analysis to the design of manifold type multiplexers using efficient minimax optimization, and an implementation with realistic and nonideal effects included.

(5) Presentation of a new formulation for modelling which exploits multi-circuit measurements with a discussion of its implementation.

(6) Establishing the relationship between physical and model parameters of a multi-coupled cavity filter using efficient modelling.

2

MINIMAX AND ℓ_1 OPTIMIZATION TECHNIQUES – NEW ADVANCES

2.1 INTRODUCTION

A wide class of microwave circuit and system design problems can be formulated as minimax optimization problems. Therefore, efficient minimax algorithms have been of great interest to microwave engineers and researchers for the past 20 years. On the other hand, ℓ_1 optimization has just begun to gain popularity in the microwave area and it is the author's belief that the formulation of the modelling problem using the ℓ_1 norm marks one of the first attempts to solve a well-known and widely encountered microwave problem with this type of optimization. Unique properties of ℓ_1 optimization and the modelling technique which utilizes such properties are discussed in this thesis.

In the context of integrated-circuit design, Brayton, Hachtel and Sangiovanni-Vincentelli (1981) have surveyed the advances in the multiple objective optimization techniques up to 1981. Many of the techniques reviewed are also used in the microwave area. In the past few years, mainly due to the work of Hald and Madsen (1981, 1985) at the Technical University of Denmark, highly efficient minimax and ℓ_1 optimization algorithms have been developed. Very recently, applications of these new methods to solve general engineering problems and particularly problems in the microwave area have been discussed (Bandler, Kellermann and Madsen 1985a, 1985b; Kellermann 1986).

In this chapter, the existing minimax and ℓ_1 optimization techniques are briefly reviewed. In both cases, we conclude the discussion by describing the efficient algorithms of Hald and Madsen.

For the ℓ_1 problem, the necessary conditions for optimality and the role of zero-valued functions are discussed in detail due to their significance in the modelling technique which utilizes them. Also, an ℓ_1 approximation example is presented for direct comparison with the least squares (ℓ_2) approximation.

To extend the practical applications for gradient-based minimax and ℓ_1 optimizations, efficient gradient approximations are described. Such approximations become extremely useful for problems in which exact gradient evaluation is not feasible.

2.2 MINIMAX OPTIMIZATION TECHNIQUES

From its early applications in the design of microwave filters with Chebyshev type responses, minimax optimization has been used extensively in many circuit design problems. Most commonly, the minimax functions result from lower and/or upper specifications on a performance function of interest. In this section, formulation of minimax optimization problems and minimax algorithms are reviewed.

2.2.1 Design Specifications and Error Functions

In a general design problem there are λ response functions $F^1(\boldsymbol{\phi}, \psi^1)$, $F^2(\boldsymbol{\phi}, \psi^2), \ldots, F^\lambda(\boldsymbol{\phi}, \psi^\lambda)$ that have to meet given specifications. $\boldsymbol{\phi}$ represents the network parameters and ψ^j, $j = 1,2, \ldots, \lambda$ is an independent parameter such as frequency, time, temperature, etc. (Bandler and Rizk 1979). As an example, a filter

can be designed to meet desired specifications in both the frequency and time domain as illustrated in Fig. 2.1 (Rizk, 1979). The performance specifications are usually functions of the independent parameter only. They are denoted by $S^1(\psi^1)$, $S^2(\psi^2), \ldots, S^\lambda(\psi^\lambda)$. The corresponding error functions are given by

$$e^j(\boldsymbol{\Phi}, \psi^j) = w^j(\psi^j)\,(F^j(\boldsymbol{\Phi}, \psi^j) - S^j(\psi^j)) \,, \qquad j = 1,2,\ldots,\lambda \,, \tag{2.1}$$

where w^j is a positive weighting function. It is necessary in practice, to consider a discrete set of samples for each ψ^j, such that satisfying the specifications at these sample points implies satisfying them almost everywhere. Thus, for the discrete case, taking I^j as the index set for the jth functions,

$$e^j_i(\boldsymbol{\Phi}) \triangleq e^j(\boldsymbol{\Phi}, \psi^j_i) = w^j_i\,(F^j_i\,(\boldsymbol{\Phi}) - S^j_i) \,, \qquad i \in I^j \tag{2.2a}$$

is the error function evaluated at the ith sample point for the independent variable ψ^j. Notice the following notation:

$$w^j_i \triangleq w^j\,(\psi^j_i) \,, \tag{2.2b}$$

$$F^j_i(\boldsymbol{\Phi}) \triangleq F^j(\boldsymbol{\Phi}, \psi^j_i) \tag{2.2c}$$

and

$$S^j_i \triangleq S^j(\psi^j_i) \,. \tag{2.2d}$$

In typical microwave design problems, we have only one independent variable, namely, frequency. Therefore, superscript j is dropped and ω is used in place of ψ in the following formulations. Considering upper and lower specifications, the error functions will be of the form

$$e_{ui}(\boldsymbol{\Phi}) \triangleq e_u(\boldsymbol{\Phi}, \omega_i) = w_{ui}(F_i(\boldsymbol{\Phi}) - S_{ui}) \,, \qquad i \in I_u \tag{2.3a}$$

and

$$e_{\ell i}(\boldsymbol{\Phi}) \triangleq e_\ell(\boldsymbol{\Phi}, \omega_i) = w_{\ell i}(F_i(\boldsymbol{\Phi}) - S_{\ell i}) \,, \qquad i \in I_\ell \,, \tag{2.3b}$$

where subscripts u and ℓ refer to the upper and lower specifications, respectively. I_u and I_ℓ are not necessarily disjoint. Let

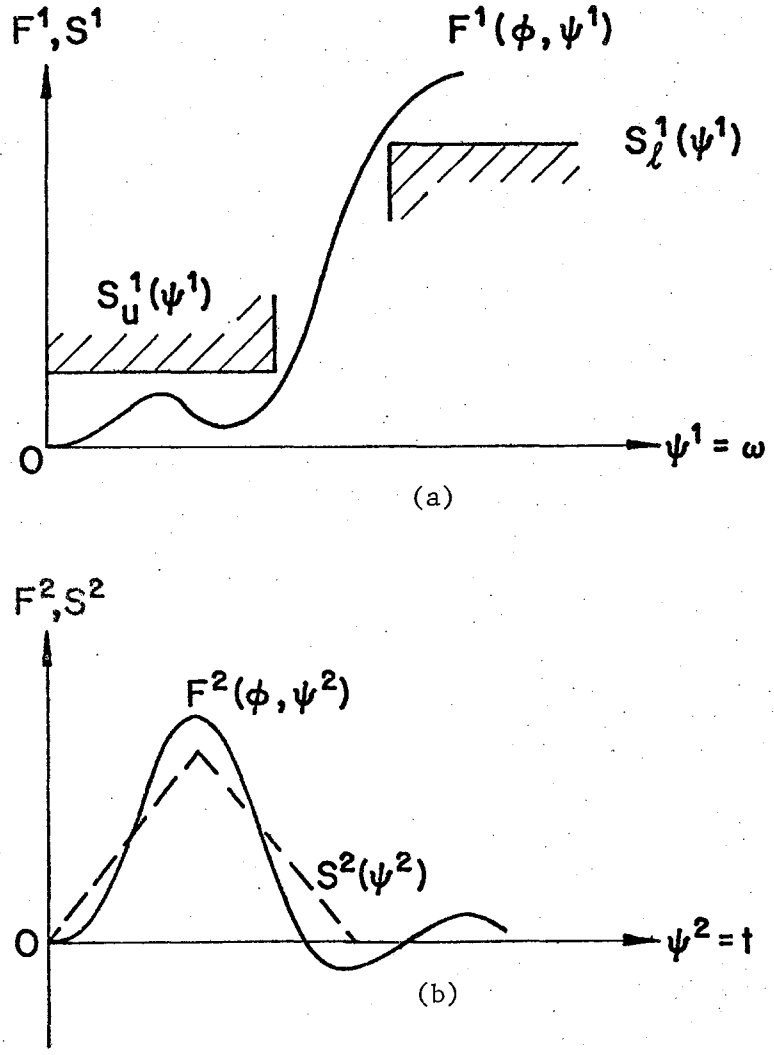

Fig. 2.1 An example of multiple objectives in filter design, (a) the insertion loss specification in the frequency domain of a lowpass filter, (b) an impulse response specification in the time domain of the lowpass filter (Rizk 1979).

$$f_i \triangleq \begin{cases} e_{uj}, & j \in I_u, \\ -e_{\ell k}, & k \in I_\ell, \end{cases} \qquad i \in I_c, \tag{2.4}$$

where

$$I_u \triangleq \{1,2,\ldots,n_u\}, \tag{2.5}$$

$$I_\ell \triangleq \{1,2,\ldots,n_\ell\}, \tag{2.6}$$

$$I_c \triangleq \{1,2,\ldots,m\} \tag{2.7}$$

and $m = n_u + n_\ell$. The m functions

$$\mathbf{f} = [f_1\ f_2 \ldots f_m]^T \tag{2.8}$$

characterize the circuit performance which is monitored during the optimization process. If we let

$$M_f(\boldsymbol{\phi}) \triangleq \max_{i \in I_c} f_i(\boldsymbol{\phi}), \tag{2.9}$$

then the sign of M_f indicates whether the specifications are satisfied or violated.

2.2.2 Formulation of the Minimax Optimization Problem

The mathematical formulation of the linearly constrained minimax problem, which is applicable to design problems addressed in this thesis, is the following. Let

$$f_j(\mathbf{x}) \triangleq f_j(x_1, x_2, \ldots, x_n), \qquad j=1,2,\ldots,m,$$

be a set of m nonlinear, continuously differentiable functions. The vector

$$\mathbf{x} \triangleq [x_1\ x_2\ \ldots\ x_n]^T$$

is the set of n parameters to be optimized.

We consider the optimization problem

$$\underset{\mathbf{x}}{\text{minimize}}\ F(\mathbf{x}) \triangleq \max_j f_j(\mathbf{x}), \tag{2.10a}$$

subject to

$$\mathbf{a}_i^T \mathbf{x} + b_i = 0 , \qquad i=1,2,\ldots,\ell_{eq} , \tag{2.10b}$$

$$\mathbf{a}_i^T \mathbf{x} + b_i \geq 0 , \qquad i=(\ell_{eq}+1),\ldots,\ell , \tag{2.10c}$$

where $\mathbf{a}_i$ and b_i, $i = 1,2,\ldots,\ell$, are constants.

2.2.3 Nonlinear Programming Using Minimax Optimization

In problems such as tolerance optimization and tuning where usually a cost function is to be minimized, the specifications on circuit responses are handled by nonlinear constraints. An efficient and robust minimax algorithm, in addition to its application in designs which are directly formulated as minimax problems, can be used in general nonlinear programming. The transformation of a general nonlinear programming problem to minimax optimization often results in a singular minimax problem (defined in Section 2.2.4) for which only minimax algorithms using second-order information are efficient. The minimax algorithms will be described in more detail in the next section. Here, the transformation is presented.

Consider the problem

$$\underset{\mathbf{x}}{\text{minimize}}\ U(\mathbf{x}) \tag{2.11a}$$

subject to

$$g_i(\mathbf{x}) \geq 0 , \qquad i=1,2,\ldots,\ell , \tag{2.11b}$$

where U and g_i, $i = 1,2,\ldots,\ell$, are nonlinear functions of $\mathbf{x}$. Charalambous (1973) and Bandler and Charalambous (1974) suggested the transformation of (2.11) to an equivalent unconstrained minimax problem, namely,

$$\text{minimize } M(\mathbf{x}, \boldsymbol{\alpha}) \triangleq \max_j [U(\mathbf{x}), U(\mathbf{x}) - \alpha_i g_i(\mathbf{x})] , \quad i = 1, 2, \cdots, \ell, \tag{2.12a}$$

where

$$\alpha_i > 0, \quad i = 1,2,\ldots,\ell. \tag{2.12b}$$

Any design problem which is naturally formulated as a nonlinear programming problem is transformed to the minimax problem via (2.12) and then solved using minimax optimization algorithms.

2.2.4 Review of Minimax Algorithms

Linear Programming Methods

Methods of solving the minimax problem via linear programming techniques have been considered by many researchers over the past fifteen years. Here the method suggested by Madsen et al. (1975) is presented. At the kth stage of the method, let $\mathbf{x}_k$ be the current best point. Each function $f_j(\mathbf{x})$ is linearized at $\mathbf{x}_k$. Let

$$\mathbf{f}_j'(\mathbf{x}_k) = \frac{\partial f_j(\mathbf{x}_k)}{\partial \mathbf{x}} \quad . \tag{2.13}$$

Then $f_j(\mathbf{x})$ is approximated by

$$f_j(\mathbf{x}_k + \mathbf{h}) \simeq f_j(\mathbf{x}_k) + \mathbf{f}_j'(\mathbf{x}_k)^T \mathbf{h} \ , \qquad j=1,2,...,m \ . \tag{2.14}$$

A step $\mathbf{h} = [h_1 \ h_2 \ldots h_n]^T$ which simultaneously decreases each f_j is found by the linear program

$$\underset{\gamma, \mathbf{h}}{\text{minimize}} \ \gamma \tag{2.15a}$$

subject to

$$f_j(\mathbf{x}_k) + \mathbf{f}_j'(\mathbf{x}_k)^T \mathbf{h} \le \gamma \ , \qquad j=1,2,...,m \ , \tag{2.15b}$$

$$-\delta_k \le h_i \le \delta_k \ , \qquad i=1,2,..,n \ . \tag{2.15c}$$

The value of the scalar δ_k controls the step size $\mathbf{h}$ so that a decrease in max $\{f_j(\mathbf{x})\}$ is made. If δ_k is small enough, then the linear approximations to the f_j are accurate and a decrease is guaranteed. The value of δ_k is adjusted at each step. For example, suppose $\mathbf{h}_k$ is the solution to (2.15). The new point, $\mathbf{x}_{k+1} = \mathbf{x}_k + \mathbf{h}_k$, may not have achieved a decrease in max $\{f_j(\mathbf{x})\}$ since (2.15) only uses a linear approximation to $f_j(\mathbf{x})$. If no decrease is obtained, then the last step $\mathbf{h}_k$ is rejected and δ_k is replaced by $\beta\|\mathbf{h}_k\|_\infty$

where $\beta<1$. If a decrease in max $\{f_j(\mathbf{x})\}$ occurs, then δ_k may be increased if a test, measuring the goodness of linear approximations, succeeds.

This method may work well if $m>n$, i.e., the number of functions exceeds the number of parameters. However, if $m<n$, the method may behave like the steepest descent method with slow convergence. If $m>n$, then in many cases the solution can be expected to be a point $(\mathbf{x}, \gamma)$, where $n+1$ of the function f_j's are equal to each other as well as being equal to γ. Thus, in effect, we are solving a system of equations where $\mathbf{x}$ and γ are the unknowns. The linearization of each function $f_j(\mathbf{x})$ would correspond to the same linearization found in Newton's method on the above equations and quadratic convergence is expected. In general, one can expect this method to work quite well when the final answer is tightly constrained, (called the regular case), but may revert to a method related to steepest descent if fewer than $n+1$ of the functions are constraining the final answer (singular case). Madsen and Schjaer-Jacobsen (1976) give a complete discussion of when quadratic convergence is expected for this method.

Methods Using Second-Order Information

All linear programming methods are first-order methods, i.e., the search is based on first-order derivatives only. They all have problems with singular solutions in which the rate of convergence may be very slow. In order to overcome this problem, some second-order (or approximate second-order) information must be used. Hettich (1976) was the first who proposed doing this. He used a Newton iteration for solving a set of equations which expresses the necessary condition for an optimum. Hettich's method is only local and requires the initial point to be close to the solution. Han (1981) suggested nonlinear programming techniques for solving the minimax

problem. He uses a nonlinear programming formulation of the minimax problem which is solved via successive quadratic programming (Powell 1978). A line search is incorporated using the minimax objective function as merit function.

Watson (1979) introduced a method that switches between a first-order and a second-order method. Hald and Madsen (1981) use a similar method, however their method has the following advantages over Watson's method: 1) the user is required to provide only exact first-order derivatives, 2) a suitable set of criteria for switching between the first-order and the second-order methods are defined, 3) the method has guaranteed convergence to the set of stationary points.

The Hald and Madsen Algorithm

The Hald and Madsen algorithm for nonlinear minimax optimization (Hald and Madsen 1981) is a two-stage one. Initially, Stage 1 is used and at each point the nonlinear residual functions are approximated by linear functions using the first-order derivative information (provided by the user). If a smooth valley through the solution is detected, a switch to Stage 2 is made and the quasi-Newton iteration is used. Necessary second derivative estimates are generated by the algorithm. If it turns out that the Stage 2 iteration is unsuccessful (for instance, if the set of active functions has been wrongly chosen) then a switch is made back to Stage 1. The algorithm may switch several times between Stage 1 and Stage 2 but normally only a few switches will take place and the iteration will terminate in either Stage 1 with quadratic rate of convergence or in Stage 2 with superlinear rate of convergence.

The algorithm, which handles linear equality and inequality constraints, is a feasible point algorithm. This means that the residual functions are only evaluated

at points satisfying the linear constraints. Initially a feasible point is determined by the algorithm, and from that point feasibility is retained.

For this thesis, we have used the MMLC version of the algorithm (Bandler and Zuberek 1982).

2.3 ℓ_1 OPTIMIZATION TECHNIQUES

2.3.1 Formulation of the Problem

The optimization problem to be considered has the following mathematical formulation. Let $f_j(\mathbf{x})$, $j = 1,2,\ldots,m$, be a set of m nonlinear, continuously differentiable functions. The vector

$$\mathbf{x} \triangleq [x_1\ x_2\ \ldots\ x_n]^T$$

is the set of n parameters to be optimized. We consider the following problem:

$$\underset{\mathbf{x}}{\text{minimize}}\ F(\mathbf{x}) \triangleq \sum_{j=1}^{m} |f_j(\mathbf{x})| \tag{2.16a}$$

subject to

$$\mathbf{a}_i^T\mathbf{x} + b_i = 0\ , \qquad i=1,2,\ldots,\ell_{eq}\ , \tag{2.16b}$$

$$\mathbf{a}_i^T\mathbf{x} + b_i \geq 0\ , \qquad i=\ell_{eq}+1,\ldots,\ell\ , \tag{2.16c}$$

where $\mathbf{a}_i$ and b_i, $i = 1,2,\ldots,\ell$, are constants. This is called the linearly constrained ℓ_1 problem.

2.3.2 Review of ℓ_1 Algorithms

One of the first attempts to solve the ℓ_1 problem was published by Osborne and Watson (1971). The method is iterative and at the kth iterate $\mathbf{x}_k$ the following approximation of the nonlinear ℓ_1 problem is used:

$$\underset{\mathbf{h}}{\text{minimize}}\ F(\mathbf{x}_k, \mathbf{h}) \triangleq \sum_{j=1}^{m} |f_j(\mathbf{x}_k) + \mathbf{f}_j'(\mathbf{x}_k)^T \mathbf{h}| . \tag{2.17}$$

This is similar to the linearization of minimax functions as given by (2.14). The linear model problem is solved using linear programming. The direction $\mathbf{h}_k$ found is then used in a line search. The global convergence properties of this method are rather poor and the method may provide convergence to a nonstationary point, i.e., a point which is not a local minimum.

The more recent papers on the ℓ_1 problem use some second-order information. Most of the methods require that the user supplies exact second (as well as first) derivatives.

The linearly constrained ℓ_1 problem can be formulated as a nonlinear programming problem. Then, it can be solved by standard techniques from that field. When Powell's method (Powell 1978) for nonlinear programming is applied to the ℓ_1 problem, we obtain a method which in its final stages is similar to the Hald and Madsen method (Hald and Madsen 1985). However, in the neighbourhood of a solution, Hald and Madsen have to solve only a set of linear equations whereas in Powell's method a quadratic program must be solved in every iteration.

The Hald and Madsen Algorithm

The Hald and Madsen algorithm (Hald and Madsen 1985) is a hybrid method combining a first-order method with an approximate second-order method. The user supplies only first derivatives. The first-order method is based on the linear model problems of the type (2.17). These are solved subject to the constraints of the original problem (2.16) and a bound on the step length $\|\mathbf{h}\|$. The latter bound reflects the neighbourhood of the iterate $\mathbf{x}_k$ in which the kth model function (see (2.17)) is a

good approximation to the nonlinear ℓ_1 function. If the solution approached by the first-order method is "singular" (see definition which follows), then a higher-order method must be used in order to obtain a fast ultimate rate of convergence. Therefore, a switch is made to a quasi-Newton method that solves a set of nonlinear equations that necessarily hold at a solution of (2.16). This method has superlinear final convergence. Several switches between the first-order and the quasi-Newton method may take place. The reason for allowing this is that the latter method works only close to a solution, so if it started too early, a switch back to the more robust first method is necessary. The second derivative information required in the quasi-Newton method is generated by the algorithm.

Definition

We say that the solution $\mathbf{x}^*$ of the linearly constrained ℓ_1 problem is regular if the set

$$\left\{\mathbf{f}_j'(\mathbf{x}^*) \mid f_j(\mathbf{x}^*) = 0\right\} \cup \left\{\mathbf{a}_i \mid \mathbf{a}_i^T \mathbf{x}^* + b_i = 0\right\}$$

spans the space R^n. Otherwise the solution is singular (Bandler, Kellermann and Madsen 1985c).

The set of zero functions, i.e., the functions which are equal to zero at the solution, are called active functions for the ℓ_1 problem. A problem is regular if the (total) number of zero-valued functions (active functions) and active contraints is at least n. For regular problems the method of Hald and Madsen is quadratically convergent. For singular problems the convergence is superlinear.

2.3.3 Necessary Condition for Optimality of ℓ_1 Problems

The use of the ℓ_1 norm in the problem of approximating a function to data that might contain some wild points has been discussed by many researchers. Recently, ℓ_1 optimization has found new applications in many circuit and system problems based on its unique properties which result from the necessary conditions for optimality. The applications include fault isolation techniques for linear analog circuits (Bandler and Salama 1985a), functional approach to postproduction tuning (Bandler and Salama 1985b) and microwave modelling (Bandler, Chen and Daijavad 1986b). The insensitivity of ℓ_1 optimization to a few large f_j's in (2.16) and the fact that many f_j's are zero at the solution, has led to formulations that are designed to exploit these properties.

In this section, we follow the approach of Kellermann (1986) based on the earlier work of El-Attar, Vidyasagar and Dutta (1979) to derive the necessary conditions for optimality of the nonlinear ℓ_1 problem with nonlinear constraints. Therefore, we derive some insight into the features of the ℓ_1 norm in engineering problems in general, and the microwave device modelling approach presented in Chapter 6 in particular.

The nonlinear ℓ_1 problem with nonlinear constraints may be stated as

$$\text{minimize } F(\mathbf{x}) \triangleq \sum_{j=1}^{m} |f_j(\mathbf{x})| \tag{2.18a}$$

subject to

$$g_i(\mathbf{x}) \geq 0, \qquad i=1,\ldots,m_c\ , \tag{2.18b}$$

where the g_i's are, in general, nonlinear constraints.

Problem (2.18) can be transformed into the following nonlinear programming problem

$$\underset{\mathbf{x},\,\mathbf{y}}{\text{minimize}}\ F(\mathbf{x},\mathbf{y}) \triangleq \sum_{i=1}^{m} y_i \tag{2.19a}$$

subject to

$$y_i - f_i(\mathbf{x}) \geq 0\ , \qquad i=1,2,\ldots,m\ , \tag{2.19b}$$

$$y_i + f_i(\mathbf{x}) \geq 0\ , \qquad i=1,2,\ldots,m\ , \tag{2.19c}$$

$$g_i(\mathbf{x}) \geq 0\ , \qquad i=1,\ldots,m_c\ , \tag{2.19d}$$

where the $f_i(\mathbf{x})$, $g_i(\mathbf{x})$ are as in (2.18) and $F{:}R^{n+m}\rightarrow R$ is a new objective.

The gradient of the objective function is

$$\mathbf{F}' = \begin{bmatrix} \mathbf{u} \\ \mathbf{0} \end{bmatrix}\ , \tag{2.20}$$

where $\mathbf{u} = [1\ 1\ \ldots\ 1]^T$ is an m-dimensional vector representing the gradient with respect to $\mathbf{y}$ and $\mathbf{0} = [0\ 0\ \ldots\ 0]^T$ is an n-dimensional vector representing the gradient with respect to $\mathbf{x}$.

Suppose that $(\mathbf{x}^*, \mathbf{y}^*)$ is a solution to (2.19), then

$$y_i^* = |f_i(\mathbf{x}^*)|\ , \qquad i=1,2,\ldots,m\ . \tag{2.21}$$

Define the sets

$$I(\mathbf{x}^*) \triangleq \{i\,|\,f_i(\mathbf{x}^*)>0\}\ , \tag{2.22}$$

$$J(\mathbf{x}^*) \triangleq \{i\,|\,f_i(\mathbf{x}^*)<0\}\ , \tag{2.23}$$

$$Z(\mathbf{x}^*) \triangleq \{i\,|\,f_i(\mathbf{x}^*)=0\}\ , \tag{2.24}$$

$$A(\mathbf{x}^*) \triangleq \{i\,|\,g_i(\mathbf{x}^*)=0\}\ . \tag{2.25}$$

The gradients of the active constraints for the problem (2.19) are given by

$$\begin{bmatrix} \mathbf{e}_i \\ -\mathbf{f}_i'(\mathbf{x}^*) \end{bmatrix}\ , \qquad i\in I(\mathbf{x}^*)\ , \tag{2.26}$$

$$\begin{bmatrix} \mathbf{e}_i \\ \mathbf{f}_i'(\mathbf{x}^*) \end{bmatrix}, \qquad i \in J(\mathbf{x}^*), \tag{2.27}$$

$$\begin{bmatrix} \mathbf{e}_i \\ -\mathbf{f}_i'(\mathbf{x}^*) \end{bmatrix}, \begin{bmatrix} \mathbf{e}_i \\ \mathbf{f}_i'(\mathbf{x}^*) \end{bmatrix}, \qquad i \in Z(\mathbf{x}^*), \tag{2.28}$$

$$\begin{bmatrix} \mathbf{0} \\ \mathbf{g}_i'(\mathbf{x}^*) \end{bmatrix}, \qquad i \in A(\mathbf{x}^*), \tag{2.29}$$

where $\mathbf{e}_i$ is an m-dimensional vector with 1 in the ith position and zeros elsewhere.

By applying the Kuhn-Tucker conditions we get the following necessary conditions for optimality

$$\begin{bmatrix} \mathbf{u} \\ \mathbf{0} \end{bmatrix} + \sum_{i \in I} \lambda_i \begin{bmatrix} -\mathbf{e}_i \\ \mathbf{f}_i'(\mathbf{x}^*) \end{bmatrix} + \sum_{i \in J} \lambda_i \begin{bmatrix} -\mathbf{e}_i \\ -\mathbf{f}_i'(\mathbf{x}^*) \end{bmatrix} + \sum_{i \in Z} \left\{ \lambda_i \begin{bmatrix} -\mathbf{e}_i \\ \mathbf{f}_i'(\mathbf{x}^*) \end{bmatrix} + \mu_i \begin{bmatrix} -\mathbf{e}_i \\ -\mathbf{f}_i'(\mathbf{x}^*) \end{bmatrix} \right\} + \sum_{i \in A} \lambda_i \begin{bmatrix} \mathbf{0} \\ -\mathbf{g}_i'(\mathbf{x}^*) \end{bmatrix} = \begin{bmatrix} \mathbf{0} \\ \mathbf{0} \end{bmatrix}, \tag{2.30}$$

where $\lambda_i \geq 0$, and $\mu_i \geq 0$ are the corresponding multipliers.

Splitting equation (2.30) we get

$$\sum_{i \in I} \lambda_i \mathbf{f}_i'(\mathbf{x}^*) + \sum_{i \in J} \lambda_i \left(-\mathbf{f}_i'(\mathbf{x}^*)\right) + \sum_{i \in Z} (\lambda_i - \mu_i) \mathbf{f}_i'(\mathbf{x}^*) + \sum_{i \in A} \lambda_i \left(-\mathbf{g}_i'(\mathbf{x}^*)\right) = \mathbf{0},$$

$$\left.\begin{array}{l} \lambda_i = 1, \qquad i \in I \\ \lambda_i = 1, \qquad i \in J \\ \lambda_i + \mu_i = 1 \\ \lambda_i \geq 0, \mu_i \geq 0 \end{array}\right\}, \qquad i \in Z, \tag{2.31}$$

$$\lambda_i \geq 0, \qquad i \in A$$

or

$$\sum_{i\notin Z} \sigma_i \mathbf{f}_i'(\mathbf{x}^*) + \sum_{i\in Z} \delta_i \mathbf{f}_i'(\mathbf{x}^*) = \sum_{i\in A} \lambda_i \mathbf{g}_i'(\mathbf{x}^*)$$

$$-1 \le \delta_i \le 1 , \qquad i\in Z \tag{2.32}$$

$$\lambda_i \ge 0 , \qquad i\in A ,$$

where

$$\sigma_i \triangleq \operatorname{sign} f_i(\mathbf{x}^*) . \tag{2.33}$$

The necessary conditions for optimality of the nonlinear ℓ_1 problem indicate that zero-valued functions $f_i(\mathbf{x}^*)$, $i\in Z$, play an important role in the characteristics of the ℓ_1 problem. This fact can be exploited in formulating practical engineering problems in which zero (or nonzero) functions at an ℓ_1 solution have physical interpretations.

2.3.4 Illustration of ℓ_1 Approximation

The robustness of the ℓ_1 optimization in dealing with large f_j's in (2.16), as discussed in the literature (Hald and Madsen 1985, Bartels and Conn 1981), is a consequence of the optimality conditions. Since the ℓ_1 solution is usually situated at a point where one or more f_j's are equal to zero, some large f_j's are in effect ignored completely. In Chapter 5, we introduce a formulation for modelling in which some f_j's are designed to have large values at the solution, justifying the use of ℓ_1 as opposed to the other norms ℓ_p with $p>1$. In that formulation which uses the concept of multi-circuit measurements, the change in parameters between different circuits form part of the objective, i.e., they are some of the f_j's. These f_j's are expected to have only a few large values but many zeros at the solution.

In this section, we illustrate the unique properties of ℓ_1 optimization by considering a rational approximation problem. In particular, the insensitivity of ℓ_1

optimization to a few large f_j's will become evident when the same problem is solved using ℓ_1 and the least squares (ℓ_2) and the results are compared.

We want to find the rational approximant of the form (El-Attar, Vidyasagar and Dutta 1979)

$$K(\mathbf{x}) = \frac{x_1 + x_2\omega + x_3\omega^2}{1 + x_4\omega + x_5\omega^2} \tag{2.34}$$

to the function $\sqrt{\omega}$ on the interval $\omega \in [0, 1]$. Using 51 uniformly spaced sample points on the given interval, parameter vector $\mathbf{x}$ was obtained by ℓ_1 and ℓ_2 optimizations. The results are summarized in Table 2.1 under case A. Using both sets of parameters, the approximating function virtually duplicates the actual function over the whole interval. We now introduce a few large deviations in the actual function in two separate cases. In case B, the actual function value is replaced by zero at 5 points in the interval, namely, at 0.2, 0.4, . . .,1.0. In case C, we use zero at 0.4 and 0.8 and one at 0.2 and 0.6. In both cases, ℓ_1 and ℓ_2 optimizations are performed and the parameters obtained are summarized in Table 2.1.

The parameters obtained by ℓ_1 optimization in cases B and C are consistent with their values in case A. On the other hand, the presence of large deviations has affected the ℓ_2 optimization results severely, and inconsistent parameters are obtained. Figs. 2.2(a) and 2.2(b) illustrate the approximating and the actual functions for cases B and C. Whereas the approximation using ℓ_1 has ignored the large deviations completely and has achieved an excellent match for both cases, the ℓ_2 approximation which was as good as ℓ_1 in case A, has deteriorated. For instance, the particular arrangement of deviations in case B has caused the approximating function to underestimate the actual function over the whole interval.

TABLE 2.1

APPROXIMATION PROBLEM USING ℓ_1 AND ℓ_2 OPTIMIZATION

	Case A		Case B		Case C	
Parameter	ℓ_1	ℓ_2	ℓ_1	ℓ_2	ℓ_1	ℓ_2
x_1	0.0	0.0071	0.0	0.0391	0.0	−0.0261
x_2	8.5629	8.5660	8.6664	5.8050	8.5506	12.8828
x_3	29.3124	29.7515	30.5684	30.0523	29.1070	26.0012
x_4	24.7375	25.0108	25.4261	19.6892	24.6452	32.1023
x_5	12.2285	12.3699	12.9234	21.8794	12.0887	7.4300

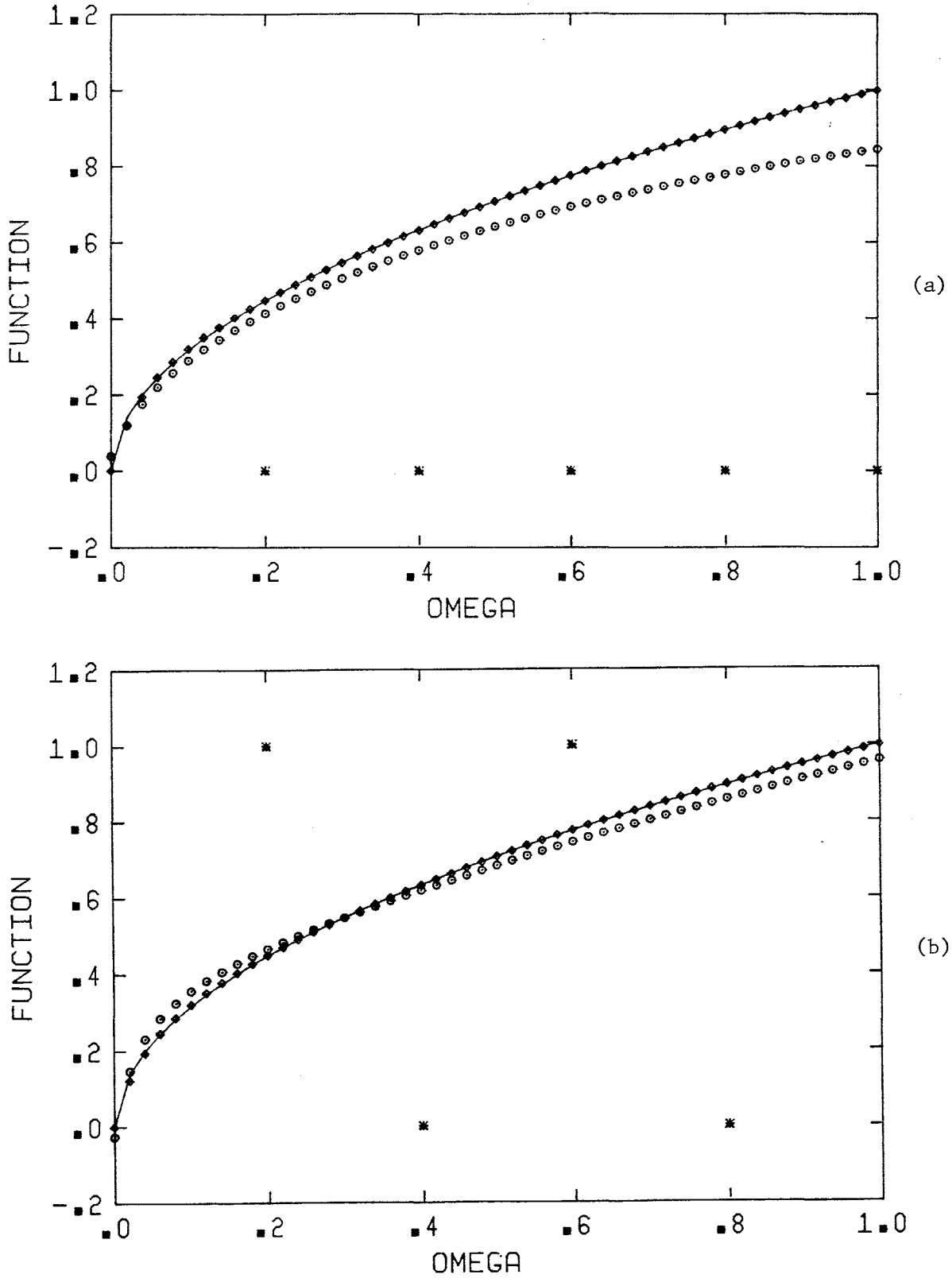

Fig. 2.2 Approximations using ℓ_1 and ℓ_2 optimizations. The solid line is the actual function. Diamonds identify the approximation using ℓ_1 and circles represent approximations with ℓ_2. Stars represent data points after large deliberate deviations. (a) and (b) correspond to cases B and C.

2.4 EFFICIENT GRADIENT APPROXIMATIONS

2.4.1 Introductory Remarks

One difficulty in extending the practical applications for powerful gradient-based minimax and ℓ_1 optimization described previously is that exact gradients of all functions with respect to all variables are required. For some applications, either an explicit expression of the exact gradients is not available or the computational labor for evaluating such gradients is prohibitive. Moreover, it is highly desirable to utilize many existing circuit simulation programs which provide only the values of the functions (or responses).

Recently, Bandler, Chen, Daijavad and Madsen (1986) proposed a flexible and powerful approach to gradient approximation for nonlinear optimization. It is a hybrid method which utilizes parameter perturbations (i.e., finite differencing), the Broyden update (Broyden, 1965) and the special iterations of Powell (1970). Finite differencing requires one additional function evaluation to obtain the gradient with respect to each variable. It is the most reliable but also the most expensive method. The Broyden rank-one formula has been used in conjunction with the special iterations of Powell to update the approximate gradients. See, for example, the work by Madsen (1975) and Zuberek (1984). Such an update does not require additional function evaluations but its accuracy may not be satisfactory for some highly nonlinear problems or for a certain stage of optimization. Bandler, Chen, Daijavad and Madsen (1986) use parameter perturbations to obtain an initial approximation and to provide regular corrections. The subsequent approximations are updated using the Broyden formula. Special iterations are introduced to improve the performance of the Broyden update. The Broyden formula is also modified to incorporate a

knowledge, if available, of the structure of the Jacobian (e.g., the sparsity of the Jacobian).

The gradient approximation is rather independent of the optimization technique and can be used in conjunction with both the minimax and ℓ_1 algorithms described in Sections 2.2.4 and 2.3.2.

2.4.2 Method of Perturbations

For a nonlinear optimization problem with m functions $f_j(\mathbf{x})$, $j = 1, \ldots, m$, the first-order derivative of $f_j(\mathbf{x})$ with respect to x_i can be approximated by

$$\frac{\partial f_j(\mathbf{x})}{\partial x_i} \simeq \frac{f_j(\mathbf{x}+t\mathbf{e}_i) - f_j(\mathbf{x})}{t}, \tag{2.35}$$

where $\mathbf{e}_i$ is a unit vector and t is the perturbation on x_i. An approximation of the Jacobian

$$\mathbf{J}(\mathbf{x}) \triangleq \left[\frac{\partial \mathbf{f}^T}{\partial \mathbf{x}}\right]^T$$

using perturbations requires $n+1$ evaluations of the functions $\mathbf{f}(\mathbf{x})$ where n is the number of variables.

2.4.3 Broyden Update

Having an approximate Jacobian $\mathbf{J}_k$ at a point $\mathbf{x}_k$ and the function values at $\mathbf{x}_k$ and $\mathbf{x}_k + \mathbf{h}_k$, we can obtain $\mathbf{J}_{k+1}$ using the Broyden rank-one update (Broyden 1965)

$$\mathbf{J}_{k+1} = \mathbf{J}_k + \frac{\mathbf{f}(\mathbf{x}_k+\mathbf{h}_k) - \mathbf{f}(\mathbf{x}_k) - \mathbf{J}_k\mathbf{h}_k}{\mathbf{h}_k^T\mathbf{h}_k}\mathbf{h}_k^T. \tag{2.36}$$

The new approximation $\mathbf{J}_{k+1}$ provides a linearized model between two points $\mathbf{x}_k$ and $\mathbf{x}_k + \mathbf{h}_k$:

$$\mathbf{f}(\mathbf{x}_k+\mathbf{h}_k) - \mathbf{f}(\mathbf{x}_k) = \mathbf{J}_{k+1}\mathbf{h}_k. \tag{2.37}$$

Notice that if $\mathbf{x}_k$ and $\mathbf{x}_k + \mathbf{h}_k$ are iterates of optimization the Broyden formula does not require additional function evaluations.

The application of the original Broyden update has shortcomings. As has been observed by Zuberek (1984), if some functions are linear in some variables and if the corresponding components of $\mathbf{h}_k$ are nonzero, then the approximation to constant derivatives are updated by nonzero values. Applying the Broyden formula to each $f_j(\mathbf{x})$ as a single function and associating with f_j a weighting vector defined by

$$\mathbf{w}_j \triangleq [w_{j1} \cdots w_{jn}]^T , \qquad w_{ji} \geq 0 , \tag{2.38}$$

we have

$$(\mathbf{f}_j')_{k+1} = (\mathbf{f}_j')_k + \frac{f_j(\mathbf{x}_k + \mathbf{h}_k) - f_j(\mathbf{x}_k) - (\mathbf{f}_j')_k^T \mathbf{h}_k}{\mathbf{q}_{jk}^T \mathbf{h}_k} \mathbf{q}_{jk} , \tag{2.39}$$

where

$$\mathbf{q}_{jk} \triangleq [w_{j1} h_{k1} \cdots w_{jn} h_{kn}]^T . \tag{2.40}$$

If f_j is linear in x_i, we set $w_{ji} = 0$. In circuit design problems, it may be known that the performance function is linear or independent of some parameters over certain frequency or time intervals. An approximate Jacobian evaluated using (2.39) also satisfies (2.37).

2.4.4 Special Iterations of Powell

The Broyden formula updates the approximate gradients along the direction $\mathbf{h}_k$. If the directions of some consecutive steps of optimization are collinear, the Broyden update may not converge. To cure this problem, Powell (1970) suggested the method of "strictly linearly independent directions" generated by special iterations. Unlike an ordinary iteration where a step is taken in order to reduce the objective function, a special iteration is intended to improve the gradient approximation. After every p ordinary iterations the function values are calculated at

a point obtained using the formula given by Powell (1970) and a Broyden update is applied. As suggested by Powell and also Madsen (1975), p = 2 gives satisfactory results.

2.5 CONCLUDING REMARKS

In this chapter, we reviewed minimax and ℓ_1 optimization techniques which are used for design and modelling of microwave circuits in this thesis. The emphasis was on the efficient and new techniques developed in the past few years. In particular, we have described the Hald and Madsen algorithms for both minimax and ℓ_1 optimizations.

The necessary conditions for optimality and the role of zeros of the nonlinear functions and active constraints in ℓ_1 optimization were discussed and a simple illustration of the ℓ_1 approximation compared with the ℓ_2 was presented.

We described efficient gradient approximation techniques which use a hybrid method utilizing parameter perturbations, the Broyden update and special iterations of Powell. These techniques, which are rather independent of the optimization method, can be used in conjunction with minimax and ℓ_1 algorithms. Their use obviates exact calculation of gradients and hence expands the range of applications for powerful gradient-based algorithms to many microwave problems in which exact gradient evaluation is not feasible.

3

SENSITIVITY ANALYSIS OF TWO-PORTS AND CASCADED STRUCTURES – SIMPLE ALGEBRAIC APPROACHES

3.1 INTRODUCTION

In Chapter 2, we reviewed recent gradient-based minimax and ℓ_1 optimization techniques. When these techniques are applied to the design and modelling of electrical circuits, exact and efficient evaluation of circuit response sensitivities with respect to equivalent network parameters becomes of significant interest. For linear networks, Director and Rohrer (1969) introduced the concept of the adjoint network, which is used in efficient calculation of sensitivities based on Tellegen's theorem. They showed that the sensitivities of a particular response with respect to all the parameters in a linear network can be evaluated with two network analyses: one corresponding to the original network and one corresponding to a hypothetical network called the adjoint. Director (1971) showed that, once the original circuit has been analyzed, the analysis of the adjoint network is performed with minimal extra effort.

In this chapter, we develop a systematic way of evaluating sensitivities without appealing to the adjoint network concept. The computations involve simple algebraic manipulations of vectors and matrices. This simple treatment was originally suggested by Branin (1973). Starting with the admittance or impedance matrix description of a network, we develop formulas to evaluate first- and second-order sensitivities of its two-port equivalent with respect to a generic variable ϕ appearing in the matrix. These formulas are then used to evaluate input and output

port response sensitivities. To accommodate active devices, we consider the use of controlled sources in the network and present formulas for sensitivities of two-port S-parameters which are commonly used for both active and passive devices.

Recently, an important result in sensitivity analysis of lossless two-ports was presented by Orchard et al.(1983, 1985). Using the matrix notation of this chapter, we prove their result in an elegant and simple way and further develop it to the computation of group delay.

Finally, in preparation for the design of multiplexing networks which belong to the class of branched cascaded networks, we review some of the concepts in sensitivity analysis of cascaded 2-ports by Bandler et al. (1978, 1981). Utilizing a method which obviates the use of auxiliary or adjoint networks, we discuss the sensitivity of branched cascaded circuits with examples on specific frequency responses.

3.2 GENERAL TWO-PORTS

3.2.1 Unterminated Two-Ports

Assume that the admittance matrix description of an equivalent circuit model is available. All derivations and formulas presented in this chapter have dual counterparts for the case of a circuit described by its impedance matrix. The general case of a hybrid matrix could also be handled, however, we avoid generalization for the sake of the simplicity of notation.

From the four types of controlled sources, the voltage controlled current source (VCCS) can be easily handled in an admittance matrix description. The other three types are converted into VCCS through an intermediate step involving gyrators. This is an exercise described in Chua and Lin (1975), as well as other text books.

Consider an n×n admittance matrix **Y** arranged such that the input and output responses of interest are evaluated using the voltages at nodes 1 and n. In this section, we develop a comprehensive set of formulas for first- and second-order sensitivities of the two-port open-circuit impedance matrix obtained from **Y**. Figure 3.1 illustrates the block representation of the circuit and its two-port equivalent. We have

$$\mathbf{Y}\,\mathbf{V} = \mathbf{I} \tag{3.1}$$

where $\mathbf{I} = [I_1\ 0 \ldots 0\ I_n]^T$ and $\mathbf{V} = [V_1\ V_2 \ldots V_n]^T$ are the current excitation and the voltages, respectively. Denote the two-port currents and voltages by $\mathbf{I}_p = [I_1\ \ I_n]^T$ and $\mathbf{V}_p = [V_1\ \ V_n]^T$. By defining

$$\mathbf{U} = [\mathbf{e}_1\ \ \mathbf{e}_n] \tag{3.2}$$

where $\mathbf{e}_1 = [1\ 0 \ldots 0]^T$ and $\mathbf{e}_n = [0 \ldots 0\ 1]^T$, we have

$$\mathbf{V}_p = \mathbf{U}^T\mathbf{V} \tag{3.3}$$

and

$$\mathbf{I} = \mathbf{U}\mathbf{I}_p\,. \tag{3.4}$$

From (3.1), (3.3) and (3.4) we can solve for

$$\mathbf{V}_p = \mathbf{U}^T\,\mathbf{Y}^{-1}\,\mathbf{I} = \mathbf{U}^T\,\mathbf{Y}^{-1}\,\mathbf{U}\,\mathbf{I}_p \tag{3.5}$$

which gives

$$\mathbf{z} = \mathbf{U}^T\,\mathbf{Y}^{-1}\,\mathbf{U} = \begin{bmatrix} \mathbf{e}_1^T\mathbf{Y}^{-1}\mathbf{e}_1 & \mathbf{e}_1^T\mathbf{Y}^{-1}\mathbf{e}_n \\ \mathbf{e}_n^T\mathbf{Y}^{-1}\mathbf{e}_1 & \mathbf{e}_n^T\mathbf{Y}^{-1}\mathbf{e}_n \end{bmatrix}, \tag{3.6}$$

using the definition of two-port open-circuit impedance matrix **z**. By solving the system of equations

$$\mathbf{Y}\,\mathbf{p} = \mathbf{e}_1 \tag{3.7a}$$

and

$$\mathbf{Y}\mathbf{q} = \mathbf{e}_n\,, \tag{3.7b}$$

we evaluate $\mathbf{z}$ as

$$\mathbf{z} = \begin{bmatrix} \mathbf{e}_1^T\mathbf{p} & \mathbf{e}_1^T\mathbf{q} \\ \mathbf{e}_n^T\mathbf{p} & \mathbf{e}_n^T\mathbf{q} \end{bmatrix} = \begin{bmatrix} p_1 & q_1 \\ p_n & q_n \end{bmatrix} . \tag{3.8}$$

Differentiating (3.6) with respect to a variable ϕ in $\mathbf{Y}$, we have

$$\mathbf{z}_\phi = -\mathbf{U}^T \mathbf{Y}^{-1} \mathbf{Y}_\phi \mathbf{Y}^{-1} \mathbf{U}, \tag{3.9}$$

where $\mathbf{z}_\phi$ and $\mathbf{Y}_\phi$ denote the derivative of $\mathbf{z}$ and $\mathbf{Y}$ with respect to ϕ. Now,

$$\mathbf{U}^T\mathbf{Y}^{-1} = \begin{bmatrix} \mathbf{e}_1^T\mathbf{Y}^{-1} \\ \mathbf{e}_n^T\mathbf{Y}^{-1} \end{bmatrix} = \begin{bmatrix} \hat{\mathbf{p}}^T \\ \hat{\mathbf{q}}^T \end{bmatrix} = [\hat{\mathbf{p}} \;\; \hat{\mathbf{q}}]^T , \tag{3.10}$$

where $\hat{\mathbf{p}}$ and $\hat{\mathbf{q}}$ are obtained by solving the systems of equations

$$\mathbf{Y}^T \hat{\mathbf{p}} = \mathbf{e}_1 \tag{3.11a}$$

and

$$\mathbf{Y}^T \hat{\mathbf{q}} = \mathbf{e}_n . \tag{3.11b}$$

Also, using the identity

$$\mathbf{Y}^{-1}\mathbf{U} = [\mathbf{Y}^{-1}\mathbf{e}_1 \quad \mathbf{Y}^{-1}\mathbf{e}_n] = [\mathbf{p} \;\; \mathbf{q}] , \tag{3.12}$$

(3.9) becomes

$$\mathbf{z}_\phi = -[\hat{\mathbf{p}} \;\; \hat{\mathbf{q}}]^T \mathbf{Y}_\phi [\mathbf{p} \;\; \mathbf{q}] . \tag{3.13}$$

As an example, suppose that ϕ appears in $\mathbf{Y}$ in the following positions:

$$\mathbf{Y} = \begin{array}{c} \\ i \\ \\ j \\ \\ \end{array} \begin{array}{c} \begin{array}{ccccc} & k & & \ell & \end{array} \\ \begin{bmatrix} & \vdots & & \vdots & \\ \cdots & \phi & \cdots & -\phi & \cdots \\ & \vdots & & \vdots & \\ \cdots & -\phi & \cdots & \phi & \cdots \\ & \vdots & & \vdots & \end{bmatrix} \end{array} , \tag{3.14}$$

then (3.13) becomes

$$\mathbf{z}_\phi = -\begin{bmatrix} (\hat{p}_i - \hat{p}_j)(p_k - p_\ell) & (\hat{p}_i - \hat{p}_j)(q_k - q_\ell) \\ (\hat{q}_i - \hat{q}_j)(p_k - p_\ell) & (\hat{q}_i - \hat{q}_j)(q_k - q_\ell) \end{bmatrix} . \tag{3.15}$$

Having evaluated $\mathbf{z}_\phi$, we can calculate $\mathbf{z}_x$, i.e., the sensitivity of $\mathbf{z}$ with respect to actual circuit parameters, by applying the chain rule of differentiation. Table 3.1

shows some possible circuit parameters and the relationship between $\mathbf{z}_x$ and $\mathbf{z}_\phi$. The circuit parameters considered are conductance G, resistance R, capacitance C, inductance L, and two parameters associated with a VCCS with a transconductance $g_m e^{-j2\pi f\tau}$, namely delay τ and g_m which denotes the magnitude of transconductance at dc.

3.2.2 Second-Order Sensitivities

In optimization of responses such as group delay and gain slope, second-order derivatives of $\mathbf{z}$ are needed. In such cases, $\mathbf{z}_\omega$, which denotes the sensitivity of $\mathbf{z}$ with respect to angular frequency ω, is used to evaluate the response itself. The sensitivities with respect to circuit parameters are then calculated using $\mathbf{z}_{\phi\omega}$, which is a second-order sensitivity expression.

Using (3.9) we have

$$\mathbf{z}_\omega = -\mathbf{U}^T \mathbf{Y}^{-1} \mathbf{Y}_\omega \mathbf{Y}^{-1} \mathbf{U}, \tag{3.16}$$

which can be differentiated with respect to ϕ as

$$\begin{aligned} \mathbf{z}_{\phi\omega} &= \mathbf{U}^T\mathbf{Y}^{-1}(\mathbf{Y}_\phi \mathbf{Y}^{-1}\mathbf{Y}_\omega - \mathbf{Y}_{\phi\omega} + \mathbf{Y}_\omega \mathbf{Y}^{-1}\mathbf{Y}_\phi)\mathbf{Y}^{-1}\mathbf{U} \\ &= [\hat{\mathbf{p}}\ \hat{\mathbf{q}}]^T \mathbf{Y}_\phi [\bar{\mathbf{p}}\ \bar{\mathbf{q}}] - [\hat{\mathbf{p}}\ \hat{\mathbf{q}}]^T \mathbf{Y}_{\phi\omega} [\mathbf{p}\ \mathbf{q}] + [\mathbf{p}'\,\mathbf{q}']^T \mathbf{Y}_\phi [\mathbf{p}\ \mathbf{q}]. \end{aligned} \tag{3.17}$$

Four systems of equations are solved to obtain $[\bar{\mathbf{p}}\ \bar{\mathbf{q}}]$ and $[\mathbf{p}'\ \mathbf{q}']$. They are

$$\mathbf{Y}\,\bar{\mathbf{p}} = \mathbf{Y}_\omega \mathbf{p}, \tag{3.18a}$$

$$\mathbf{Y}\,\bar{\mathbf{q}} = \mathbf{Y}_\omega \mathbf{q}, \tag{3.18b}$$

$$\mathbf{Y}^T \mathbf{p}' = \mathbf{Y}_\omega^T \hat{\mathbf{p}}, \tag{3.18c}$$

and

$$\mathbf{Y}^T \mathbf{q}' = \mathbf{Y}_\omega^T \hat{\mathbf{q}}. \tag{3.18d}$$

TABLE 3.1

SENSITIVITIES OF OPEN-CIRCUIT IMPEDANCE MATRIX

W.R.T. SOME POSSIBLE NETWORK PARAMETERS

x	$\mathbf{z}_x$
G	$\mathbf{z}_\phi$
R	$\left(\frac{-1}{R^2}\right)\mathbf{z}_\phi$
C	$s\mathbf{z}_\phi$
L	$\frac{-1}{sL^2}\mathbf{z}_\phi$
g_m	$e^{-s\tau}\mathbf{z}_\phi$
τ	$-sg_m e^{-s\tau}\mathbf{z}_\phi$

$s = j\omega = j2\pi f$ is the complex frequency

3.2.3 Computational Considerations

For a general two-port, it has been established that solving eight systems of equations, namely (3.7), (3.11) and (3.18), provides complete information for evaluation of first- and second-order sensitivities of the open-circuit impedance matrix **z**, which in turn leads to sensitivity evaluation of input and output responses. From a computational point of view, this means one LU factorization of matrix **Y** followed by eight forward and backward substitutions (FBS). If matrix **Y** is symmetrical, only four FBS are required since $\hat{\mathbf{p}} = \mathbf{p}$, $\hat{\mathbf{q}} = \mathbf{q}$, $\mathbf{p}' = \overline{\mathbf{p}}$ and $\mathbf{q}' = \overline{\mathbf{q}}$.

For those familiar with the concept of the adjoint network, an explanation is in order here to justify the need for performing as many as eight FBS's in a complete sensitivity analysis. Using the adjoint network approach, the first-order sensitivity of a particular response is calcuated via 2 FBS's and the second-order sensitivity requires 4 FBS's for any linear network. An example of second-order sensitivity evaluation can be found in calculation of group delay sensitivities discussed by Bandler, Rizk and Tromp (1976). The important difference here is that with the unterminated two-port, we have not committed ourselves to excitation or termination at either port and this freedom has doubled the number of possible FBS's required. By designating excitation and termination ports, the matrix manipulation method is computationally equivalent to the adjoint network approach with the difference that algebra has replaced circuit interpretation.

The use of an unterminated two-port model has the advantage that we can obtain the transmission matrix and its first- and second-order sensitivities of a two-port equivalent for a complicated subnetwork inside a large network in an independent fashion. This means that the excitations and terminations in other parts of the large network are ignored. Later in this chapter, we will describe efficient

methods for simulation and sensitivity analysis of cascaded networks with the requirement that the transmission matrix and its sensitivities for each two-port be known.

3.2.4 Terminated Two-Ports

If the two-port equivalent obtained by reduction of admittance or impedance matrix is part of a larger network, e.g., a filter in a multiplexer structure, then we evaluate the transmission matrix and its sensitivities for the two-port and use the cascaded network approach. However, in many of the examples in this thesis, such as modelling of multi- coupled cavity filters and GaAs FET's, the entire analysis is almost completed after reduction to two-ports since the input and output responses and their sensitivities could be readily evaluated once the unterminated two-port analysis is done.

Assume that the two-port is terminated by an arbitrary load Y_L and a source $J = 1$ A with an admittance Y_S. We have

$$I_1 = 1 - Y_S V_1 \tag{3.19}$$

and

$$I_n = -Y_L V_n . \tag{3.20}$$

Denoting

$$\mathbf{T} \triangleq \begin{bmatrix} Y_S & 0 \\ 0 & Y_L \end{bmatrix}, \tag{3.21}$$

we write (3.19) and (3.20) in a compact form, as

$$\mathbf{I}_p = \mathbf{e}_1 - \mathbf{T}\,\mathbf{V}_p . \tag{3.22}$$

Using the fact that $\mathbf{V}_p = \mathbf{z}\,\mathbf{I}_p$ subject to (3.22), we solve for $\mathbf{V}_p$ as

$$\mathbf{V}_p = (1 + \mathbf{z}\,\mathbf{T})^{-1}\,\mathbf{z}\,\mathbf{e}_1 = \mathbf{H}\,\mathbf{z}\,\mathbf{e}_1 , \tag{3.23}$$

where

$$\mathbf{H} \triangleq (1 + \mathbf{z}\,\mathbf{T})^{-1}\,. \tag{3.24}$$

Furthermore, the first-order sensitivities of $\mathbf{V}_p$ can be derived as

$$\begin{aligned}(\mathbf{V}_p)_\phi &= [\mathbf{H}_\phi\,\mathbf{z} + \mathbf{H}\,\mathbf{z}_\phi]\,\mathbf{e}_1 \\ &= [-\mathbf{H}\,(\mathbf{H}^{-1})_\phi\,\mathbf{H}\mathbf{z} + \mathbf{H}\mathbf{z}_\phi]\,\mathbf{e}_1 \\ &= \mathbf{H}\,[-(\mathbf{z}_\phi\,\mathbf{T} + \mathbf{z}\,\mathbf{T}_\phi)\,\mathbf{H}\,\mathbf{z} + \mathbf{z}_\phi]\,\mathbf{e}_1 \\ &= \mathbf{H}\,[-(\mathbf{z}_\phi\,\mathbf{T} + \mathbf{z}\,\mathbf{T}_\phi)\,\mathbf{V}_p + \mathbf{z}_\phi\,\mathbf{e}_1] \\ &= \mathbf{H}\,[\mathbf{z}_\phi\,(-\mathbf{T}\,\mathbf{V}_p + \mathbf{e}_1) - \mathbf{z}\,\mathbf{T}_\phi\,\mathbf{V}_p] \\ &= \mathbf{H}\,(\mathbf{z}_\phi\,\mathbf{I}_p - \mathbf{z}\,\mathbf{T}_\phi\,\mathbf{V}_p).\end{aligned} \tag{3.25}$$

The derivation of the second-order derivative is similar. Here we state the result, which is derived in Appendix A, as

$$\begin{aligned}(\mathbf{V}_p)_{\phi\omega} = -\mathbf{H}\,\{&\mathbf{z}_\omega\,[\mathbf{T}_\phi\,\mathbf{V}_p + \mathbf{T}\,(\mathbf{V}_p)_\phi] + \mathbf{z}_\phi\,[\mathbf{T}_\omega\,\mathbf{V}_p + \mathbf{T}\,(\mathbf{V}_p)_\omega] \\ &+ \mathbf{z}\,[\mathbf{T}_\phi\,(\mathbf{V}_p)_\omega + \mathbf{T}_\omega\,(\mathbf{V}_p)_\phi + \mathbf{T}_{\phi\omega}\,\mathbf{V}_p] - \mathbf{z}_{\phi\omega}\,\mathbf{I}_p\}.\end{aligned} \tag{3.26}$$

Sometimes, as for the evaluation of the output reflection coefficient, it is also of interest to solve the network excited at the output port. The solution, denoted by $\hat{\mathbf{V}}_p$, can be obtained by simply replacing $\mathbf{e}_1$ by $\mathbf{e}_n$ in (3.23), where $\mathbf{e}_n = [0\ \ 1]^T$. The sensitivity expressions of $\hat{\mathbf{V}}_p$ are the same as those of $\mathbf{V}_p$ except that $\mathbf{e}_1$, $\mathbf{I}_p$ and $\mathbf{V}_p$ are replaced by $\mathbf{e}_n$, $\hat{\mathbf{I}}_p$ and $\hat{\mathbf{V}}_p$, as appropriate.

Various frequency responses and their sensitivities can be calculated using the formulas obtained for the two-port. Table 3.2 summarizes some useful formulas for various responses. The formulas have been derived from their conventional definitions, having in mind that we have already presented formulas for $\mathbf{V}_p = [V_1\ \ V_n]^T$ and its first- and second-order sensitivities. The sensitivities for each response are obtained by simple differentiation, e.g., for the group delay denoted by T_G, we have

TABLE 3.2

VARIOUS FREQUENCY RESPONSE EXPRESSIONS

Response	Formula
input reflection coefficient (ρ_{in})	$\frac{Y_S}{Y_S^*}[2G_S V_1 - 1]$
input return loss	$-20 \log_{10}\lvert\rho_{in}\rvert$
transducer loss	$-10 \log_{10}[4\lvert V_n\rvert^2 G_S G_L]$
insertion loss	$-20 \log_{10}\lvert V_n Y_T\rvert$
gain slope	$\frac{-20}{\ell n\, 10} \mathrm{Re}\left[\frac{(V_n)_\omega}{V_n} + \frac{(Y_T)_\omega}{Y_T}\right]$
group delay	$-\mathrm{Im}\left[\frac{(V_n)_\omega}{V_n} + \frac{(Y_S)_\omega}{Y_S}\right]$

$G_S \triangleq \mathrm{Re}(Y_S)$ $\quad G_L \triangleq \mathrm{Re}(Y_L)$ $\quad Y_T \triangleq Y_S + Y_L$

$$(T_G)_\phi = -\mathrm{Im}\left[\frac{(V_n)_{\phi\omega}}{V_n} - \frac{(V_n)_\phi (V_n)_\omega}{V_n^2} + \frac{(Y_S)_{\phi\omega}}{Y_S} - \frac{(Y_S)_\phi (Y_S)_\omega}{Y_S^2}\right]. \tag{3.27}$$

As mentioned earlier, starting with the impedance matrix description of a network, we can derive dual formulas for all equations derived in this chapter. Such formulas for a symmetrical impedance matrix have been presented by Bandler, Chen and Daijavad (1985a, 1986a).

3.2.5 S-parameter Sensitivities

The use of scattering coefficients or S-parameters is popular in the microwave area. Scattering coefficients are usually defined from a wave point of view. However, in this section we relate two-port S-parameters to the open-circuit impedance matrix of the two-port and derive their sensitivities.

From the definition of S-parameters, we have

$$\begin{bmatrix} a_1 \\ a_2 \end{bmatrix} = \frac{1}{2\sqrt{Z_0}} \left\{ \begin{bmatrix} V_1 \\ V_n \end{bmatrix} + Z_0 \begin{bmatrix} I_1 \\ I_n \end{bmatrix} \right\}, \tag{3.28a}$$

$$\begin{bmatrix} b_1 \\ b_2 \end{bmatrix} = \frac{1}{2\sqrt{Z_0}} \left\{ \begin{bmatrix} V_1 \\ V_n \end{bmatrix} - Z_0 \begin{bmatrix} I_1 \\ I_n \end{bmatrix} \right\}, \tag{3.28b}$$

$$\begin{bmatrix} b_1 \\ b_2 \end{bmatrix} = \begin{bmatrix} S_{11} & S_{12} \\ S_{21} & S_{22} \end{bmatrix} \begin{bmatrix} a_1 \\ a_2 \end{bmatrix}, \tag{3.28c}$$

where I_1, V_1 and I_n, V_n are the current and voltage at ports 1 and 2, respectively, of a two-port network, a_1, b_1 and a_2, b_2 are the incident and reflected waves at ports 1 and 2, respectively, and Z_0 is the normalizing impedance. The reason for using subscript n for voltage and current at port 2 is to be consistent with the previous notation.

Denoting the normalized open-circuit impedance by $\bar{\mathbf{z}}$, we have

$$\bar{\mathbf{z}} = \frac{1}{Z_0}\,\mathbf{z}\,, \tag{3.29}$$

where $\mathbf{z}$ and its sensitivity with respect to ϕ denoted by $\mathbf{z}_\phi$ have been derived in (3.8) and (3.13). From the definition of $\bar{\mathbf{z}}$, we have

$$\begin{bmatrix} V_1 \\ V_n \end{bmatrix} = Z_0\,\bar{\mathbf{z}} \begin{bmatrix} I_1 \\ I_n \end{bmatrix}, \tag{3.30}$$

and after simple manipulation of (3.28) and (3.30), we get

$$\begin{bmatrix} \bar{z}_{11}-1 & \bar{z}_{12} \\ \bar{z}_{21} & \bar{z}_{22}-1 \end{bmatrix} = \begin{bmatrix} S_{11} & S_{12} \\ S_{21} & S_{22} \end{bmatrix} \begin{bmatrix} \bar{z}_{11}+1 & \bar{z}_{12} \\ \bar{z}_{21} & \bar{z}_{22}+1 \end{bmatrix} \tag{3.31}$$

or

$$(\bar{\mathbf{z}} - 1) = \mathbf{S}(\bar{\mathbf{z}} + 1)\,. \tag{3.32}$$

From (3.32), it follows that

$$\mathbf{S} = \frac{1}{\Delta} \begin{bmatrix} \Delta - 2(\bar{z}_{22}+1) & 2\,\bar{z}_{12} \\ 2\,\bar{z}_{21} & \Delta - 2(\bar{z}_{11}+1) \end{bmatrix}, \tag{3.33}$$

where

$$\Delta = (\bar{z}_{11}+1)\,(\bar{z}_{22}+1) - \bar{z}_{12}\,\bar{z}_{21}\,. \tag{3.34}$$

Also, differentiating both sides of (3.32) w.r.t. ϕ, after simplification, gives

$$\mathbf{S}_\phi = \frac{1}{2Z_0}\,(1-\mathbf{S})\,\mathbf{z}_\phi(1-\mathbf{S})\,, \tag{3.35}$$

i.e., $\mathbf{S}_\phi$ can be readily evaluated from $\mathbf{z}_\phi$.

3.3 LOSSLESS TWO-PORTS

Lossless reciprocal two-ports, usually arranged as ladder networks, have been the preferred circuit arrangement for filters from the time that filters were first used. Many types of filters, e.g., microwave, RC-active, digital, and, most recently, switched capacitor filters, are often modelled on a prototype lossless ladder. Recently, Orchard, Temes and Cataltepe (1983, 1985) presented new and simple first-order

sensitivity expressions for reciprocal lossless two-ports. From the time the formulas were introduced by Orchard et al. (1983) until their proof was presented in 1985, three different and original proofs were presented by Bandler, Chen and Daijavad (1984a, 1984b, 1985b). In this section, we present a proof which is based on the ideas of the previous publications, however, it is consistent with the notation used in this chapter.

Starting with an admittance matrix $\mathbf{Y}$ and assuming excitation J with its corresponding conductance G_S at port 1 and the load conductance G_L at port 2, we have

$$\mathbf{Y}\,\mathbf{V} = \mathrm{J}\,\mathbf{e}_1\,, \tag{3.36}$$

where

$$\mathbf{Y} = G_S\,\mathbf{e}_1\mathbf{e}_1^T + G_L\mathbf{e}_n\mathbf{e}_n^T + \mathbf{Y}'\,. \tag{3.37}$$

The reason for the partitioning of $\mathbf{Y}$ will become clear as we proceed. We will now show that it is possible to obtain $\partial V_1/\partial\phi$ and $\partial V_n/\partial\phi$ by solving only (3.36), i.e., by avoiding any auxiliary system, given certain conditions on $\mathbf{Y}'$.

From (3.36), it immediately follows that

$$\begin{aligned}\frac{\partial V_1}{\partial\phi} &= -\mathbf{e}_1^T\mathbf{Y}^{-1}\frac{\partial\mathbf{Y}}{\partial\phi}\,\mathbf{V} \\ &= -\frac{1}{\mathrm{J}}\,\mathbf{V}^T\frac{\partial\mathbf{Y}}{\partial\phi}\,\mathbf{V}\,,\end{aligned} \tag{3.38}$$

given that $\mathbf{Y}$ is symmetrical, which requires $\mathbf{Y}'$ to be symmetrical, i.e.,

$$(\mathbf{Y}')^T = \mathbf{Y}'\,. \tag{3.39}$$

Also, differentiating (3.36) with respect to ϕ and premultiplying it by $(\mathbf{V}^*)^T$ gives

$$(\mathbf{V}^*)^T\,\mathbf{Y}\,\frac{\partial\mathbf{V}}{\partial\phi} = -(\mathbf{V}^*)^T\frac{\partial\mathbf{Y}}{\partial\phi}\,\mathbf{V}\,. \tag{3.40}$$

If $\mathbf{Y}'$ has the property that

$$\mathbf{Y}' = -(\mathbf{Y}')^*\,, \tag{3.41}$$

then

$$\mathbf{Y}+(\mathbf{Y}^*)^T = 2\{G_S\mathbf{e}_1\mathbf{e}_1^T+G_L\mathbf{e}_n\mathbf{e}_n^T\}+\mathbf{Y}'+[(\mathbf{Y}')^*]^T \tag{3.42}$$

$$= 2\{G_S\mathbf{e}_1\mathbf{e}_1^T+G_L\mathbf{e}_n\mathbf{e}_n^T\}.$$

Evaluating $\mathbf{Y}$ from (3.42) and substituting the result in (3.40) gives

$$(\mathbf{V}^*)^T\left[2\{G_S\mathbf{e}_1\mathbf{e}_1^T+G_L\mathbf{e}_n\mathbf{e}_n^T\}-(\mathbf{Y}^*)^T\right]\frac{\partial\mathbf{V}}{\partial\Phi}=-(\mathbf{V}^*)^T\frac{\partial\mathbf{Y}}{\partial\Phi}\mathbf{V}. \tag{3.43}$$

Now, by noticing that

$$(\mathbf{V}^*)^T(\mathbf{Y}^*)^T=J\mathbf{e}_1^T, \tag{3.44}$$

(3.43) gives

$$2G_SV_1^*\frac{\partial V_1}{\partial\Phi}+2G_LV_n^*\frac{\partial V_n}{\partial\Phi}-J\frac{\partial V_1}{\partial\Phi}=-(\mathbf{V}^*)^T\frac{\partial\mathbf{Y}}{\partial\Phi}\mathbf{V}. \tag{3.45}$$

Finally, by substituting (3.38) in (3.45) and using the input reflection coefficient ρ_1 given by

$$\rho_1=\frac{2G_SV_1}{J}-1, \tag{3.46}$$

we get

$$\frac{\partial V_n}{\partial\Phi}=\frac{1}{2G_LV_n^*}(\rho_1^*\mathbf{V}-\mathbf{V}^*)^T\frac{\partial\mathbf{Y}}{\partial\Phi}\mathbf{V}. \tag{3.47}$$

To summarize the above derivations, it has been proved that given conditions (3.39) and (3.41) for matrix $\mathbf{Y}'$, $\partial V_n/\partial\Phi$ can be evaluated by solving only one system of equations, namely (3.36). Conditions (3.39) and (3.41) translate into having a lossless reciprocal network.

We can use (3.47) to derive some formulas in the form presented by Orchard, Temes and Cataltepe (1983) and in the calculation of group delay. Given the definition of the transducer coefficient θ as

$$\theta\triangleq\ell n\,H, \tag{3.48}$$

where

$$H\triangleq\frac{J}{2V_n}\sqrt{\frac{1}{G_SG_L}}, \tag{3.49}$$

we have

$$\frac{\partial\theta}{\partial\phi} = -\frac{1}{V_n}\frac{\partial V_n}{\partial\phi} \quad . \tag{3.50}$$

Using (3.47), we get

$$\frac{\partial\theta}{\partial\phi} = \frac{1}{2P_n}(\mathbf{V}^* - \rho_1^*\mathbf{V})^T \frac{\partial\mathbf{Y}}{\partial\phi}\mathbf{V}, \tag{3.51}$$

where P_n is the power in the load, given by $P_n = G_L V_n V_n^*$.

As an example, assume that ϕ represents y_{ij} which denotes the admittance connected between nodes i and j, therefore

$$\frac{\partial\mathbf{Y}}{\partial\phi} = (\mathbf{e}_i - \mathbf{e}_j)(\mathbf{e}_i - \mathbf{e}_j)^T, \tag{3.52}$$

and (3.51) gives

$$\begin{aligned}\frac{\partial\theta}{\partial y_{ij}} &= \frac{1}{2P_n}\left[(V_i^* - \rho_1^* V_i) - (V_j^* - \rho_1^* V_j)\right](V_i - V_j) \\ &= \frac{|V_{ij}|^2 - \rho_1^* V_{ij}^2}{2P_n},\end{aligned} \tag{3.53}$$

where $V_{ij} = V_i - V_j$ represents the voltage across nodes i and j. This form of the equation can be found in the work by Orchard et al. (1985).

We can evaluate the group delay using (3.51) as

$$T_G = \mathrm{Im}\left[\frac{\partial\theta}{\partial\omega}\right] = \frac{1}{2P_n}\mathrm{Im}\left\{(\mathbf{V}^* - \rho_1^*\mathbf{V})^T\frac{\partial\mathbf{Y}}{\partial\omega}\mathbf{V}\right\} . \tag{3.54}$$

Many elements of solution vector $\mathbf{V}$ are usually used in calculation of group delay since $\partial\mathbf{Y}/\partial\omega$ has many nonzero elements.

As has been noted by Orchard et al. (1985), for purely numerical work, the new formulas for lossless reciprocal two-ports have little to offer over other methods, e.g., the adjoint network method. Their value lies primarily in their simple analytic form. Orchard et al. have also shown the application of the new formulas to active switched-capacitor filter design. This is merely an exercise to prove the usefulness of

first-order sensitivity information in applications where nonideal effects which can be represented by a first-order change are present.

3.4 CASCADED STRUCTURES

3.4.1 Review of Concepts

The analysis of cascaded networks plays an important role in the design and optimization of microwave circuits. Bandler, Rizk and Abdel-Malek (1978, 1981) presented an attractive, exact and efficient approach to network analysis for cascaded structures using the concept of forward and reverse analysis. The fundamental assumption is that the transmission matrices for the individual components of the network and their sensitivities with respect to possible variables inside them are available. Bandler et al. discussed the use of their approach in large-change sensitivity analysis, in analysis of simple branched circuits (branches in series or parallel) and in analysis of 2p-port cascaded networks.

In this section, we use some of the original ideas by Bandler et al. and further develop them to general branched cascaded networks with arbitrary junctions, in preparation for the analysis of multiplexer structures.

To fulfill the requirement of having transmission matrices and their sensitivities for individual components of the network, we refer to Section 3.2 and specifically the discussions on the unterminated two-port. We derived the two-port impedance matrix $\mathbf{z}$ and its first- and second-order sensitivities for a complicated subnetwork represented by an $n \times n$ admittance matrix. The transmission matrix and its sensitivities can be readily evaluated from $\mathbf{z}$ and its sensitivities. We have

$$\mathbf{A} = \begin{bmatrix} A & B \\ C & D \end{bmatrix} = \frac{1}{z_{21}} \begin{bmatrix} z_{11} & z_{11}z_{22} - z_{12}z_{21} \\ 1 & z_{22} \end{bmatrix} \tag{3.55}$$

and

$$\mathbf{A}_{\phi} = \frac{1}{(z_{21})^2} \begin{bmatrix} (z_{11})_{\phi} z_{21} - (z_{21})_{\phi} z_{11} & (z_{11})_{\phi} z_{22} z_{21} + (z_{22})_{\phi} z_{11} z_{21} - (z_{12})_{\phi} z_{21}^2 - (z_{21})_{\phi} z_{11} z_{22} \\ -(z_{21})_{\phi} & (z_{22})_{\phi} z_{21} - (z_{21})_{\phi} z_{22} \end{bmatrix} . \tag{3.56}$$

In considering the cascaded structures, the network is divided into subnetworks by reference planes. We define the equivalent transmission matrix between reference planes i and j by

$$\mathbf{Q}_{ij} \triangleq [\mathbf{r}_{ij} \ \mathbf{s}_{ij}] \triangleq \begin{bmatrix} A_{ij} & B_{ij} \\ C_{ij} & D_{ij} \end{bmatrix} , \tag{3.57}$$

where

$$\mathbf{r}_{ij} \triangleq \begin{bmatrix} A_{ij} \\ C_{ij} \end{bmatrix} , \quad \mathbf{s}_{ij} \triangleq \begin{bmatrix} B_{ij} \\ D_{ij} \end{bmatrix} . \tag{3.58}$$

In a forward (reverse) analysis, $\mathbf{Q}_{ij}$ is computed by initializing row vectors $\mathbf{e}_1^T$ and $\mathbf{e}_2^T$ (column vectors $\mathbf{e}_1$ and $\mathbf{e}_2$) at reference plane i(j) and successively premultiplying (postmultiplying) each transmission matrix by the resulting row (column) vector until reference plane j(i) is reached. $\mathbf{e}_1$ and $\mathbf{e}_2$ are unit vectors given by $[1 \ \ 0]^T$ and $[0 \ \ 1]^T$, respectively.

Sensitivities of $\mathbf{Q}_{ij}$ with respect to any variable ϕ located between reference planes i and j are evaluated as

$$\frac{\partial \mathbf{Q}_{ij}}{\partial \phi} = \begin{bmatrix} (A_{ij})_{\phi} & (B_{ij})_{\phi} \\ (C_{ij})_{\phi} & (D_{ij})_{\phi} \end{bmatrix} = \sum_{\ell \in I_{\phi}} \frac{\partial}{\partial \phi} (\mathbf{Q}_{ij}^{\ell}) , \tag{3.59}$$

where I_{ϕ} is an index set whose elements identify the transmission matrices containing ϕ and $\partial \mathbf{Q}_{ij}^{\ell} / \partial \phi$ is the result of a forward or reverse analysis between reference planes i and j with the ℓth matrix replaced by its derivative with respect to ϕ. Second-order sensitivities can be derived in a similar manner as

$$\frac{\partial^2 \mathbf{Q}_{ij}}{\partial \phi \partial \omega} = \begin{bmatrix} (A_{ij})_{\phi\omega} & (B_{ij})_{\phi\omega} \\ (C_{ij})_{\phi\omega} & (D_{ij})_{\phi\omega} \end{bmatrix} = \sum_{\ell \in I_{\phi}} \sum_{m \in I_{\omega}} \frac{\partial^2 \mathbf{Q}_{ij}^{\ell m}}{\partial \phi \, \partial \omega} , \tag{3.60}$$

where I_ϕ and I_ω are index sets, not necessarily disjoint, identifying those matrices which are functions of ϕ and ω. Also we defined $\partial^2 \mathbf{Q}_{ij}^{\ell m}/(\partial\phi\partial\omega)$ as the second-order sensitivity of $\mathbf{Q}_{ij}$ as if ϕ and ω exist only in the ℓth and mth matrices, respectively.

3.4.2 Thevenin and Norton Equivalent Circuits

Using the method of forward and reverse analysis, Thevenin or Norton equivalent circuits can be evaluated at the ports of interest. The equivalents are then readily employed to calculate the responses of interest. Consider the network shown in Fig. 3.2 where it is desired to evaluate the Thevenin equivalents in a forward analysis and Norton equivalents in a reverse analysis. Denoting the Thevenin equivalent voltages and impedances at reference points i and j by V_S^i, Z_S^i, V_S^j and Z_S^j, we have

$$V_S^j = \frac{V_S^i}{A_{ij} + Z_S^i C_{ij}} \tag{3.61}$$

and

$$Z_S^j = \frac{B_{ij} + Z_S^i D_{ij}}{A_{ij} + Z_S^i C_{ij}}, \tag{3.62}$$

where reference plane i is located towards the source with respect to j. The sensitivities are obtained as

$$(V_S^j)_\phi = \frac{(V_S^i)_\phi - [(A_{ij})_\phi + Z_S^i (C_{ij})_\phi + (Z_S^i)_\phi C_{ij}]\, V_S^j}{A_{ij} + Z_S^i C_{ij}} \tag{3.63}$$

and

$$(Z_S^j)_\phi = \frac{[1 \quad Z_S^i](\mathbf{Q}_{ij})_\phi \begin{bmatrix} -Z_S^j \\ 1 \end{bmatrix} + (Z_S^i)_\phi (D_{ij} - Z_S^j C_{ij})}{A_{ij} + Z_S^i C_{ij}}. \tag{3.64}$$

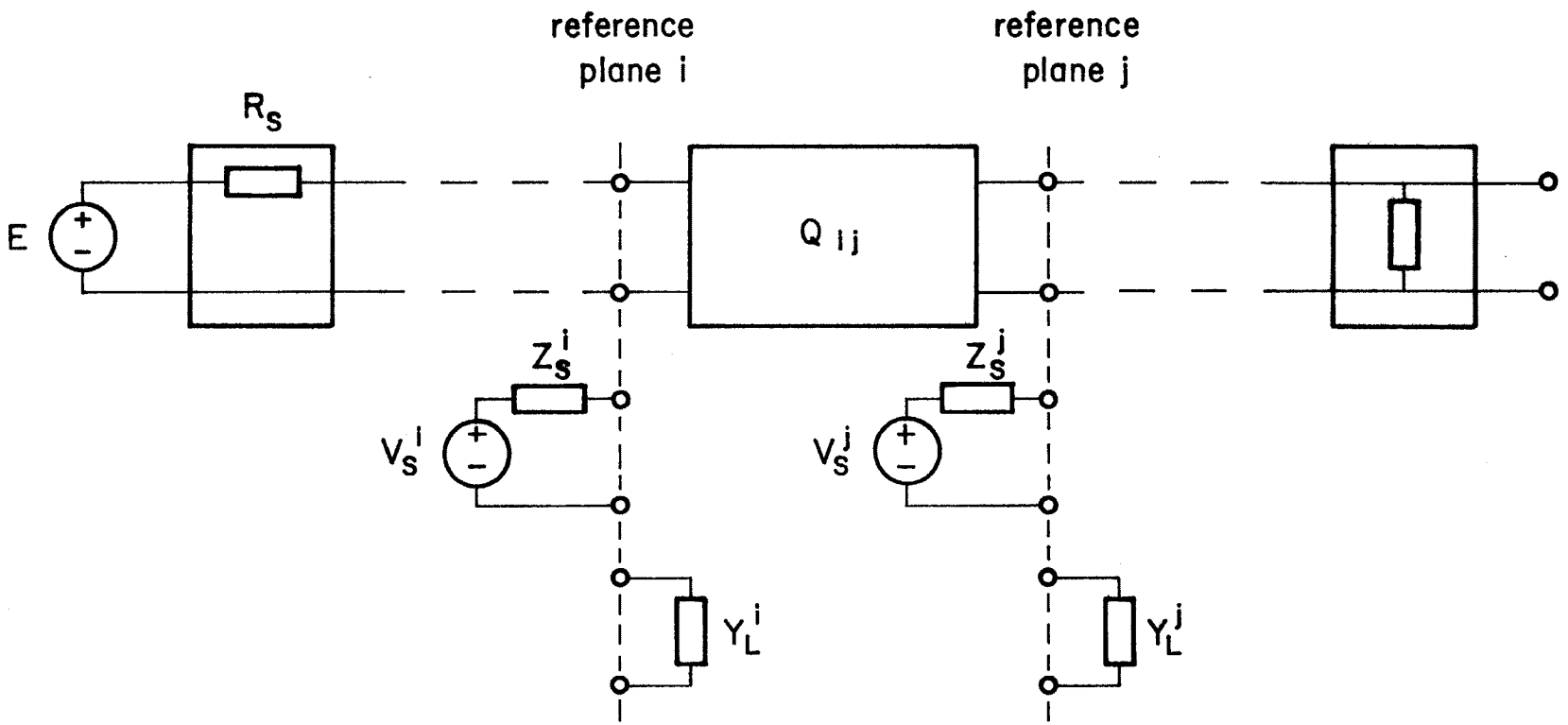

Fig. 3.2 Thevenin and Norton equivalents at reference planes i and j, where reference plane i is towards the source w.r.t. reference plane j.

Performing reverse analysis and denoting Norton equivalent currents and admittances at reference planes i and j by I_L^i, Y_L^i, I_L^j and Y_L^j, we have

$$Y_L^i = \frac{C_{ij} + Y_L^j D_{ij}}{A_{ij} + Y_L^j B_{ij}} \tag{3.65}$$

and

$$I_L^i = I_L^j = 0 . \tag{3.66}$$

Also,

$$(Y_L^i)_\Phi = \frac{[-Y_L^i \quad 1](\mathbf{Q}_{ij})_\Phi \begin{bmatrix} 1 \\ Y_L^j \end{bmatrix} + (Y_L^j)_\Phi (D_{ij} - Y_L^i B_{ij})}{A_{ij} + Y_L^j B_{ij}} . \tag{3.67}$$

The use of Thevenin and Norton equivalent circuits in evaluation of various frequency responses in branched cascaded networks will be described in Section 3.4.4.

3.4.3 Branched Cascaded Circuits

Simulation and sensitivity analysis of branched cascaded circuits using the method of forward and reverse analysis, which was considered briefly by Bandler et al. (1978), has become more important due to their application in multiplexing networks. Bandler, Daijavad and Zhang (1985a, 1985b, 1986) introduced a unified notation, considered arbitrary junctions and showed the effective use of the analysis in the design of multiplexers. The multiplexing networks will be described in more detail in Chapter 4. In this section, we consider general branched cascaded networks without describing details of subnetworks.

A branched cascaded structure is shown in Fig. 3.3. For such a structure, we want to calculate reflection coefficients at the common port and branch output

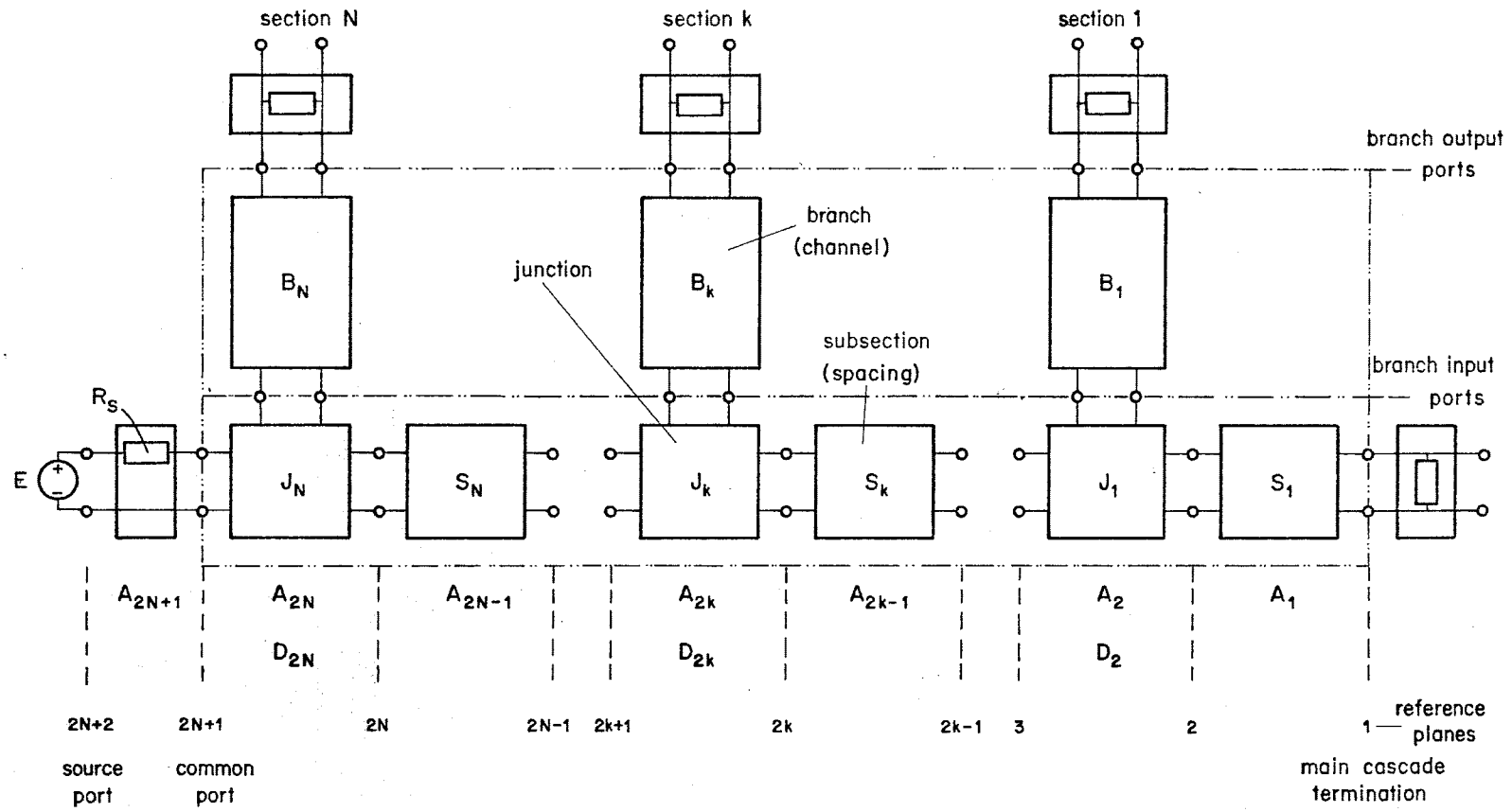

Fig. 3.3 The branched cascaded network under consideration. $J_1, J_2, ..., J_N$ are arbitrarily defined 3-port junctions. $B_1, B_2, ..., B_N$ are branches or channels which may each be represented in reduced cascade form and $S_1, S_2, ..., S_N$ represent the subsections between junctions. Principal concepts of reference planes, transmission matrices and typical ports are illustrated.

ports as well as branch output voltages. Simultaneously, first- and second-order derivatives are to be calculated.

The basic components of the structure are 2-port elements or 3-port junctions. The 2-ports, as has been mentioned before, may represent equivalents for complicated networks such as filters. For the 3-port junctions, a 3-port description in the form of an arbitrary hybrid matrix must be given. To simplify the structure to a cascade of 2-ports, the junctions are reduced to 2-port representations.

Consider the 3-port junction shown in Fig. 3.4. To carry the analysis through the junction along the main cascade, we terminate port 3, e.g., by calculating the equivalent admittance seen at this port given by $Y_3 = -I_3/V_3$ and represent the transmission matrix between ports 1 and 2 by **A**. The analysis can also be carried through the junction into the branch by terminating port 2, e.g., calculating $Y_2 = -I_2/V_2$ and denoting the transmission matrix between ports 1 and 3 by **D**.

As an example, suppose the 3-port junction is characterized by a hybrid matrix **H** such that

$$[V_1 \quad I_1 \quad I_3]^T = \mathbf{H}\,[V_2 \quad I_2 \quad V_3]^T, \tag{3.68}$$

where $\mathbf{H} = [h_{ij}]_{3x3}$. Then $\mathbf{A} = [a_{ij}]_{2x2}$ can be found from

$$a_{ij} = (-1)^{j-1}[h_{ij} - h_{i3}h_{3j}/(Y_3 + h_{33})]. \tag{3.69}$$

For various forms of hybrid matrices **H**, the 2-port representation **A** or **D** is evaluated in a similar manner using elements of **H** and the equivalent termination at port 3 or 2.

Having reduced the junctions to 2-port representations, the network structure is transformed to a simple cascade of two-ports. The reference planes in the entire network are defined uniformly and numbered consecutively beginning from the main cascade termination, which is designated reference plane 1. Refer to the

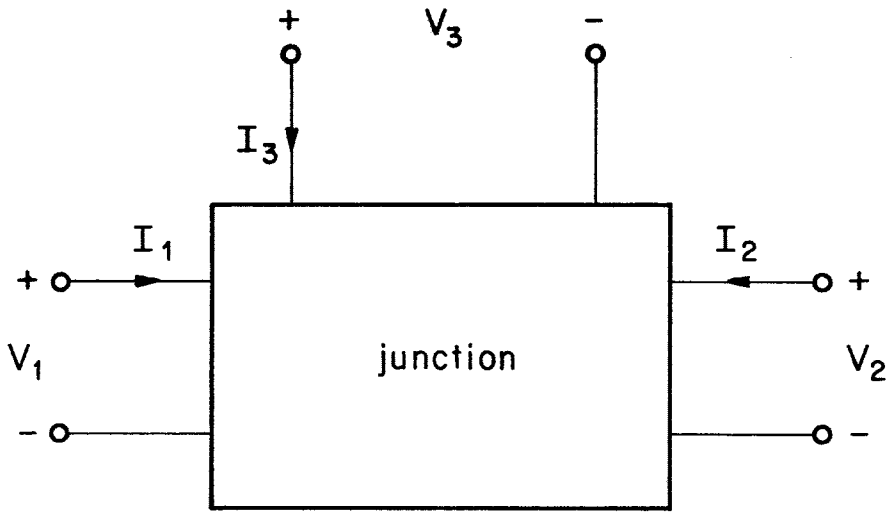

Fig. 3.4 A 3-port junction in which ports 1 and 2 are considered along a main cascade and port 3 represents a channel or branch of the main cascade.

network of Fig. 3.3 which consists of N sections. A typical section, e.g., the kth one, has a junction, n(k) cascaded elements of branch k, and a subsection along the main cascade, as shown in Fig. 3.5. Moving along the main cascade first, the source port is reference plane 2N+2. The termination of the kth branch is called reference plane $\tau(k)$ and the branch main cascade connection (branch input port) is reference plane $\sigma(k)$, k = 1,2,. . . ,N, where

$$\begin{aligned} &\tau(1) = 2N+3 \\ &\sigma(k) = \tau(k) + n(k), \quad k = 1, 2, ..., N \\ &\tau(k) = \sigma(k-1) + 1, \quad k = 2, 3, ..., N . \end{aligned} \tag{3.70}$$

3.4.4 Various Frequency Response and Sensitivity Formulas

Thevenin and Norton equivalents evaluated at reference planes of interest which were discussed for simple cascaded structures, are used for branched cascaded networks as well. By reduction of junctions to 2-ports along the main cascade, (terminating port 3 of the junction) we have a simple cascaded network as shown in Fig. 3.2. To evaluate branch output voltages, 3-port junctions are reduced to 2-ports by terminating their port 2. The result is again a simple cascaded structure as illustrated in Fig. 3.6.

Having numbered all reference planes, we use Norton equivalent admittances to evaluate admittances Y_3 and Y_2 required in reduction of junctions to 2-port representation. As special cases of (3.65), we have

$$Y_3^k = Y_L^{\sigma(k)} = \frac{C_{\sigma(k),\tau(k)}}{A_{\sigma(k),\tau(k)}}, \quad k = 1, 2, ..., N . \tag{3.71}$$

Since $Y_L{}^{\tau(k)} = 0$. To evaluate $Y_2{}^k$, main cascade termination must be given, e.g., for a short-circuit termination,

$$Y_2^k = Y_L^{2k} = \frac{D_{2k,1}}{B_{2k,1}}, \quad k = 1, 2, ..., N . \tag{3.72}$$

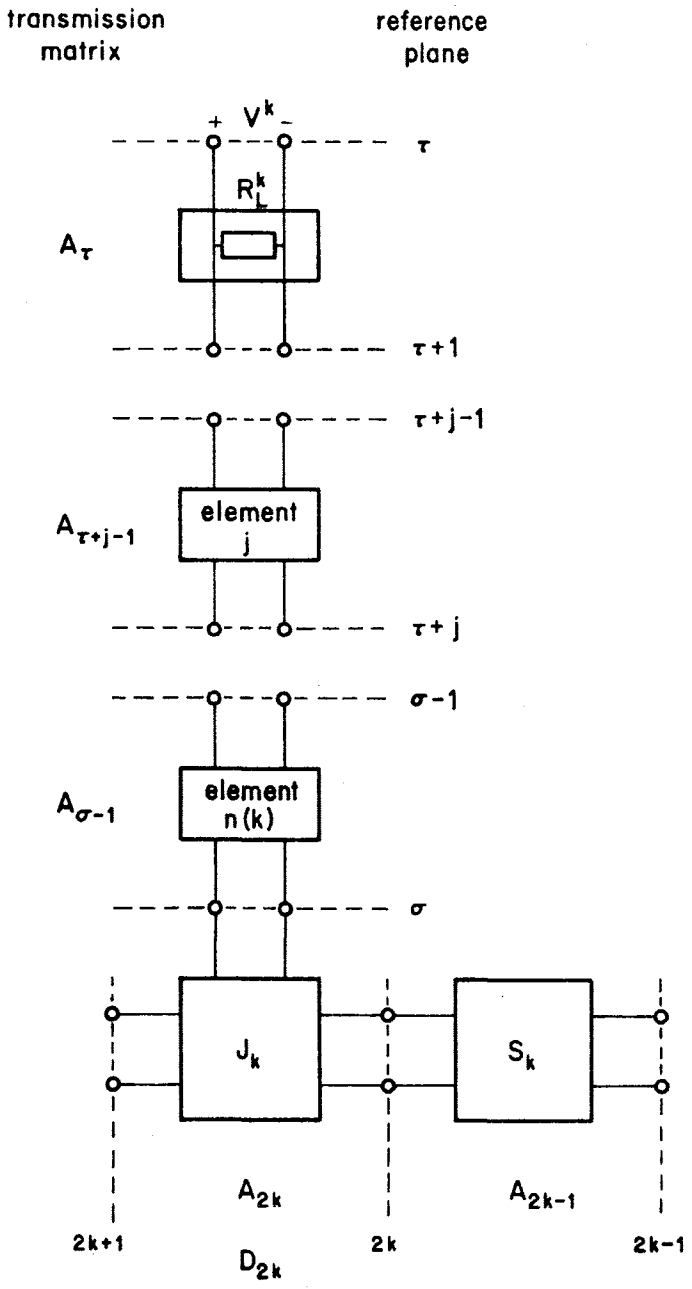

Fig. 3.5 Detail of the kth section of a branched cascaded circuit showing reference planes along the branch where $\tau = \tau(k)$ and $\sigma = \sigma(k)$.

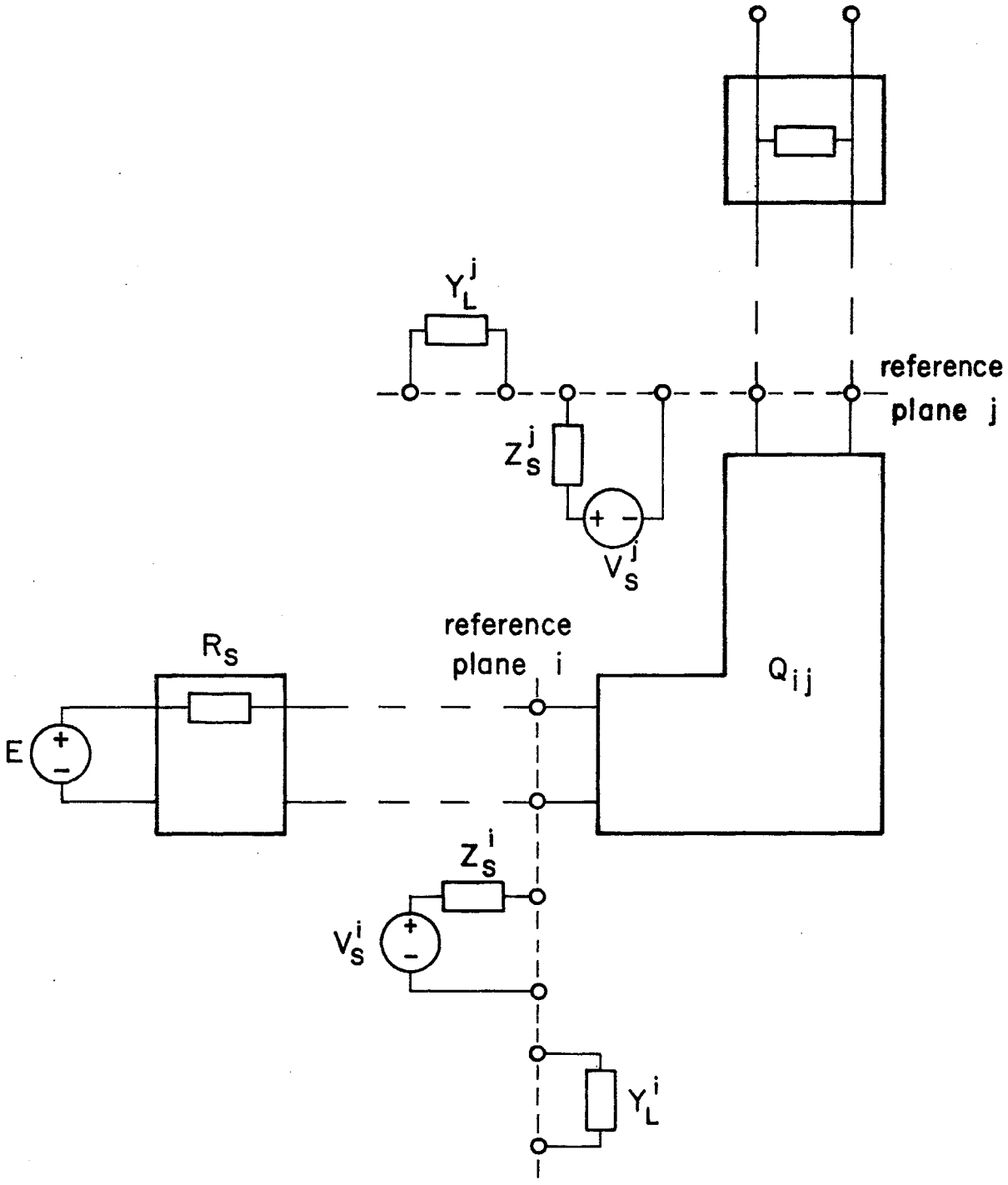

Fig. 3.6 Thevenin and Norton equivalents at reference planes i and j where reference plane j is in a branch. Q_{ij} is obtained by terminating port 2 of the junction.

since $Y_L^1 \to \infty$.

The common-port reflection coefficient is also computed using the Norton equivalent admittance (at the source reference plane) as

$$\begin{aligned} \rho^0 &= 1 - 2R_S\, Y_L^{2N+2} \\ &= 1 - \frac{2\,R_S\, D_{2N+2,1}}{B_{2N+2,1}}\,, \end{aligned} \tag{3.73}$$

again by assuming a short-circuit main cascade termination. Notice that $2N+2$ is the reference plane to the left of R_S, i.e., R_S has been taken into account in evaluation of Y_L^{2N+2}. The corresponding sensitivity formula is

$$(\rho^0)_\phi = 2\ R_S\ \frac{(B)_\phi D - (D)_\phi B}{B^2}\,, \tag{3.74}$$

where $B \equiv B_{2N+2,1}$ and $D \equiv D_{2N+2,1}$.

If the reflection coefficient at the kth branch output port is to be calculated, we use Thenevin equivalent impedance at reference plane $\tau+1$. In this case, (3.62) and (3.64) are specialized to

$$Z_S^{\tau+1} = \frac{B}{A} \tag{3.75}$$

and

$$(Z_S^{\tau+1})_\phi = \frac{(B)_\phi - (A)_\phi Z_S^{\tau+1}}{A}\,, \tag{3.76}$$

where $A \equiv A_{2N+2,\tau+1}$, $B \equiv B_{2N+2,\tau+1}$, and $\tau \equiv \tau(k)$. This is simply due to the fact that there is no impedance to the left of reference plane $2N+2$, i.e. $Z_S^{2N+2} = 0$. The corresponding output reflection coefficient is defined as

$$\rho^k \triangleq \frac{Z_S^{\tau+1} - R_L^k}{Z_S^{\tau+1} + R_L^k}\,, \tag{3.77}$$

where R_L^k is the load resistance at the kth channel output. Clearly, (3.76) is utilized in the evaluation of $(\rho^k)_\phi$ as

$$(\rho^k)_\phi = \frac{(Z_S^{\tau+1})_\phi\,(1-\rho^k)}{Z_S^{\tau+1}+R_L^k}\,. \tag{3.78}$$

The branch output voltage is also computed by utilizing the Thevenin equivalent voltage source and impedance at reference plane $\tau+1$. For the kth branch, we have

$$V^k = \frac{R_L^k}{A\,(R_L^k + Z_S^{\tau+1})}\,, \tag{3.79}$$

assuming a normalized excitation at the source port. This can be explained by noticing that V^k is evaluated using a voltage divider once $V_S{}^{\tau+1}$ is known. Using (3.61) and taking into account that $V_S{}^{2N+2} = 1$ and $Z_S{}^{2N+2} = 0$, we have $V_S{}^{\tau+1} = 1/A$. Also

$$(V^k)_\phi = -V^k\left[\frac{(A)_\phi}{A} + \frac{(Z_S^{\tau+1})_\phi}{R_L^k + Z_S^{\tau+1}}\right]. \tag{3.80}$$

The appropriate reference planes are as in the case of output reflection coefficient, i.e., $A \equiv A_{2N+2,\tau+1}$, $\tau \equiv \tau(k)$.

The second-order sensitivity of V^k with respect to ϕ and ω, i.e., $\partial^2 V_k/(\partial\phi\,\partial\omega)$, is obtained via evaluation of $\partial^2 Z_S{}^{\tau+1}/(\partial\phi\,\partial\omega)$. Substituting ω for ϕ in (3.76) and differentiating w.r.t. ϕ, gives

$$(Z_S^{\tau+1})_{\phi\omega} = \frac{(B)_{\phi\omega} - Z_S^{\tau+1}\,(A)_{\phi\omega} - (A)_\omega (Z_S^{\tau+1})_\phi - (Z_S^{\tau+1})_\omega\,(A)_\phi}{A}\,, \tag{3.81}$$

where double subscript $\phi\omega$ denotes $\partial^2/(\partial\phi\,\partial\omega)$.

Now replacing ϕ by ω in (3.80) and differentiating with respect to ϕ gives

$$(V^k)_{\phi\omega} = \frac{(V^k)_\phi (V^k)_\omega}{V^k} - V^k\left[\frac{A\,(A)_{\phi\omega} - A_\phi A_\omega}{A^2} + \frac{(Z_S^{\tau+1})_{\phi\omega}(R_L^k + Z_S^{\tau+1}) - (Z_S^{\tau+1})_\omega\,(Z_S^{\tau+1})_\phi}{(R_L^k + Z_S^{\tau+1})^2}\right]. \tag{3.82}$$

Using reflection coefficients at the common-port and branch output ports (ρ^0 and ρ^k), branch output voltages (V^k) and the first- and second-order sensitivities

$$\left(\frac{\partial \rho^0}{\partial \phi}, \frac{\partial \rho^k}{\partial \phi}, \frac{\partial V^k}{\partial \phi}, \frac{\partial V^k}{\partial \omega} \text{ and } \frac{\partial^2 V^k}{\partial \phi \, \partial \omega} \right)$$

we can tabulate some other frequency responses and their sensitivities. Table 3.3 summarizes some responses of interest and the corresponding sensitivities.

3.4.5 An Interesting Result in Sensitivity Evaluation of Branched Cascaded Networks

In reporting a novel approach for simulation and sensitivity analysis of multiplexers, Bandler, Daijavad and Zhang (1985a) presented an interesting result which can be applied to all branched cascaded networks. They proved that for a variable parameter at any part of the network, the sensitivities of insertion loss between source and a branch output port, for all branches located between the variable element and the main cascade termination, have identical values. They also introduced an elegant notation for treating terminations.

Consider the basic geometry of Fig. 3.7 in which a "channel" is equivalent to a branch. We have already discussed the reduction of 3-port junctions to 2-port equivalents. Denoting the vector containing voltage and current at an arbitrary reference plane x by $\mathbf{u}^x$, we have

$$\mathbf{u}^1 = \mathbf{A}\,\mathbf{u}^2 \tag{3.83}$$

or

$$\mathbf{u}^1 = \mathbf{D}\,\mathbf{u}^3, \tag{3.84}$$

where 1, 2 and 3 are the port reference planes for the junction (see Fig. 3.4) and **A** (**D**) is the appropriate transmission matrix. Evaluation of **A** (**D**), as discussed in section 3.4.3, requires the use of elements of the 3-port hybrid matrix **H** and

TABLE 3.3

VARIOUS FREQUENCY RESPONSES AND THEIR SENSITIVITIES

Response Type	Formula	Expression for Sensitivity w.r.t. ϕ
return loss (common port or channel output port)	$-20 \log_{10}\lvert\rho\rvert$	$\mathrm{cRe}\left[\frac{\rho_\phi}{\rho}\right]$
transducer loss †	$-10 \log_{10}\left(\frac{4\lvert V^k\rvert^2 R_S}{R_L^k}\right)$	$\mathrm{cRe}\left[\frac{(V^k)_\phi}{V^k}\right]$
insertion loss †	$-20 \log_{10}\left[\frac{\lvert V^k\rvert (R_S + R_L^k)}{R_L^k}\right]$	$\mathrm{cRe}\left[\frac{(V^k)_\phi}{V^k}\right]$
gain slope †	$\mathrm{cRe}\left[\frac{(V^k)_\omega}{V^k}\right]$	$\mathrm{cRe}\left[\frac{(V^k)_{\phi\omega}}{V^k} - \frac{(V^k)_\phi (V^k)_\omega}{(V^k)^2}\right]$
group delay †	$-\mathrm{Im}\left[\frac{(V^k)_\omega}{V^k}\right]$	$-\mathrm{Im}\left[\frac{(V^k)_{\phi\omega}}{V^k} - \frac{(V^k)_\phi (V^k)_\omega}{(V^k)^2}\right]$

$$c = -\frac{20}{\ell n\, 10}$$

† between common port and channel k output port

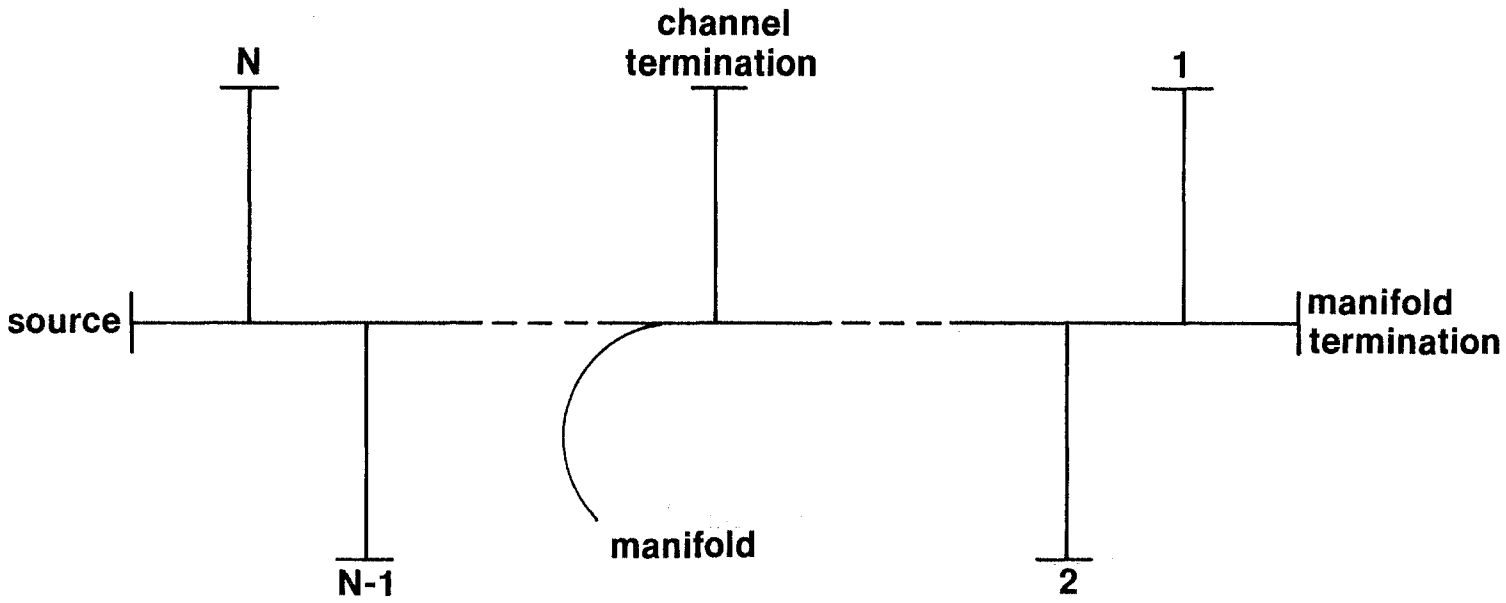

Fig. 3.7 The basic structure of an N-branched cascaded network.

equivalent termination at port 3(2). We also have

$$\boldsymbol{\alpha}^T \mathbf{u}^2 = \boldsymbol{\beta}^T \mathbf{u}^3 , \tag{3.85}$$

where $\boldsymbol{\alpha}$ and $\boldsymbol{\beta}$ are obtained from $\mathbf{H}$. For instance, for the hybrid description used in (3.68), we have

$$\boldsymbol{\alpha}^T = [-h_{31} \quad h_{32}] \tag{3.86}$$

and

$$\boldsymbol{\beta}^T = [h_{33} \quad 1] . \tag{3.87}$$

Terminations for the structure are treated in a unified manner. If t denotes a terminating reference plane (in Fig. 3.3, t could be reference plane 1, reference plane $2N+2$ or any of the branch terminations $\tau(k)$) we have

$$(\boldsymbol{\mu}^t)^T \mathbf{u}^t = c^t . \tag{3.88}$$

For example, for a short-circuit termination, a terminating load of impedance Z and a terminating voltage source E, we have $\boldsymbol{\mu} = [1 \quad 0]^T$, $c = 0$, $\boldsymbol{\mu} = [1 \quad -Z]^T$, $c = 0$ and $\boldsymbol{\mu} = [1 \quad 0]^T$, $c = E$, respectively. A termination can be transferred from one reference plane to another if the transmission matrix between the two planes is known. For instance, from $\mathbf{u}^{t_1} = \mathbf{Q}_{t_1 t_2} \mathbf{u}^{t_2}$, it is easily shown that $\boldsymbol{\mu}^{t_2}$ and c^{t_2} in $(\boldsymbol{\mu}^{t_2})^T \mathbf{u}^{t_2} = c^{t_2}$ are evaluated from

$$(\boldsymbol{\mu}^{t_2})^T = (\boldsymbol{\mu}^{t_1})^T \mathbf{Q}_{t_1 t_2} , \quad c^{t_2} = c^{t_1} , \tag{3.89}$$

where $\mathbf{Q}_{t_1 t_2}$ is the equivalent transmission matrix between planes t_1 and t_2. The concept of transferring Thevenin and Norton equivalents from one reference plane to another which was discussed before is a specialized variation of the above termination transfer.

Assuming that the branch output port at, say, reference plane τ is of interest, the structure is simplified as shown in Fig 3.8. In Fig. 3.8, $\mathbf{Q}_{x1}$ and $\mathbf{Q}_{sy}$ are the equivalent transmission matrices between the appropriate planes. Their evaluation involves the calculation of equivalent terminations looking into the

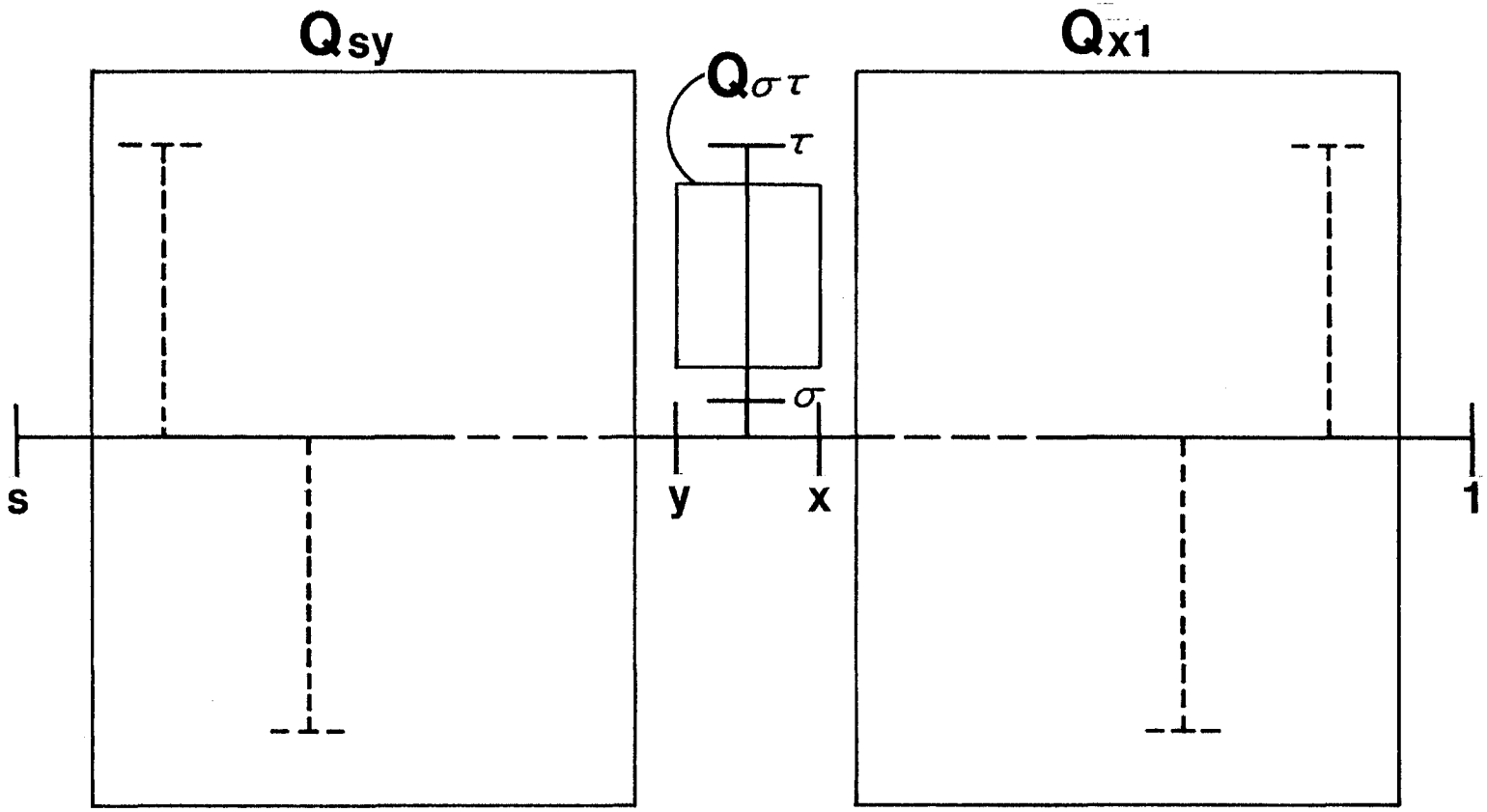

Fig. 3.8 The simplified structure of the branched cascaded network when branch output port τ is of interest.

branch from the main cascade, i.e., transferring branch output port terminating relationships to the junction and then reducing the three-port junction to two ports. By invoking (3.85) at the junction in Fig. 3.8, we get

$$\boldsymbol{\alpha}^T \mathbf{Q}_{x1}\, \mathbf{u}^1 = \boldsymbol{\beta}^T \mathbf{Q}_{\sigma\tau}\, \mathbf{u}^\tau . \tag{3.90}$$

Also, we have

$$\mathbf{u}^s = \mathbf{Q}_{s1}\, \mathbf{u}^1 \tag{3.91}$$

where $\mathbf{Q}_{s1}$ represents the equivalent transmission matrix of the whole structure between main cascade source and load terminations. To evaluate $\mathbf{u}^1$, $\mathbf{u}^\tau$ and $\mathbf{u}^s$ (6 unknowns) we use (3.90) and (3.91) (3 equations, noting that (3.91) yields two relationships) and three terminating conditions at reference planes 1, τ and s.

Consider an open-circuit termination at reference plane τ, e.g., by taking a nonzero load impedance as part of $\mathbf{Q}_{\sigma\tau}$. Also assume a load impedance Z for the main cascade and a voltage source E. We have $\mathbf{u}^1 = I^1[Z \;\; 1]^T$, $\mathbf{u}^\tau = [V^\tau \;\; 0]^T$ and $\mathbf{u}^s = [E \;\; I^s]^T$. Substituting the terminating conditions in (3.90), we get

$$\boldsymbol{\alpha}^T \mathbf{Q}_{x1}\, I^1 \begin{bmatrix} Z \\ 1 \end{bmatrix} = \boldsymbol{\beta}^T \mathbf{Q}_{\sigma\tau}\, \mathbf{e}_1\, V^\tau , \tag{3.92}$$

where $\mathbf{e}_1$ is the voltage selector vector $[1 \;\; 0]^T$. Combining (3.91) with the terminating condition at s gives

$$E = \mathbf{e}_1^T \mathbf{Q}_{s1}\, I^1 \begin{bmatrix} Z \\ 1 \end{bmatrix} . \tag{3.93}$$

Finally, eliminating I^1 between (3.92) and (3.93) results in the branch output voltage as

$$V^\tau = \frac{\boldsymbol{\alpha}^T \mathbf{Q}_{x1} \begin{bmatrix} Z \\ 1 \end{bmatrix} E}{(\boldsymbol{\beta}^T \mathbf{Q}_{\sigma\tau}\, \mathbf{e}_1)(\mathbf{e}_1^T \mathbf{Q}_{s1} \begin{bmatrix} Z \\ 1 \end{bmatrix})} . \tag{3.94}$$

For a short-circuit termination of the main cascade, $[Z \;\; 1]^T$ is simply replaced by $\mathbf{e}_2 = [0 \;\; 1]^T$ in (3.94), since $Z = 0$. On the other hand, for an open- circuit termination, we replace $[Z \;\; 1]^T$ by $\mathbf{e}_1$. (notice that $[Z \;\; 1]^T = Z[1 \;\; (1/Z)]^T$ and $Z \to \infty$ for the open-circuit).

Evalution of the branch output voltage and the corresponding insertion loss using (3.94) is an alternative method to what was described in Section 3.4.4. Using (3.94) we can also show an interesting property for the insertion loss sensitivities. From Table 3.3 we know that the sensitivity of insertion loss between the source and the branch output port τ is directly proportional to $(V^\tau)_\phi \,/V^\tau$. Now, for a variable ϕ located between the branch considered and the source (i.e., inside $\mathbf{Q}_{sy}$), $\mathbf{Q}_{x1}$ and $\mathbf{Q}_{\sigma\tau}$ are independent of ϕ. Applying the mathematical property

$$x = \frac{a}{bc} \to \frac{1}{x}\frac{\partial x}{\partial \phi} = -\frac{1}{c}\frac{\partial c}{\partial \phi}$$

if a and b are independent of ϕ, and using (3.94), we have

$$\frac{(V^\tau)_\phi}{V^\tau} = -\frac{\mathbf{e}_1^T(\mathbf{Q}_{s1})_\phi \begin{bmatrix} Z \\ 1 \end{bmatrix}}{\mathbf{e}_1^T \mathbf{Q}_{s1} \begin{bmatrix} Z \\ 1 \end{bmatrix}} . \tag{3.95}$$

It is clear that $\mathbf{Q}_{s1}$ and $(\mathbf{Q}_{s1})_\phi$ are independent of τ, i.e., for all other branches to the right of the branch considered, the insertion loss sensitivity w.r.t. the same ϕ, has the same value. An example clarifies the result of the above argument. For a variable in section N of the structure, the insertion loss (between source and branch output port) for branches $N-1, N-2, \cdots, 1$ have identical sensitivities. Similarly, for a variable in section $N-1$, the insertion loss sensitivities corredponding to branches $N-2, \cdots, 1$ are identical.

The result reported in this section leads to considerable computational saving in evaluation of insertion loss sensitivities for branched cascaded networks.

3.5 CONCLUDING REMARKS

In this chapter we used simple algebraic manipulation of vectors and matrices to develop a unified approach for sensitivity analysis of a general class of networks, namely, the branched cascaded structures. We provided a general scheme and useful formulas to evaluate the unterminated two-port equivalents and their first- and second- order sensitivities for complicated subnetworks. This allows us to conduct the sensitivity analysis of subnetworks inside a cascaded structure in an independent fashion. Once the transmission matrices of all subnetworks and their derivatives w.r.t. possible variables in them are evaluated, an organized and elegant method is used to perform simulation and sensitivity analysis of large branched cascaded structures.

Our method of dealing with the sensitivities is straightforward, since the use of the adjoint network concept has been avoided. The method is applicable to almost any complex linear circuit structure in the frequency domain.

We provided the proof for a recent and general sensitivity formula for lossless reciprocal 2-ports and derived an interesting result for insertion loss sensitivities in branched cascaded structures.

The importance of efficient sensitivity analysis becomes evident when the performance of modern gradient-based optimization algorithms are compared with the slow non-gradient older methods.

4

DESIGN OF MULTIPLEXING NETWORKS

4.1 INTRODUCTION

The design of contiguous band multiplexers consisting of multi-coupled cavity filters distributed along a waveguide manifold was a problem of significant theoretical interest for several years (Atia 1974; M.H. Chen, Assal and Mahle 1976), however, the manufacturing of such structures with more than five channels did not appear to be feasible. Recently, the subject has turned into an important development area in microwave engineering practice due to reports by leading manufacturers of successful production of 12-channel contiguous band multiplexers for satellite applications. The works by Tong et al. (1982,1984) of ComDev, M.H. Chen (1983, 1985) of TRW, Egri, Williams and Atia (1983) of COMSAT, Holme (1984) of Ford Aerospace, and Nomoto (1984) of NHK (Japan) can be referred to. The employment of optimization techniques to determine the best multiplexer parameters has been an indispensable part of the design procedures reported. The use of a powerful gradient-based minimax optimization technique (Bandler, Chen, Daijavad and Kellermann 1984; Bandler, Kellermann and Madsen 1985a; Bandler, Daijavad and Zhang 1986) has reduced significantly the CPU time required in the design procedure.

Among the many types of contiguous band waveguide multiplexers, we only consider the manifold type in this thesis. M.H. Chen (1985) has discussed the advantages of this kind of multiplexer compared to the older types such as common junction multiplexers or circulator coupled structures. Only the manifold type can provide a large number of channels without performance degradation. The equi-

valent network model of a manifold type multiplexer falls into the category of branched cascaded structures.

Evaluation of the exact sensitivities for the mulitplexer structure is based on the sensitivity analysis of individual filters using the methods described for 2-ports in Chapter 3 and an application of the branched cascaded network sensitivity analysis, also covered in Chapter 3.

In this chapter we describe details of a multiplexer structure, i.e., the subnetworks involved. We discuss models for filters, junctions and possible nonideal effects. A minimax formulation of possible optimization problems is presented and a particular implementation is described in detail. Finally, specific multiplexer design examples are solved which effectively demonstrate the efficiency of the method of analysis and the optimization procedure, reflected in the low CPU times required.

4.2 BASIC COMPONENTS OF A MULTIPLEXER STRUCTURE

4.2.1 The Overall Configuration

The structure used for a multiplexer throughout this chapter can be utilized in both contiguous and noncontiguous band multiplexer designs depending on the way in which performance specifications are defined. The possible equivalent circuit of a multiplexer is illustrated in Fig. 4.1. This is a specialization of the general branched cascaded network of Fig. 3.3, hence the sensitivity analysis and formulas in Chapter 3 are readily applicable. A branch (channel) consists of a coupled-cavity filter, together with input-output transformers, and an impedance inverter. A waveguide section separates two adjacent channels, and the junction is the equivalent circuit model for the physical junction between channel filters and the manifold. The main cascade is short-circuited and the responses of interest are common-port return

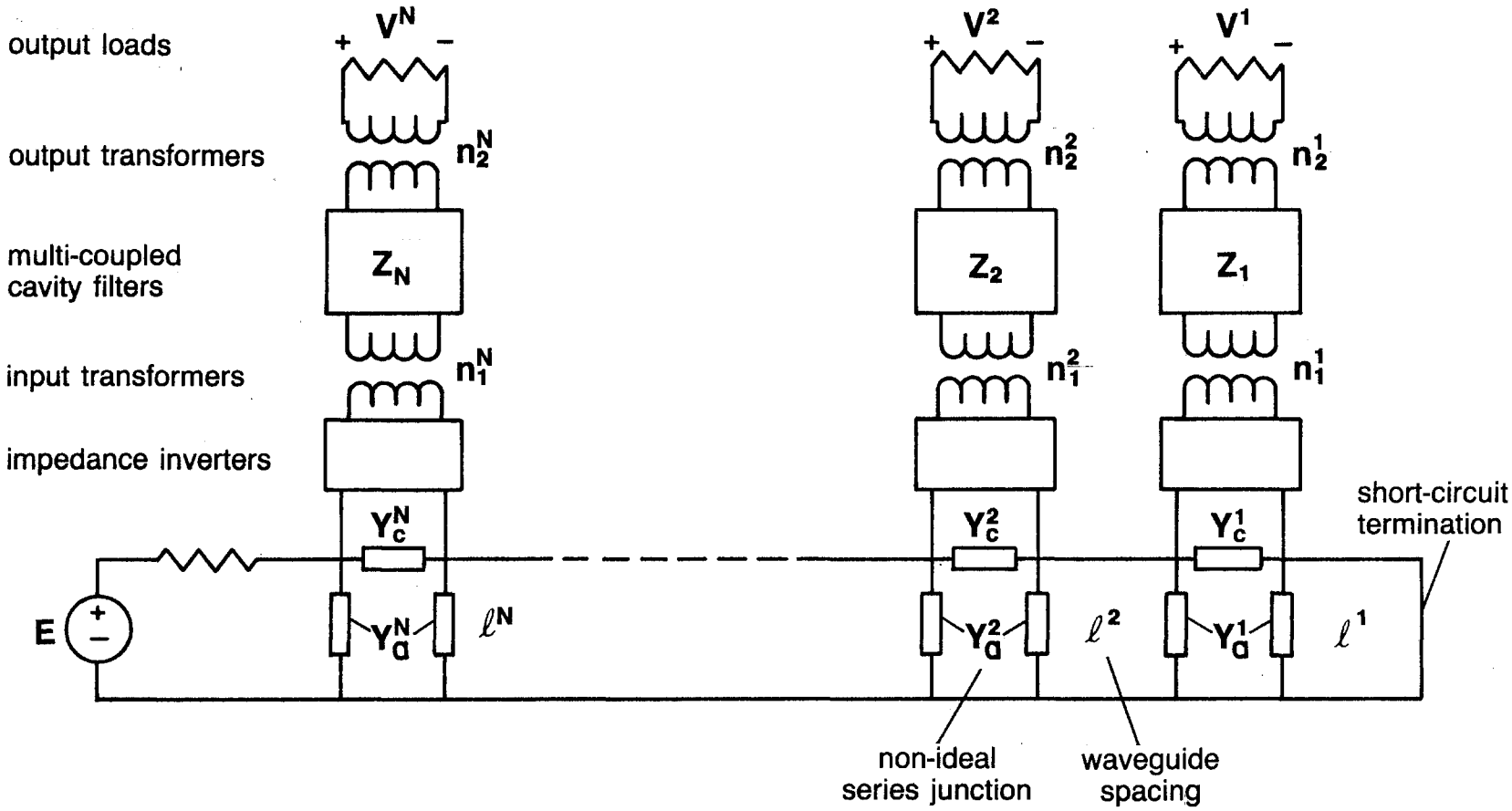

Fig. 4.1 Equivalent circuit of a contiguous band multiplexer. Each channel has a multi-coupled cavity filter with input and output transformers as well as an impedance inverter. The main cascade is a waveguide manifold with a short-circuit termination. Branches are connected to the main cascade through nonideal series junctions.

loss, channel output return loss, insertion loss, gain-slope and group delay between common-port and channel output ports.

A typical optimization problem could be finding parameters for which common-port return loss and individual channel insertion losses satisfy the specifications shown in Fig. 4.2 (3-channel multiplexer).

To apply the general method of Chapter 3 for simulation and sensitivity analysis, the subnetworks, namely, channel filters, waveguide spacings, and junctions must be represented by 2-port transmission matrices. We deal with subnetworks in the following sections.

4.2.2 Multi-Coupled Cavity Filters

The application of multi-coupled cavity microwave filters in modern communication systems has received increasing attention since the early 70's. Williams (1970) of COMSAT constructed a fourth-order elliptic function filter, in which two circular waveguide cavities, each excited by two orthogonal TE_{111} modes, were coupled together by a cross slot. Atia and Williams (1971,1972) introduced the theory of narrowband coupled cavities and described a synthesis procedure. More recent advances have been reported by Cameron (1982) and Kudsia (1982). Typical structures for longitudinal dual-mode cavity filters are illustrated in Fig. 4.3.

In recent years, the growing variety and complexity of the design and manufacture of these filters has necessitated the employment of modern computer-aided design techniques. The traditional approach to an analytical solution becomes cumbersome or inappropriate when asynchronous tuning realizing asymmetric characteristics of nonminimum phase designs necessary to meet tight amplitude and delay specifications are of interest. To facilitate the CAD approach, Bandler, Chen

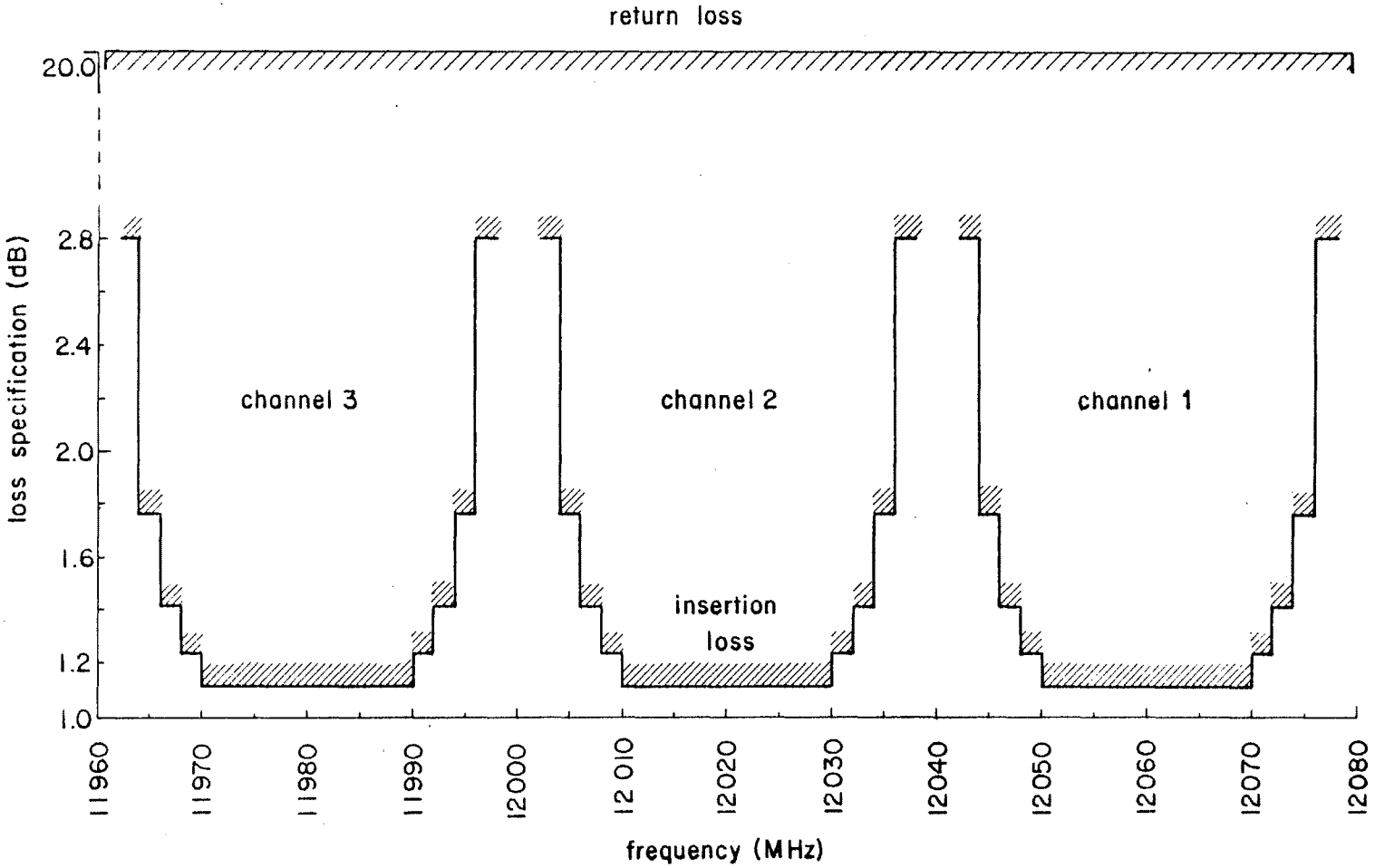

Fig. 4.2 Illustration of specifications for a 3-channel multiplexer.

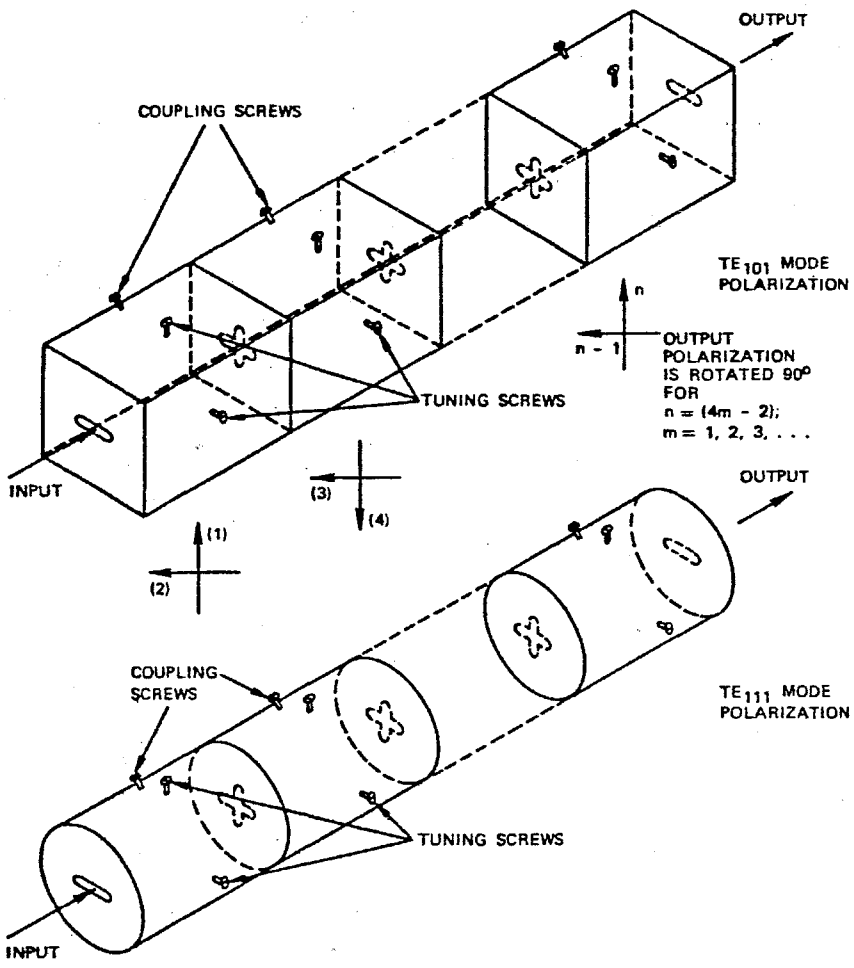

Fig. 4.3 Typical structures for longitudinal dual-mode cavity filters. (Reproduced from Atia and Williams 1971).

Daijavad (1986a) described a systematic and efficient approach to the simulation and exact sensitivity evaluation of narrowband multi-coupled cavity filters. The approach is based on the reduction of a network described by its impedance matrix to a 2-port model.

In Chapter 3, where 2-ports were considered in detail, we emphasized that starting with the impedance matrix instead of the admittance matrix description leads to dual formulas. Working with the impedance matrix, we first obtain the 2-port short-circuit admittance matrix and then calculate the transmission matrix required in the cascaded analysis. In this chapter we describe the impedance matrix model and refer to Chapter 3 or the work by Bandler, Chen and Daijavad (1986a) for reduction to 2-ports as well as sensitivity analysis.

The symmetrical impedance matrix for a narrowband lumped model of an unterminated filter is given by

$$\mathbf{Z} = j(s\mathbf{1} + \mathbf{M}) + r\mathbf{1} \tag{4.1}$$

where 1 denotes an $n \times n$ identity matrix and s is the normalized frequency variable given by

$$s \triangleq \frac{\omega_0}{\Delta\omega}\left(\frac{\omega}{\omega_0} - \frac{\omega_0}{\omega}\right) = \frac{f_0}{\Delta f}\left(\frac{f}{f_0} - \frac{f_0}{f}\right), \tag{4.2}$$

$\omega_0(f_0)$ and $\Delta\omega(\Delta f)$ being the synchronously tuned cavity resonant frequency and the bandwidth parameter, respectively. Notice that we could use either frequency or angular frequency because of the normalization. We assume uniform dissipation for all cavities indicated by parameter r where

$$r = \frac{\omega_0}{\Delta\omega\, Q_f}, \tag{4.3}$$

Q_f representing the unloaded Q-factor. In (4.1), **M** is the coupling matrix whose (a,b) element represents the normalized coupling between the ath and bth cavities, as

illustrated in Fig. 4.4, and the diagonal entries M_{aa} represent the deviations from synchronous tuning. Element M_{ab} does not necessarily correspond to a desirable and designable coupling. It may as well represent a stray coupling which is excluded from the nominal electrical equivalent circuit. Dispersion effects on the filter are modelled by both waveguide dispersion and dispersion effects on couplings, the latter causing a frequency dependent **M** matrix. We now describe the dispersion effects in detail to complete the discussion on multi- coupled cavity filters.

Assume circular cavities for the filters with the diameter d. For a TE_{11} mode (the dominant mode in circular waveguides), the cut-off wavelength is 1.706d (or 3.41r, for a radius r). The filter cut-off frequency is then calculated as

$$f_c^F = \frac{v_0}{1.706\,d}\,, \tag{4.4}$$

where v_0 is the velocity of light in free space. Superscript F is used to distinguish the filter cut-off frequency from the cut-off frequency for the waveguide manifold in the multiplexer structure. At an operating frequency f, the guide wavelength for the filter is calculated as

$$\lambda_g^F = \frac{v_0}{\sqrt{f^2 - (f_c^F)^2}}\,. \tag{4.5}$$

Similarly, the guide wavelengths corresponding to the band edges of the filter are obtained as

$$\lambda_{g\ell} = \frac{v_0}{\sqrt{(f_\ell)^2 - (f_c^F)^2}} \tag{4.6a}$$

and

$$\lambda_{gh} = \frac{v_0}{\sqrt{(f_h)^2 - (f_c^F)^2}}\,, \tag{4.6b}$$

where

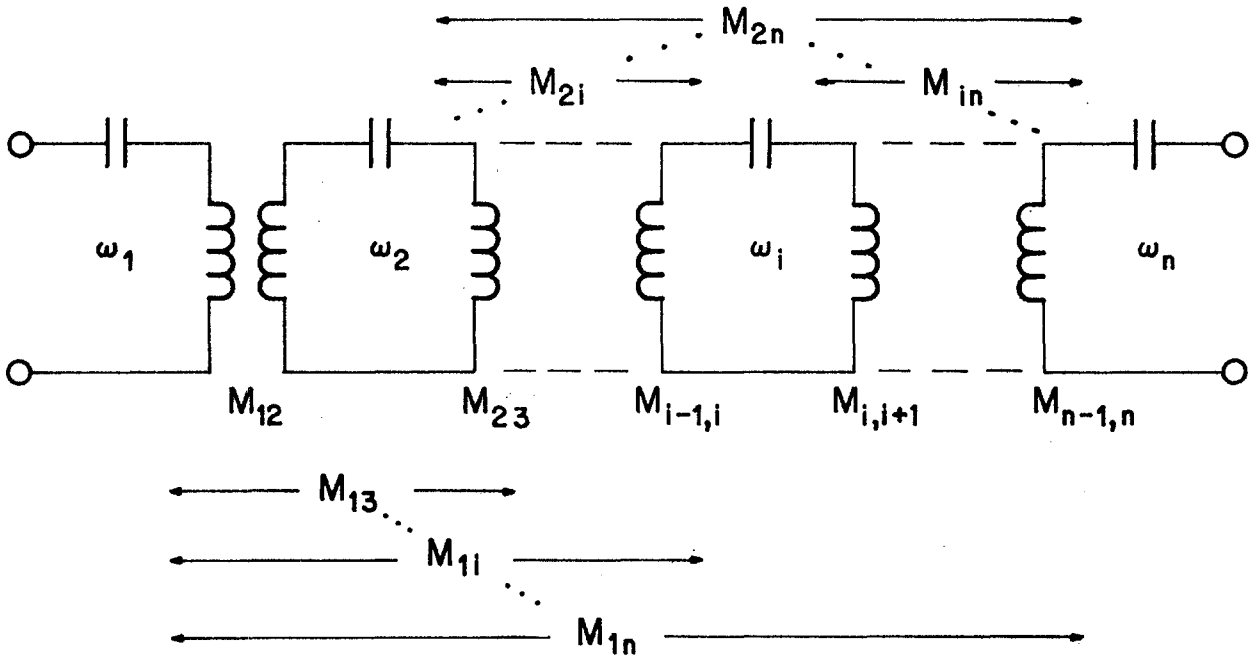

Fig. 4.4 Unterminated coupled-cavity filter illustrating the coupling coefficients.

$$f_\ell = f_0 - \frac{\Delta f}{2} \tag{4.7a}$$

and

$$f_h = f_0 + \frac{\Delta f}{2} . \tag{4.7b}$$

The guide wavelength corresponding to the filter resonant frequency is defined as

$$\lambda_{g0} \triangleq (\lambda_{gh} + \lambda_{g\ell})/2 \tag{4.8}$$

and corresponding to the bandwidth parameter, we have

$$\Delta\lambda_g \triangleq \lambda_{g\ell} - \lambda_{gh} . \tag{4.9}$$

The impedance matrix **Z** is now defined as

$$\mathbf{Z} = j(\lambda_n \mathbf{1} + \mathbf{M}) + r\mathbf{1} \tag{4.10}$$

where λ_n is the normalized wavelength parameter given by

$$\lambda_n = \frac{2(\lambda_{g0} - \lambda_g^F)}{\Delta\lambda_g} . \tag{4.11}$$

Notice the analogy between this case and the nondispersive model, where for narrowband applications, the approximate equivalence

$$s = \frac{\omega_0}{\Delta\omega}\left(\frac{\omega}{\omega_0} - \frac{\omega_0}{\omega}\right) \simeq \frac{2(\omega - \omega_0)}{\Delta\omega} \tag{4.12}$$

is often conveniently used. Compare (4.1) with (4.10) and (4.11) with (4.12).

So far, the waveguide dispersion effects have been included based on classical textbook material (see, for example, Matthaei, Young and Jones, 1964). Dispersion effects on the coupling matrix are now considered. An element of the coupling matrix, namely M_{ab}, is modified as (ComDev, 1983)

$$M_{ab} \leftarrow M_{ab}\left(\frac{\lambda_g^F}{\lambda_{g0}}\right)^{K_{ab}} , \tag{4.13}$$

where

$$K_{ab} = \begin{cases} 1, & \text{if } M_{ab} \text{ is screw coupled,} \\ -1, & \text{if } M_{ab} \text{ is iris coupled,} \\ 0, & \text{if } a = b. \end{cases} \tag{4.14}$$

This concludes the formulation of the impedance matrix for the network equivalent of a lossy and dispersive multi-coupled cavity filter. Given **Z**, the 2-port short-circuit admittance matrix **y** of the network equivalent for the filter, using a similar approach as in Chapter 3, is evaluated as

$$\mathbf{y} = \begin{bmatrix} y_{11} & y_{12} \\ y_{21} & y_{22} \end{bmatrix} = \begin{bmatrix} p_1 & q_1 \\ q_1 & q_n \end{bmatrix}, \tag{4.15}$$

where p_1, q_1 and q_n are elements of vectors **p** and **q** obtained from solving

$$\mathbf{Z}\,\mathbf{p} = \mathbf{e}_1 \tag{4.16a}$$

and

$$\mathbf{Z}\,\mathbf{q} = \mathbf{e}_n . \tag{4.16b}$$

Since matrix **Z** is symmetrical, **p** and **q** also provide complete information for evaluation of first-order sensitivities. Recall that for a general **Z** matrix, similar to a general **Y** matrix, 4 systems of equations are to be solved (refer to Section 3.2.1).

Given the **y** matrix, the transmission matrix for the filter 2-port equivalent, which is required in the cascaded analysis, is evaluated as

$$\mathbf{A} = \begin{bmatrix} A & B \\ C & D \end{bmatrix} = \frac{-1}{y_{21}} \begin{bmatrix} y_{22} & 1 \\ y_{11}y_{22} - y_{12}y_{21} & y_{11} \end{bmatrix} = \frac{-1}{q_1} \begin{bmatrix} q_n & 1 \\ p_1 q_n - q_1^2 & p_1 \end{bmatrix}. \tag{4.17}$$

4.2.3 Waveguide Manifold

In a rectangular waveguide, for a TE_{10} mode (the dominant mode) the cut-off wavelength is 2a, where a is the manifold width. The cut-off frequency is then calculated as

$$f_c = \frac{v_0}{2a}, \tag{4.18}$$

where, as in Section 4.2.2, v_0 denotes the velocity of light in free space. The guide wavelength, at an operating frequency f, is calculated as

$$\lambda_g = \frac{v_0}{\sqrt{f^2 - f_c^2}} \tag{4.19}$$

and the phase constant β is given by

$$\beta = \frac{2\pi}{\lambda_g} . \tag{4.20}$$

For a waveguide section with a characteristic impedance Z_0 and length ℓ, the transmission matrix is given by

$$\mathbf{A} = \begin{bmatrix} \cos\theta & jZ_0 \sin\theta \\ \dfrac{j \sin\theta}{Z_0} & \cos\theta \end{bmatrix} , \tag{4.21}$$

where

$$\theta = \beta\ell . \tag{4.22}$$

4.2.4 Junctions

Consider the network equivalent model of the physical junction between channel filters and the waveguide manifold, as illustrated in Fig. 4.1. A series admittance Y_c and two equal shunt admittances Y_a constitute the junction model. Recalling the discussions in Section 3.4.3 on the reduction of general 3-port junctions (Fig. 3.4) to 2-ports with the terminating port given, the transmission matrix for the junction is evaluated as

$$\mathbf{A} = \frac{1}{Y} \begin{bmatrix} Y + Y_a & 1 \\ 2Y_a Y + Y_a^2 & Y + Y_a \end{bmatrix} , \tag{4.23}$$

where $Y = Y_c + Y_3$, and port 3 is terminated by Y_3. Similarly, we have

$$\mathbf{D} = \frac{1}{Y} \begin{bmatrix} Y + Y_c & 1 \\ Y(Y_a + Y_c) + Y_a Y_c & Y + Y_a \end{bmatrix} , \tag{4.24}$$

where $Y = Y_a + Y_2$, and port 2 is terminated by Y_2. In either case, the junction model is complete when Y_a and Y_c are given.

By considering the equivalent circuit for a T-junction that connects two rectangular waveguides through a slot in Marcuvitz (1951) and experimental results, M.H. Chen et al. (1976) suggested the following formulas

$$\frac{Y_c}{Y_0} = -jC_m \frac{f_c}{2\sqrt{f^2 - f_c^2}} \tag{4.25}$$

and

$$\frac{Y_a}{Y_0} = \frac{-jf_c}{[C_c(\frac{v_0}{f})^2 - 1]\sqrt{f^2 - f_c^2}}, \tag{4.26}$$

where $Y_0 = 1/Z_0$ is the inverse of the characteristic impedance, and f_c and v_0 are as defined in Section 4.2.3. Chen et al. (1976) recommended the values $C_c = 20$ and $C_m = -1.0$ based on their experiments. Note that $C_c = 20$ can be used when v_0/f is given in inches.

4.2.5 Input-Output Transformers, Impedance Inverters and Summarizing Tables

Referring to Fig. 4.1, input and output transformers and the impedance inverters are the only components of the multiplexer structure, which have not been discussed so far. The transmission matrix description of an $1:n_1$ input transformer, an $n_2:1$ output transformer and an impedance inverter are given by

$$\mathbf{A} = \begin{bmatrix} \frac{1}{n_1} & 0 \\ 0 & n_1 \end{bmatrix}, \tag{4.27}$$

$$\mathbf{A} = \begin{bmatrix} n_2 & 0 \\ 0 & \frac{1}{n_2} \end{bmatrix} \tag{4.28}$$

and

$$\mathbf{A} = \begin{bmatrix} 0 & j \\ j & 0 \end{bmatrix}, \tag{4.29}$$

respectively, using basic definitions.

Having described the individual components of the multiplexer structure, we summarize all the transmission matrices involved and their sensitivities with respect to relevant parameters and frequency in Tables 4.1 and 4.2. Recall from Chapter 3, that for a 3-port junction the transmission matrix is denoted by **A** or **D** depending on the terminating port. The branched cascaded analysis of Chapter 3 is now readily applicable.

4.3 MULTIPLEXER OPTIMIZATION

A wide range of possible multiplexer optimization problems can be formulated and solved by appropriately defining specifications on various frequency responses of interest. The branched cascaded analysis of Chapter 3 with or without exact sensitivities is used in conjunction with the original gradient-based minimax algorithm (Bandler, Chen, Daijavad and Kellermann 1984; Bandler, Kellermann and Madsen 1985a) or with the modified approximate gradient algorithm (Bandler, Chen, Daijavad and Madsen, 1986). All design parameters of interest, as related to the individual components of the multiplexer structure described in this chapter, can be directly optimized. For instance, based on specifications on the common port return loss and individual channel insertion losses, waveguide spacing, filter coupling parameters and input-output transformer ratios may be optimized.

TABLE 4.1

TRANSMISSION MATRICES FOR SUBNETWORKS
IN THE MULTIPLEXER OF FIG. 4.1

Subnetwork	Transmission Matrix	
	Expression	Notation
output transformer n_2:1	$\begin{bmatrix} n_2 & 0 \\ 0 & \frac{1}{n_2} \end{bmatrix}$	**A**
multi-coupled cavity filter†	$\frac{1}{q_1}\begin{bmatrix} -q_n & -1 \\ q_1^2 - p_1 q_n & -p_1 \end{bmatrix}$	**A**
input transformer 1:n_1	$\begin{bmatrix} \frac{1}{n_1} & 0 \\ 0 & n_1 \end{bmatrix}$	**A**
series junction terminated at port 3 by Y_3, $(Y = Y_c + Y_3)$	$\frac{1}{Y}\begin{bmatrix} Y + Y_a & 1 \\ 2Y_a Y + Y_a^2 & Y + Y_a \end{bmatrix}$	**A**
series junction terminated at port 2 by Y_2, $(Y = Y_a + Y_2)$	$\frac{1}{Y}\begin{bmatrix} Y + Y_c & 1 \\ Y(Y_a + Y_c) + Y_a Y_c & Y + Y_a \end{bmatrix}$	**D**

TABLE 4.1 (continued)

Subnetwork	Transmission Matrix	
	Expression	Notation
waveguide spacing††	$\begin{bmatrix} \cos\theta & j Z_0 \sin\theta \\ \frac{j \sin\theta}{Z_0} & \cos\theta \end{bmatrix}$	**A**

† $p_i(q_i)$ is the ith element of vector $\mathbf{p}(\mathbf{q})$ which is the solution of $\mathbf{Zp} = \mathbf{e}_1$ ($\mathbf{Zq} = \mathbf{e}_n$), where $\mathbf{Z} = j(s\mathbf{1} + \mathbf{M}) + r\mathbf{1}$ and $s = (\omega_0/\Delta\omega)(\omega/\omega_0 - \omega_0/\omega)$ for a filter with coupling matrix **M** centered at ω_0 and having a bandwidth parameter $\Delta\omega$ and a uniform cavity dissipation parameter r.

†† a waveguide section has a characteristic impedance Z_0 and $\theta = \beta\ell$, $\beta = 2\pi/\lambda_g$, where ℓ is the section length and λ_g is the guide wavelength.

TABLE 4.2

FIRST-ORDER SENSITIVITIES OF THE TRANSMISSION MATRICES IN TABLE 4.1

Subnetwork	Identification	Sensitivity of the Transmission Matrix
output transformer	$\frac{\partial \mathbf{A}}{\partial n_2}$	$\begin{bmatrix} 1 & 0 \\ 0 & -\frac{1}{n_2^2} \end{bmatrix}$
multi-coupled cavity filter	$\frac{\partial \mathbf{A}}{\partial M_{ab}}$	$\frac{j c^{\dagger}}{2 q_1}(p_a q_b + q_a p_b)\mathbf{A} +$ $\frac{j c}{q_1}\begin{bmatrix} q_a q_b & 0 \\ p_1 q_a q_b + q_n p_a p_b - q_1(p_a q_b + p_b q_a) & p_a p_b \end{bmatrix}$
	$\frac{\partial \mathbf{A}}{\partial \omega}$	$\frac{s_\omega}{q_1}\left(\mathbf{p}^T\mathbf{q}\,\mathbf{A} + \begin{bmatrix} \mathbf{q}^T\mathbf{q} & 0 \\ p_1\mathbf{q}^T\mathbf{q} + q_n\mathbf{p}^T\mathbf{p} - 2q_1\mathbf{p}^T\mathbf{q} & \mathbf{p}^T\mathbf{p} \end{bmatrix}\right)$
input transformer	$\frac{\partial \mathbf{A}}{\partial n_1}$	$\begin{bmatrix} -\frac{1}{n_1^2} & 0 \\ 0 & 1 \end{bmatrix}$
series junction terminated at port 3 ††	$\frac{\partial \mathbf{A}}{\partial \phi}$, $\phi \in Y_3$	$(Y_3)_\phi \mathbf{K}_1$
	$\frac{\partial \mathbf{A}}{\partial \phi}$, $\phi \in J$	$(Y_c)_\phi \mathbf{K}_1 + (Y_a)_\phi \mathbf{K}_2$
	$\frac{\partial \mathbf{A}}{\partial \omega}$	$(Y_3 + Y_c)_\omega \mathbf{K}_1 + (Y_a)_\omega \mathbf{K}_2$

TABLE 4.2 (continued)

Subnetwork	Identification	Sensitivity of the Transmission Matrix
series junction terminated at port 2 †††	$\frac{\partial \mathbf{D}}{\partial \phi}$, $\phi \in Y_2$	$(Y_2)_\phi \mathbf{L}_1$
	$\frac{\partial \mathbf{D}}{\partial \phi}$, $\phi \in J$	$(Y_a)_\phi (\mathbf{L}_1 + \mathbf{L}_2) + (Y_c)_\phi \mathbf{L}_3$
	$\frac{\partial \mathbf{D}}{\partial \omega}$	$(Y_2 + Y_a)_\omega \mathbf{L}_1 + (Y_a)_\omega \mathbf{L}_2 + (Y_c)_\omega \mathbf{L}_3$
waveguide spacing	$\frac{\partial \mathbf{A}}{\partial \ell}$	$\beta \begin{bmatrix} -\sin\theta & j Z_0 \cos\theta \\ \frac{j\cos\theta}{Z_0} & -\sin\theta \end{bmatrix}$
	$\frac{\partial \mathbf{A}}{\partial \omega}$	$\ell(\beta)_\omega \begin{bmatrix} -\sin\theta & j Z_0 \cos\theta \\ \frac{j\cos\theta}{Z_0} & -\sin\theta \end{bmatrix}$

† $c = \begin{cases} 2 \text{ if } a \neq b \\ 1 \text{ if } a = b \end{cases}$

†† $\mathbf{K}_1 = -\frac{1}{Y^2} \begin{bmatrix} Y_a & 1 \\ Y_a^2 & Y_a \end{bmatrix}$, $\mathbf{K}_2 = \frac{1}{Y} \begin{bmatrix} 1 & 0 \\ 2(Y_a + Y) & 1 \end{bmatrix}$

††† $\mathbf{L}_1 = -\frac{1}{Y^2} \begin{bmatrix} Y_c & 1 \\ Y_a Y_c & Y_a \end{bmatrix}$, $\mathbf{L}_2 = \frac{1}{Y} \begin{bmatrix} 0 & 0 \\ Y_c + Y & 1 \end{bmatrix}$, $\mathbf{L}_3 = \frac{1}{Y} \begin{bmatrix} 1 & 0 \\ Y_a + Y & 0 \end{bmatrix}$

4.3.1 Formulation of the Problem

From the possible responses tabulated in Table 3.3, consider a common port response, namely, the common port return loss and a channel dependent response, namely, the insertion loss. Typical specifications for optimum performance of contiguous multiplexers in satellite communication applications require the common port return loss to be above a certain value, e.g. 20 dB, over the entire communication band. Individual channels are required to have insertion losses below a value of, say 1 dB, in their pass-bands and above a value of say 30 dB, in their stop-bands. In general, we can formulate an appropriate optimization problem as follows.

The objective function to be minimized is given by

$$F(\boldsymbol{\phi}) = \max_{j \in J} f_j(\boldsymbol{\phi}) , \tag{4.30}$$

where $\boldsymbol{\phi}$ is a vector of design parameters (waveguide spacings, couplings, etc.) and $J \triangleq \{1,2,\ldots,m\}$ is an index set. The minimax functions $f_j(\boldsymbol{\phi})$, $j \in J$, can be of the form

$$w^1_{Uk}(\omega_i)\,(F^1_k(\boldsymbol{\phi}\,,\omega_i) - S^1_{Uk}(\omega_i))\,, \tag{4.31}$$

$$-w^1_{Lk}(\omega_i)\,(F^1_k(\boldsymbol{\phi}\,,\omega_i) - S^1_{Lk}(\omega_i))\,, \tag{4.32}$$

$$w^2_{U}(\omega_i)\,(F^2(\boldsymbol{\phi}\,,\omega_i) - S^2_{U}(\omega_i))\,, \tag{4.33}$$

$$w^2_{L}(\omega_i)\,(F^2(\boldsymbol{\phi}\,,\omega_i) - S^2_{L}(\omega_i))\,, \tag{4.34}$$

where $F_k{}^1(\boldsymbol{\phi}, \omega_i)$ is the insertion loss for the kth channel at the ith frequency, $F^2(\boldsymbol{\phi}, \omega_i)$ is the return loss at the common port at the ith frequency, $S_{Uk}{}^1(\omega_i)(S_{Lk}{}^1(\omega_i))$ is the upper (lower) specification on insertion loss of the kth channel at the ith frequency, $S_U{}^2(\omega_i)(S_L{}^2(\omega_i))$ is the upper (lower) specification on the return loss at ith frequency, and $w_{Uk}{}^1$, $w_{Lk}{}^1$, $w_U{}^2$, $w_L{}^2$ are the arbitrary user-chosen nonnegative weighting factors.

A typical example of the specifications that can be handled for a five-channel multiplexer is shown in Fig. 4.5. Frequently, linear constant or piecewise-linear constant specifications, such as the ones shown in Fig. 4.2 are to be met.

4.3.2 The Overall Structure of a Computer Implementation

The sensitivity analysis described in Chapter 3 was specialized to the multiplexer structure and the models discussed in this chapter were utilized to develop a highly efficient, state-of-the-art computer program package in Fortran for simulation, sensitivity analysis and optimization. Having described the general approach for simulation and sensitivity analysis of branched-cascaded structures, we discuss the details of a particular implementation in Section 4.3.3. It should be emphasized that this implementation is highly specialized to the multiplexer structure and the generality of the approach in Chapter 3 has been sacrificed. In this section, we present the high-level overall structure of the implementation. The computer program developed was tested in close cooperation with members of ComDev (1983), directly involved in multiplexer design and postproduction tuning. Functional blocks of the package are shown in Fig. 4.6, which illustrates the user-selected options as related to the required mode of operation.

Options of the Optimization Mode

If the multiplexer optimization option is selected, three modes of optimization are allowed for, namely, only return loss optimization, only insertion loss optimization or simultaneous return and insertion loss optimizaton, all at user-defined sets of frequency points. Lower, upper, both or no specifications on a response of interest at a certain frequency point can be handled.

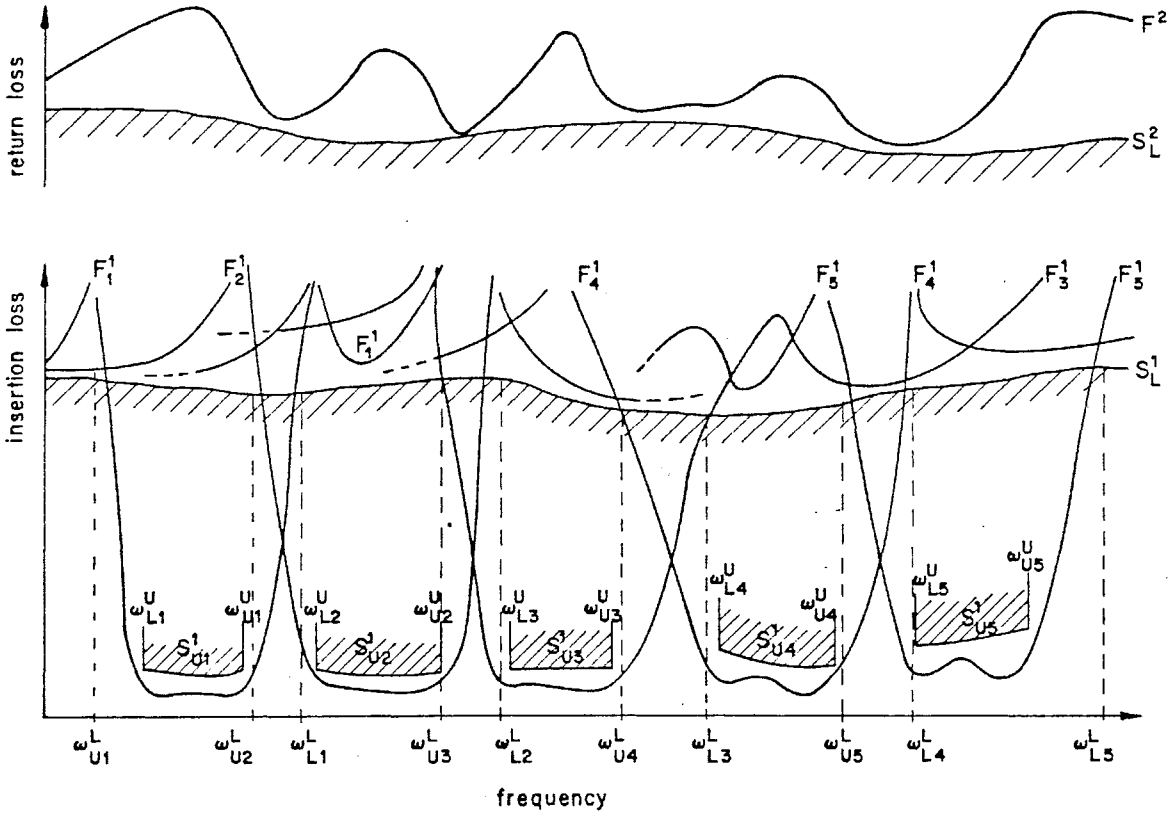

Fig. 4.5 Five channel example, illustrating the flexibility in choice of responses to be optimized and frequency bands of interest. See the text for some definitions.

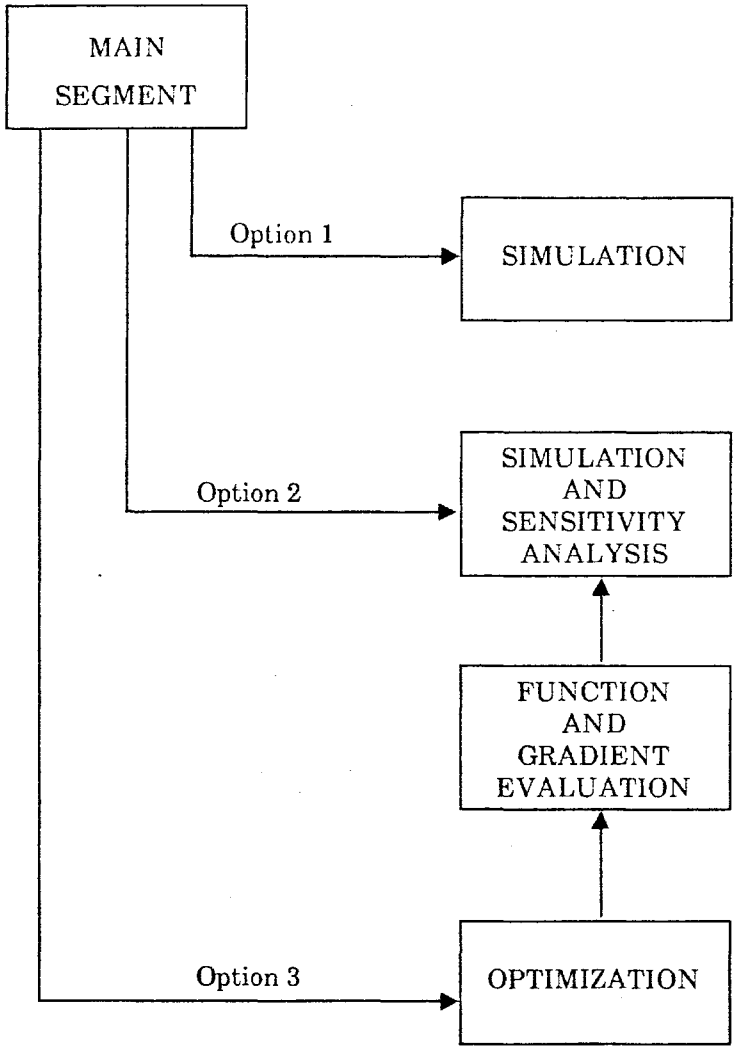

Fig. 4.6 Functional blocks of the computer package for multiplexer simulation, sensitivity analysis and optimization.

Options Related to the Selection of Optimization Variables

The package allows a flexible choice of optimization variables. In general, all parameters are candidates for optimization variables, however, the user can declare any of the parameters to be fixed.

Options Related to the Model of the Multiplexer

The package allows the user to select the junctions to be ideal (no junction susceptances) or nonideal and the filters to be lossless or lossy, dispersive or non-dispersive.

4.3.3 Detailed Description of an Implementation for Response and Sensitivity Evaluation

Here we describe the details of a particular implementation for evaluating reflection coefficient at the common port and channel output voltages as well as their first-order sensitivities with respect to filter couplings, input-output transformer ratios and waveguide section lengths in the multiplexer structure of Fig. 4.1. In Table 3.3, the formulas for calculating common port return loss and channel insertion losses and their sensitivities using the reflection coefficient and channel ouput voltages and their corresponding sensitivities, are explicitly given.

Assume that there are N channels (as shown in Fig. 4.1) with channel i, $i = 1,2\ldots,N$, terminating at an output load conductance G_L^i. Also, assume a normalized excitation with a source resistance R_S. Multi-coupled cavity filters are assumed to be of the same order n for all channels.

The following step-by-step approach is designed to calculate all the required responses and sensitivities at a single frequency f. Therefore, the iteration on frequency is external to the steps below.

Step 1

We calculate the short-circuit admittance matrix for the filters in all channels by solving two systems of equations, a total of N times. The solutions will be used in sensitivity calculations as well.

The sytems of equations to be solved are

$$\mathbf{Z}_i \mathbf{p}^i = \mathbf{e}_1, \quad i = 1, 2, ..., N \tag{4.35a}$$

and

$$\mathbf{Z}_i \mathbf{q}^i = \mathbf{e}_n, \quad i = 1, 2, ..., N, \tag{4.35b}$$

where

$$\mathbf{Z}_i = \begin{cases} j(s^i \mathbf{1} + \mathbf{M}^i) + r^i \mathbf{1}, & \text{if dispersion is not included,} \\ j(\lambda_n^i \mathbf{1} + \mathbf{M}^i) + r^i \mathbf{1}, & \text{if dispersion is included.} \end{cases} \tag{4.36}$$

(see (4.16), (4.1) and (4.10)). For the sake of simplicity, subscript i for matrix $\mathbf{Z}_i$ and superscript i for all other quantities, which is used to distinguish different channels, will be omitted from here on. However, it should be clear that all the quantities defined in the following steps are channel dependent with all the calculations done for every channel separately.

Repeating (4.15) for convenience, we have the short-circuit admittance matrix

$$\mathbf{y} = \begin{bmatrix} y_{11} & y_{12} \\ y_{21} & y_{22} \end{bmatrix} = \begin{bmatrix} p_1 & q_1 \\ q_1 & q_n \end{bmatrix}. \tag{4.37}$$

Step 2

In this step, we calculate the transmission matrices of filter-junction combinations as seen in the waveguide manifold, for all channels.

For each channel, the s.c. admittance matrix **y** of (4.37) is modified to include the input and output transformer ratios as

$$\mathbf{y}' = \begin{bmatrix} n_1^2 y_{11} & n_1 n_2 y_{21} \\ n_1 n_2 y_{21} & n_2^2 y_{22} \end{bmatrix}. \tag{4.38}$$

This modification is illustrated schematically by Fig. 4.7. Next, we find the input admittance Y_{in} of the filter terminated by a load conductance G_L as

$$Y_{in} = y'_{11} - \frac{(y'_{21})^2}{y'_{22} + G_L}. \tag{4.39}$$

(see Fig. 4.8). Taking the effect of the impedance inverter into account, we assign as per Fig. 4.9

$$Y_{in} \leftarrow 1 / Y_{in}. \tag{4.40}$$

For a junction modelled by the complex series and shunt admittances Y_c and Y_a (see (4.25)) and (4.26)), respectively, we can combine Y_c and Y_{in} as

$$Y = Y_{in} + Y_c, \tag{4.41}$$

and calculate the transmission matrix of the filter-junction combination, namely $\mathbf{T}_f$, as

$$\mathbf{T}_f = \frac{1}{Y} \begin{bmatrix} Y + Y_a & 1 \\ 2Y_a Y + Y_a^2 & Y + Y_a \end{bmatrix}. \tag{4.42}$$

(see (4.23) and Fig. 4.10).

Step 3

We now calculate the transmission matrices of all waveguide spacings (one waveguide section per channel).

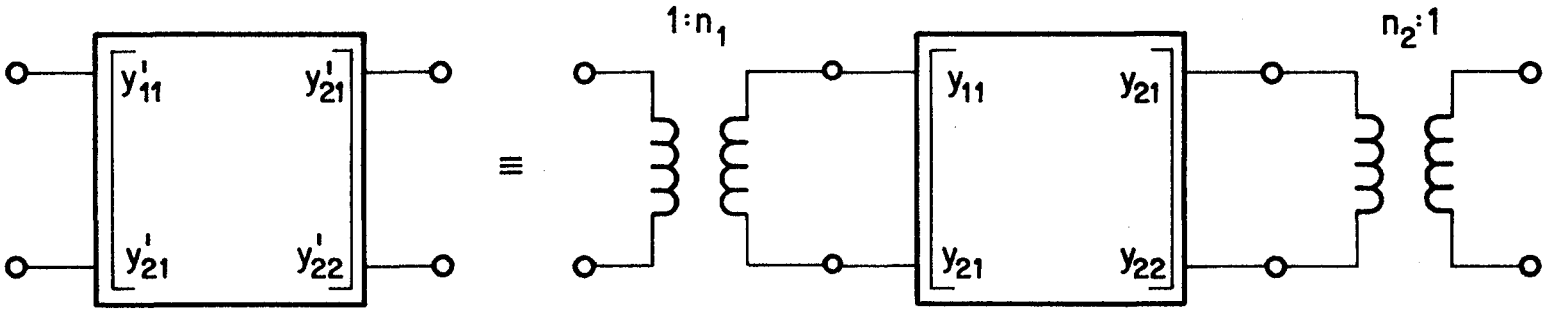

Fig. 4.7 Modification of the filter equivalent matrix y to include input and output ideal transformers.

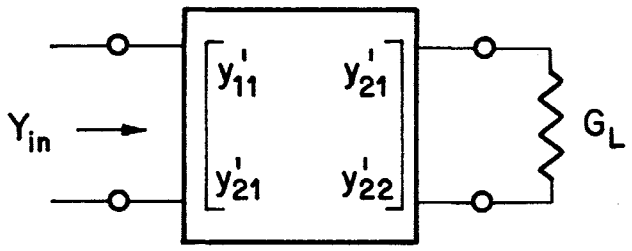

Fig. 4.8 Input admittance for a filter terminated by conductance G_L after inclusion of n_1 and n_2 as indicated by Fig. 4.7.

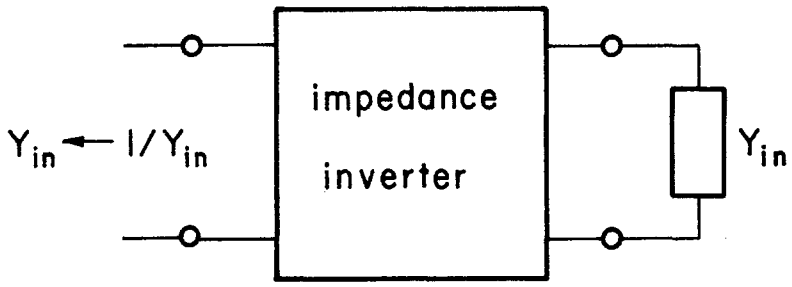

Fig. 4.9 Effect of an impedance inverter on Y_{in} of Fig. 4.8.

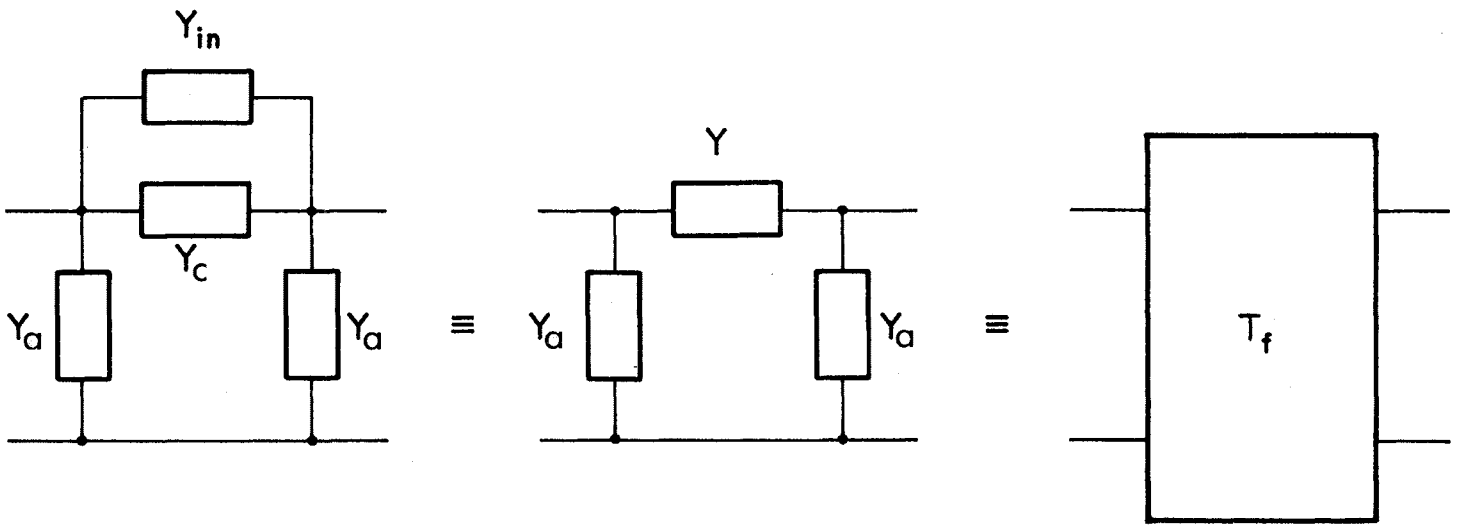

Fig. 4.10 Filter-junction combination. Y_{in} represents the filter, Y_a and Y_c the junction admittances. T_f represents the ABCD matrix of the combination.

Recalling (4.21), for a waveguide spacing of length ℓ and characteristic impedance Z_0, the transmission matrix denoted by $\mathbf{T}_g$ is given by

$$\mathbf{T}_g = \begin{bmatrix} \cos\beta\ell & j Z_0 \sin\beta\ell \\ \dfrac{j}{Z_0 \sin\beta\ell} & \cos\beta\ell \end{bmatrix}, \tag{4.43}$$

where β is calculated at the operating frequency f using (4.20), (4.19) and (4.18).

Step 4

After evaluation of $\mathbf{T}_f$ and $\mathbf{T}_g$ for each section, we find the transmission matrix of a section, namely $\mathbf{T}$, from (see Fig. 4.11)

$$\mathbf{T} = \mathbf{T}_f \mathbf{T}_g. \tag{4.44}$$

Hence, we have $\mathbf{T}_i$, $i = 1,2,\ldots,N$.

The multiplexer structure is now a simple cascade of N sections, where each section is represented by its $\mathbf{T}$ matrix (see Fig. 4.12).

To prepare for a complete sensitivity analysis, all possible products of adjacent section matrices are needed, i.e., all products shown in Fig. 4.13 should be calculated. Denoting the products by $\mathbf{A}_{ji}$, we evaluate

$$\mathbf{A}_{ji} = \begin{cases} \mathbf{T}_{i-1}\mathbf{T}_{i-2}\cdots\mathbf{T}_j, & \text{if } i > j \\ 1_{2\times 2}, & \text{if } i = j \\ \text{not defined}, & \text{if } i < j, \end{cases} \tag{4.45}$$

for $j = 1,2,\ldots,N$ and $i = 1, 2, \ldots, N+1$.

Computationally intensive calculation of all possible products, as opposed to the simple forward and reverse analysis, is required in evaluating the sensitivities of channel output voltages with respect to variables located between the corresponding channels and the short-circuit termination. If only the responses were to be evaluated (common port reflection coefficient and channel output voltages), a reverse analysis would be sufficient, i.e., only $\mathbf{A}_{1,i}$, $i = 1,2,\ldots,N+1$, were needed.

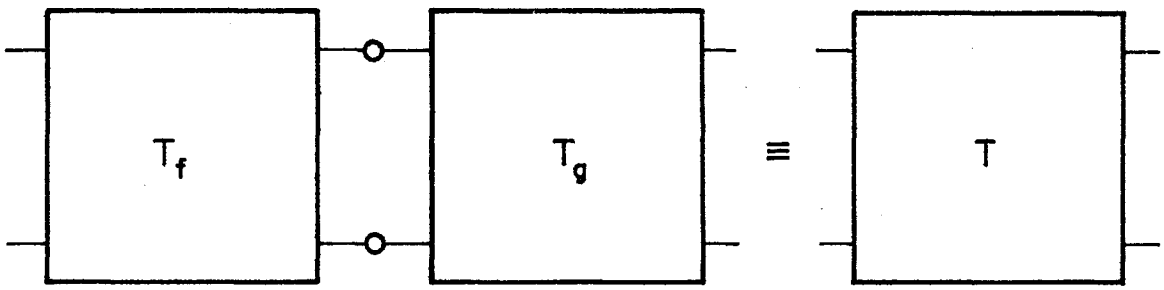

Fig. 4.11 Cascade combination of a filter-junction and waveguide spacing forming a complete section.

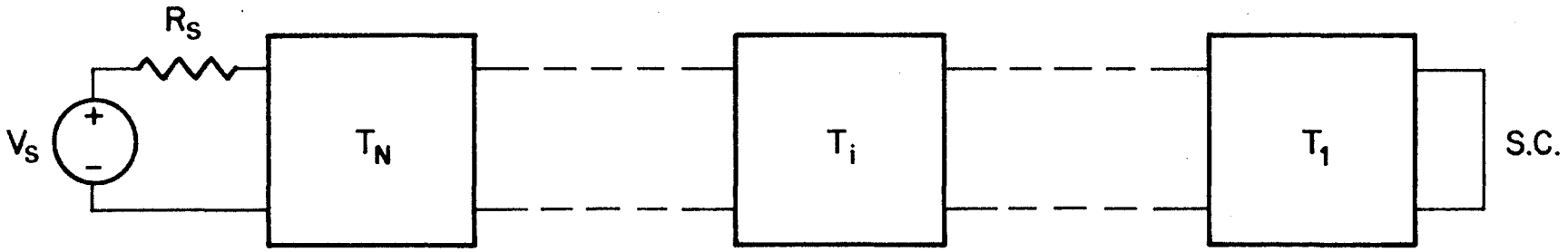

Fig. 4.12 Multiplexer structure after reduction to a simple cascaded network using the T matrices defined in Fig. 4.11.

$$
\begin{array}{lllllll}
T_1 & & & & & & \\
T_2T_1 & T_2 & & & & & \\
T_3T_2T_1 & T_3T_2 & T_3 & & & & \\
\vdots & \vdots & \vdots & \cdots & & & \\
T_N \cdots T_3T_2T_1 & T_N \cdots T_3T_2 & T_N \cdots T_3 & \cdots & \cdots & \cdots & T_NT_{N-1}
\end{array}
$$

Fig. 4.13 All the possible products of adjacent section matrices as defined by (4.45).

Step 5

The reflection coefficient at the common port and channel output voltages are calculated at this stage.

Referring to Fig. 4.14, we have

$$Z_{in} = \frac{\mathbf{e}_1^T \mathbf{A}_{1,N+1} \mathbf{e}_2}{\mathbf{e}_2^T \mathbf{A}_{1,N+1} \mathbf{e}_2} \tag{4.46}$$

and

$$\rho = \frac{Z_{in} - R_S}{Z_{in} + R_S}, \tag{4.47}$$

where $\mathbf{e}_1 = [1 \;\; 0]^T$, $\mathbf{e}_2 = [0 \;\; 1]^T$. $\mathbf{A}_{1,N+1}$ was calculated in Step 4.

To evaluate the output voltage for the ith channel, we simplify the multiplexer structure as shown in Fig 4.15, where V_S is the voltage excitation and $\mathbf{T}_{ff}$ is the transmission matrix for a multi-cavity filter including input and output transformers. After simple algebraic manipulations, we get

$$V_L^i = \frac{\mathbf{e}_2^T \begin{bmatrix} 1 & 0 \\ Y_a^i & 1 \end{bmatrix} \mathbf{T}_g^i \mathbf{A}_{1,i} \mathbf{e}_2 V_S}{\left(\mathbf{e}_2^T \begin{bmatrix} 1 & 0 \\ Y_c^i & 1 \end{bmatrix} \begin{bmatrix} 0 & j \\ j & 0 \end{bmatrix} \mathbf{T}_{ff}^i \begin{bmatrix} 1 & 0 \\ G_L^i & 1 \end{bmatrix} \mathbf{e}_1\right)\left(\mathbf{e}_1^T \begin{bmatrix} 1 & R_S \\ 0 & 1 \end{bmatrix} \mathbf{A}_{1,N+1} \mathbf{e}_2\right)}. \tag{4.48}$$

Recalling (4.17), we have

$$\mathbf{T}_{ff}^i = \frac{-1}{y'_{21}} \begin{bmatrix} y'_{22} & 1 \\ y'_{11} y'_{22} - (y'_{21})^2 & y'_{11} \end{bmatrix}, \tag{4.49}$$

and $V_L{}^i$ becomes

$$V_L^i = \frac{j[Y_a \;\; 1] \mathbf{T}_g^i \mathbf{A}_{1,i} \mathbf{e}_2 V_S}{\left(\frac{(y'_{22} + G_L)(1 + Y_c y'_{11})}{y'_{21}} - Y_c y'_{21}\right)\left([1 \;\; R_S] \mathbf{A}_{1,N+1} \mathbf{e}_2\right)}. \tag{4.50}$$

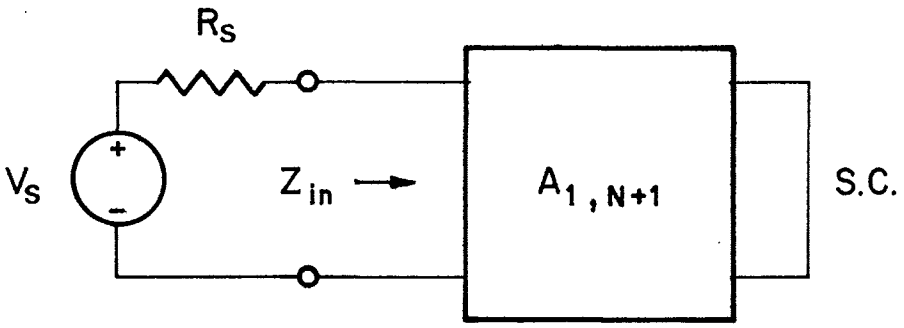

Fig. 4.14 Simplified multiplexer structure for the calculation of common port reflection coefficient.

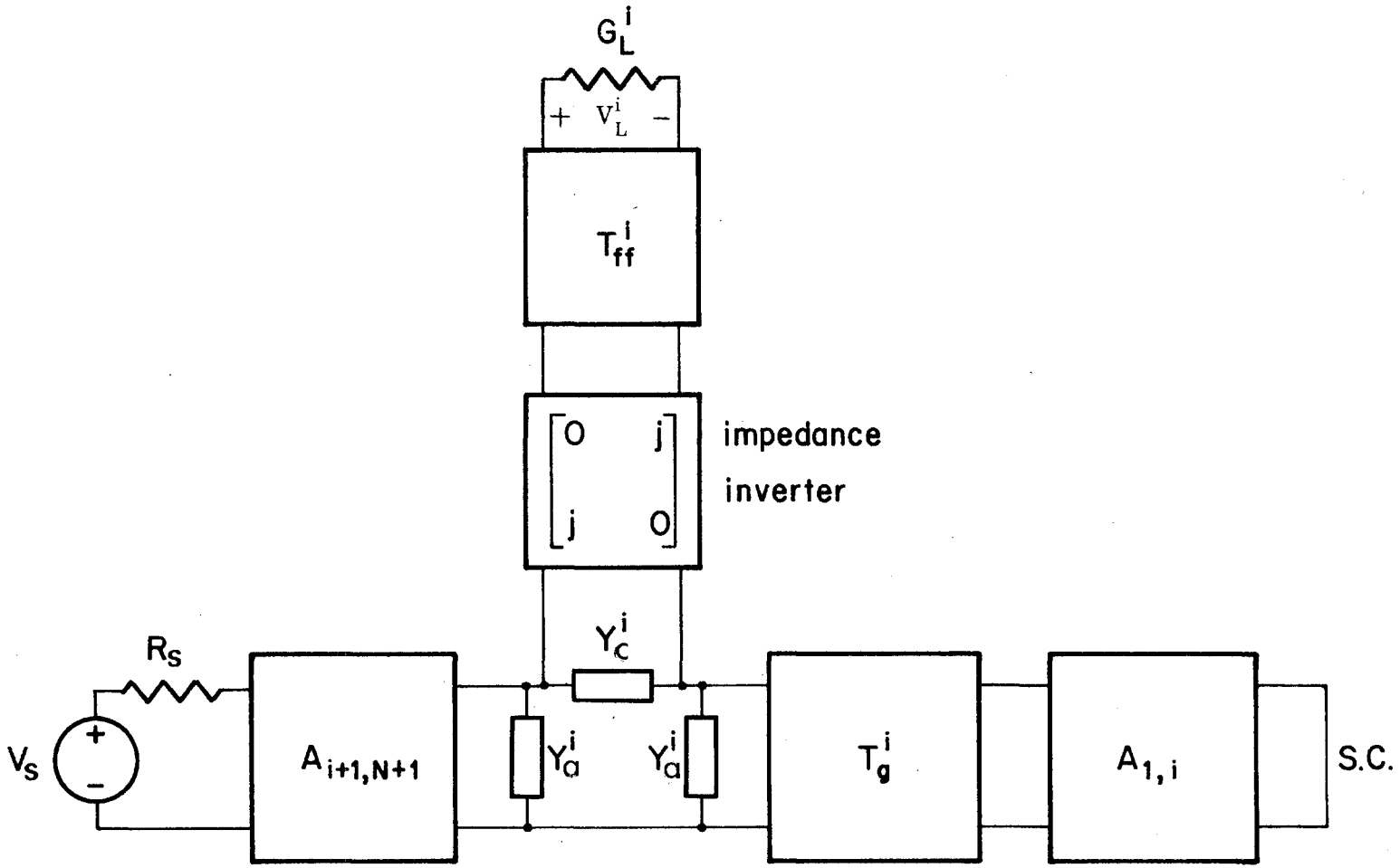

Fig. 4.15 Simplified multiplexer structure for the calculation of channel output voltage.

Note that the superscript i, needed for y_{11}', y_{21}', y_{22}', Y_c, Y_a and G_L, is omitted for simplicity.

Step 6

The remaining steps are required to evaluate the sensitivities of the responses calculated in Step 5.

In Step 6 we calculate the derivatives of individual transmission matrices **T** (a complete section) with respect to variables in them. The possible variables are filter couplings, cavity resonant frequencies (controlled by diagonal elements of the coupling matrix **M**), input-output transformer ratios and waveguide spacings.

From (4.44), we have

$$\frac{\partial \mathbf{T}}{\partial \phi} = \begin{cases} \left(\frac{\partial}{\partial \phi} \mathbf{T}_f \right) \mathbf{T}_g, & \text{if } \phi \in \{M_{ab}, n_1, n_2\} \\ \mathbf{T}_f \left(\frac{\partial}{\partial \phi} \mathbf{T}_g \right), & \text{if } \phi = \ell . \end{cases} \tag{4.51}$$

Recalling Table 4.2, or simply differentiating (4.43), we have

$$\frac{\partial}{\partial \ell} \mathbf{T}_g = \beta \begin{bmatrix} -\sin \beta\ell & j Z_0 \cos \beta\ell \\ \dfrac{j \cos \beta\ell}{Z_0} & -\sin \beta\ell \end{bmatrix}. \tag{4.52}$$

To calculate $\partial \mathbf{T}_f / \partial \phi$, we need to have $\partial Y_{in} / \partial \phi$. Using (4.41) and (4.42) and knowing that Y_a and Y_c are independent of ϕ, we have

$$\frac{\partial \mathbf{T}_f}{\partial \phi} = \frac{-1}{Y^2} \frac{\partial Y_{in}}{\partial \phi} \begin{bmatrix} Y_a & 1 \\ Y_a^2 & Y_a \end{bmatrix}, \quad \phi \in \{M_{ab}, n_1, n_2\}. \tag{4.53}$$

Now, $\partial Y_{in} / \partial \phi$ is evaluated using (4.39) and recalling (4.40) as

$$\frac{\partial Y_{in}}{\partial \phi} = -Y_{in}^2 \left[\frac{\partial}{\partial \phi} y_{11}' - \frac{2 y_{21}'}{y_{22}' + G_L} \left(\frac{\partial y_{21}'}{\partial \phi} \right) + \left(\frac{y_{21}'}{y_{22}' + G_L} \right)^2 \left(\frac{\partial y_{22}'}{\partial \phi} \right) \right]. \tag{4.54}$$

This means that the sensitivities of matrix $\mathbf{y}'$ are needed. From (4.38), we have

$$\frac{\partial \mathbf{y}'}{\partial \Phi} = \begin{cases} \begin{bmatrix} n_1^2 \dfrac{\partial y_{11}}{\partial \Phi} & n_1 n_2 \dfrac{\partial y_{21}}{\partial \Phi} \\ n_1 n_2 \dfrac{\partial y_{21}}{\partial \Phi} & n_2^2 \dfrac{\partial y_{22}}{\partial \Phi} \end{bmatrix}, & \text{if } \Phi = M_{ab} \\ \begin{bmatrix} 2n_1 y_{11} & n_2 y_{21} \\ n_2 y_{21} & 0 \end{bmatrix}, & \text{if } \Phi = n_1 \\ \begin{bmatrix} 0 & n_1 y_{21} \\ n_1 y_{21} & 2n_2 y_{22} \end{bmatrix}, & \text{if } \Phi = n_2 . \end{cases} \tag{4.55}$$

Finally, $\partial \mathbf{y}/\partial M_{ab}$ is obtained using (4.35), (4.36) and (4.37) as

$$\frac{\partial \mathbf{y}}{\partial M_{ab}} = -j\, w_1 w_2 \begin{bmatrix} 2p_a p_b & p_a q_b + p_b q_a \\ p_a q_b + p_b q_a & 2q_a q_b \end{bmatrix}, \tag{4.56}$$

where

$$w_1 = \begin{cases} 1, & \text{if } a \neq b \\ 0.5, & \text{if } a = b \end{cases} \tag{4.57}$$

and

$$w_2 = \begin{cases} \left(\dfrac{\lambda_g^F}{\lambda_{g0}} \right)^{K_{ab}}, & \text{if dispersion is included,} \\ 1, & \text{if dispersion is not included.} \end{cases} \tag{4.58}$$

(recall (4.13)).

Step 7

In this step, we calculate the sensitivities of the common port reflection coefficient with respect to all variables in the multiplexer structure.

Differentiating (4.47), we have

$$\frac{\partial \rho}{\partial \Phi} = \frac{2 R_S}{(Z_{in} + R_S)^2} \frac{\partial Z_{in}}{\partial \Phi} . \tag{4.59}$$

From (4.46) we can calculate $\partial Z_{in}/\partial \Phi$ as

$$\frac{\partial Z_{in}}{\partial \phi} = \frac{F^{(1,2)} A^{(2,2)}_{1,N+1} - F^{(2,2)} A^{(1,2)}_{1,N+1}}{\left(A^{(2,2)}_{1,N+1}\right)^2}, \tag{4.60}$$

where superscripts (1,2) and (2,2) indicate that elements (1,2) and (2,2) of the 2×2 matrices $\mathbf{F}$ and $\mathbf{A}_{1,N+1}$ are taken, e.g.,

$$\mathbf{A}^{(1,2)}_{1,N+1} = \mathbf{e}_1^T \mathbf{A}_{1,N+1} \mathbf{e}_2. \tag{4.61}$$

$\mathbf{F}$ denotes the derivative matrix $\partial\mathbf{A}_{1,N+1}/\partial\phi$ and is calculated as

$$\mathbf{F} = \frac{\partial}{\partial \phi}(\mathbf{A}_{1,N+1}) = \mathbf{A}_{j+1,N+1}\left(\frac{\partial}{\partial \phi}\mathbf{T}_j\right)\mathbf{A}_{1j} \tag{4.62}$$

where ϕ is assumed to be in section j.

Step 8

Finally, we evaluate the sensitivities of channel output voltages with respect to all variables.

Referring to (4.50), we can write

$$V^i_L = \frac{j K_1}{K_2 K_3}, \tag{4.63}$$

where

$$K_1 = [Y^i_a \quad 1]\mathbf{T}^i_g \mathbf{A}_{1,i} \mathbf{e}_2 V_S, \tag{4.64a}$$

$$K_2 = \frac{((y'_{22})^i + G^i_L)(1 + Y^i_c (y'_{11})^i)}{(y'_{21})^i} - Y^i_c (y'_{21})^i, \tag{4.64b}$$

$$K_3 = [1 \quad R_S]\mathbf{A}_{1,N+1}\mathbf{e}_2 \tag{4.64c}$$

and $i = 1, \ldots, N$.

If we assume that the variable ϕ is in section j, we can consider three different cases for evaluating sensitivities of (4.63).

Case 1: Section j is to the right of section i in Fig. 4.15, i.e., $j<i$. In this case, K_2 is independent of the variable and we have

$$\frac{\partial V_L^i}{\partial \Phi} = \frac{j\left[\left(\frac{\partial K_1}{\partial \Phi}\right)K_2 K_3 - \left(\frac{\partial K_3}{\partial \Phi}\right)K_1 K_2\right]}{(K_2 K_3)^2}. \tag{4.65}$$

We can write

$$\frac{\partial K_1}{\partial \Phi} = [Y_a^i \quad 1]\, T_g^i \left(\frac{\partial}{\partial \Phi} \mathbf{A}_{1,i}\right) \mathbf{e}_2 V_S\,, \tag{4.66}$$

and

$$\frac{\partial}{\partial \Phi}\mathbf{A}_{1,i} = \mathbf{A}_{j+1,i}\left(\frac{\partial}{\partial \Phi} T_j\right)\mathbf{A}_{1,j}. \tag{4.67}$$

Recall that the product $(\partial \mathbf{T}_j/\partial\Phi)\ \mathbf{A}_{1,j}$ has already been calculated in evaluation of $\mathbf{F}$ in (4.62). Also we have

$$\begin{aligned}\frac{\partial K_3}{\partial \Phi} &= [1 \quad R_S]\,\frac{\partial \mathbf{A}_{1,N+1}}{\partial \Phi}\,\mathbf{e}_2 \\ &= [1 \quad R_S]\,\mathbf{F}\,\mathbf{e}_2\,.\end{aligned} \tag{4.68}$$

Case 2: The variable is in the same section as the output voltage, i.e., i = j. In this case we have

$$\frac{\partial V_L^i}{\partial \Phi} = \begin{cases} j\left[\dfrac{\dfrac{\partial K_1}{\partial \Phi}}{K_2 K_3} - \dfrac{\left(\dfrac{\partial K_3}{\partial \Phi}\right)K_1 K_2}{(K_2 K_3)^2}\right], & \text{if } \Phi = \ell \\ \dfrac{-j\left[\left(\dfrac{\partial K_2}{\partial \Phi}\right)K_1 K_3 + \left(\dfrac{\partial K_3}{\partial \Phi}\right)K_1 K_2\right]}{(K_2 K_3)^2}, & \text{if } \Phi \in \{M_{ab}, n_1, n_2\} \end{cases} \tag{4.69}$$

and

$$\frac{\partial K_1}{\partial \Phi} = [Y_a^i \quad 1]\left(\frac{\partial \mathbf{T}_g^i}{\partial \Phi}\right)\mathbf{A}_{1,i}\,\mathbf{e}_2 V_S\,, \tag{4.70}$$

where $\partial \mathbf{T}_g{}^i/\partial \ell$ has already been calculated in Step 6. Also,

$$\frac{\partial K_2}{\partial \Phi} = \frac{(y'_{22}+G_L)Y_c}{y'_{21}}\left(\frac{\partial y'_{11}}{\partial \Phi}\right)+\frac{(1+Y_c y'_{11})}{y'_{21}}\left(\frac{\partial y'_{22}}{\partial \Phi}\right)$$

$$-\left(Y_c+\frac{(y'_{22}+G_L)(1+Y_c y'_{11})}{(y'_{21})^2}\right)\left(\frac{\partial y'_{21}}{\partial \Phi}\right), \tag{4.71}$$

where superscipt i is again omitted. $\partial K_3/\partial\Phi$ is calculated as in (4.68).

Case 3: Section j is to the left of section i in Fig. 4.15, i.e., $j>i$. In this case, we have

$$\frac{\partial V_L^i}{\partial \Phi} = \frac{-j K_1 K_2 \dfrac{\partial K_3}{\partial \Phi}}{(K_2 K_3)^2}, \tag{4.72}$$

where $\partial K_3/\partial\Phi$ is calculated as in (4.68).

4.4 EXAMPLES

4.4.1 12-Channel 12 GHz Multiplexer

A 12-channel, 12 GHz multiplexer without dummy channels was considered. The contiguous band multiplexer has a channel frequency separation of 40 MHz and a usable bandwidth of 39 MHz with the center frequency of the first channel at 12180 MHz. 6th-order multi-coupled cavity filters with screw couplings M_{12}, M_{34} and M_{56} and iris couplings M_{23}, M_{45} and M_{36} are used for all channels. Filter cavities are circular waveguides with a diameter of 1.07 inches. The estimated unloaded Q-factor for filters is 12000. The width of the waveguide manifold is 0.75 inches.

Suppose we want to design this multiplexer such that a lower specification of 20 dB on the common-port return loss is satisfied over the entire frequency band of interest. We start the design process with twelve identical 6th order filters with the coupling coefficients given in the following matrix (Tong and Smith 1984):

$$\mathbf{M} = \begin{bmatrix} 0 & 0.594 & 0 & 0 & 0 & 0 \\ 0.594 & 0 & 0.535 & 0 & 0 & 0 \\ 0 & 0.535 & 0 & 0.425 & 0 & -0.400 \\ 0 & 0 & 0.425 & 0 & 0.834 & 0 \\ 0 & 0 & 0 & 0.834 & 0 & 0.763 \\ 0 & 0 & -0.400 & 0 & 0.763 & 0 \end{bmatrix} . \tag{4.73}$$

In selecting the starting values of waveguide spacings, for each section the half-guide wavelength evaluated at the center frequency of the corresponding channel filter, as suggested by Atia (1974) was used. This means that for the kth channel $\lambda_{gk}/2$ was used, where λ_{gk} is calculated by evaluating (4.19) at the center frequency of the kth channel filter. The spacing evaluated in this way is measured along the manifold from the adjacent $(k-1)$th channel. For the first channel the spacing is the distance from the short-circuit. Waveguide dispersion for both manifold and filters were taken into account. Nonideal junctions with Y_a calculated from (4.26) and $Y_c = 0$ were assumed.

Figure 4.16 shows the common-port return loss and channel insertion loss responses of the multiplexer at the start of the optimization process. The specification on the common-port return loss is seriously violated, especially in the lower frequency range.

The optimization was performed in several stages with the judicious addition of new variables at each stage to improve the overall response or the response over some specific portions of the total frequency band. In particular, the first stage was the optimization with respect to only waveguide spacings, i.e., 12 variables and the last stage involved 60 variables, namely, 12 section lengths, 14 variables for each

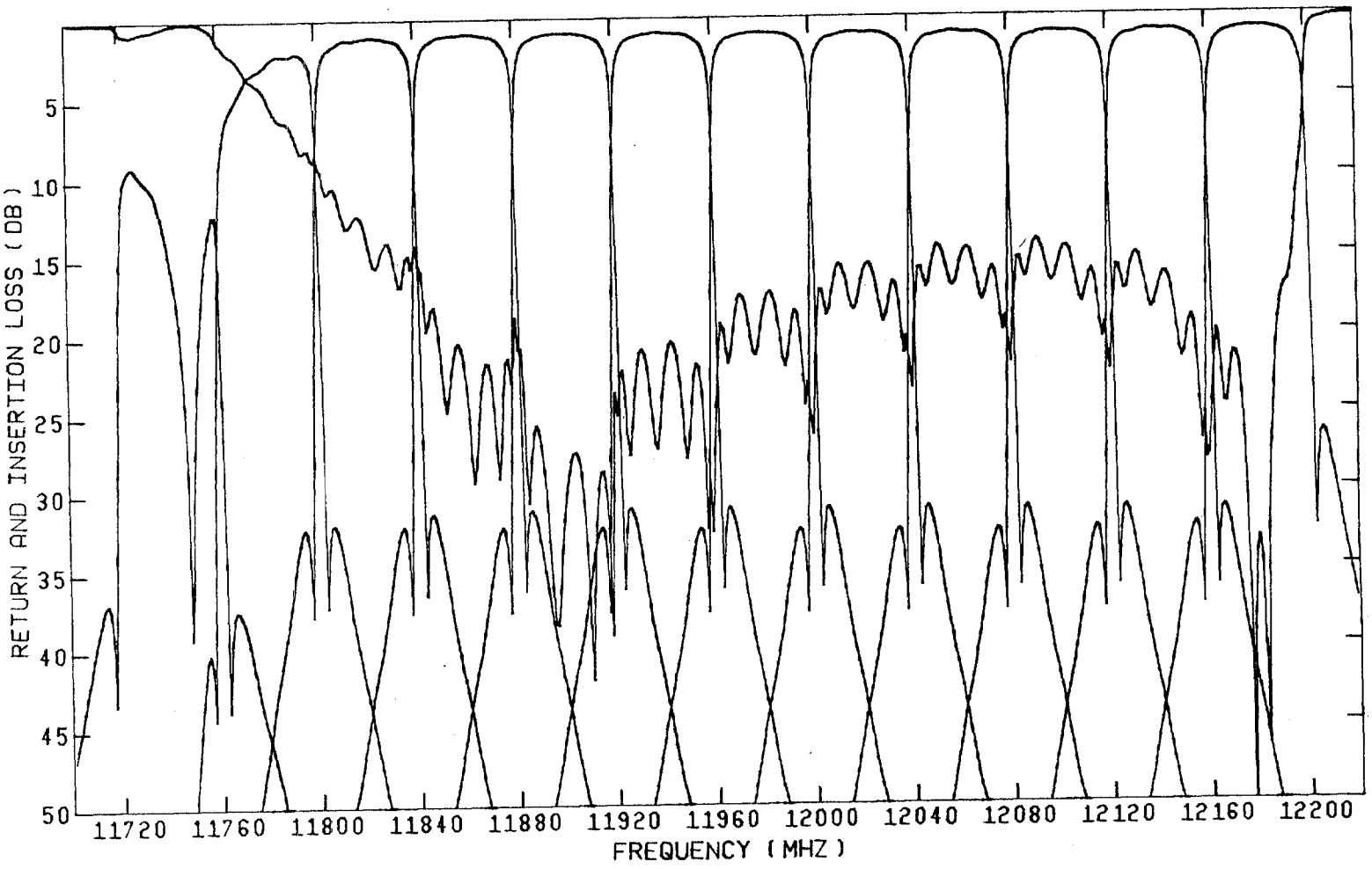

Fig. 4.16 Responses of the 12-channel multiplexer at the start of the optimization process.

of channels 1 and 12 (all six possible intercavity couplings, six cavity resonant frequencies, input and output transformer ratios), and four variables for each of channels 2, 8, 9, 10 and 11 (input and output transformer ratios, resonant frequency of the first cavity, and coupling M_{12}). In selection of the frequency points, uniformly distributed points, 10 MHz apart over the whole 500 MHz band, are taken in the early stages. However, a simple interpolation technique effectively treating sample points 1 MHz apart is introduced in the final stages of the optimization. The total CPU time on the Cyber 170/815 system was about ten minutes. The results of the final optimization are shown in Fig. 4.17. Equi-ripple return loss response satisfying the requirements over the entire communication band has been achieved.

4.4.2 3-Channel Multiplexer Design without Network Sensitivities

The 12-channel example was solved using the original minimax algorithm which requires exact sensitivities. Therefore, complete sensitivity analysis of the structure was performed. As discussed in Chapter 2, the use of efficient gradient approximation techniques obviates the evaluation of network sensitivities. Therefore, a modified minimax algorithm may be used (Bandler, Chen, Daijavad and Madsen 1986). To examine the efficiency of the new algorithm in large problems, we considered the design of a 3-channel multiplexer with 45 nonlinear variables without network sensitivities, i.e., by only evaluating the responses themselves. Using the same types of filters as in the 12-channel example, a lower specification of 20 dB on return loss over the whole band of interest should be satisfied. Also, the following upper specifications on insertion loss for all three channels should be met

$$\omega_0 \pm 10\ \text{MHz} \qquad 1.12\ \text{dB}$$

$$\omega_0 \pm 12\ \text{MHz} \qquad 1.24\ \text{dB}$$

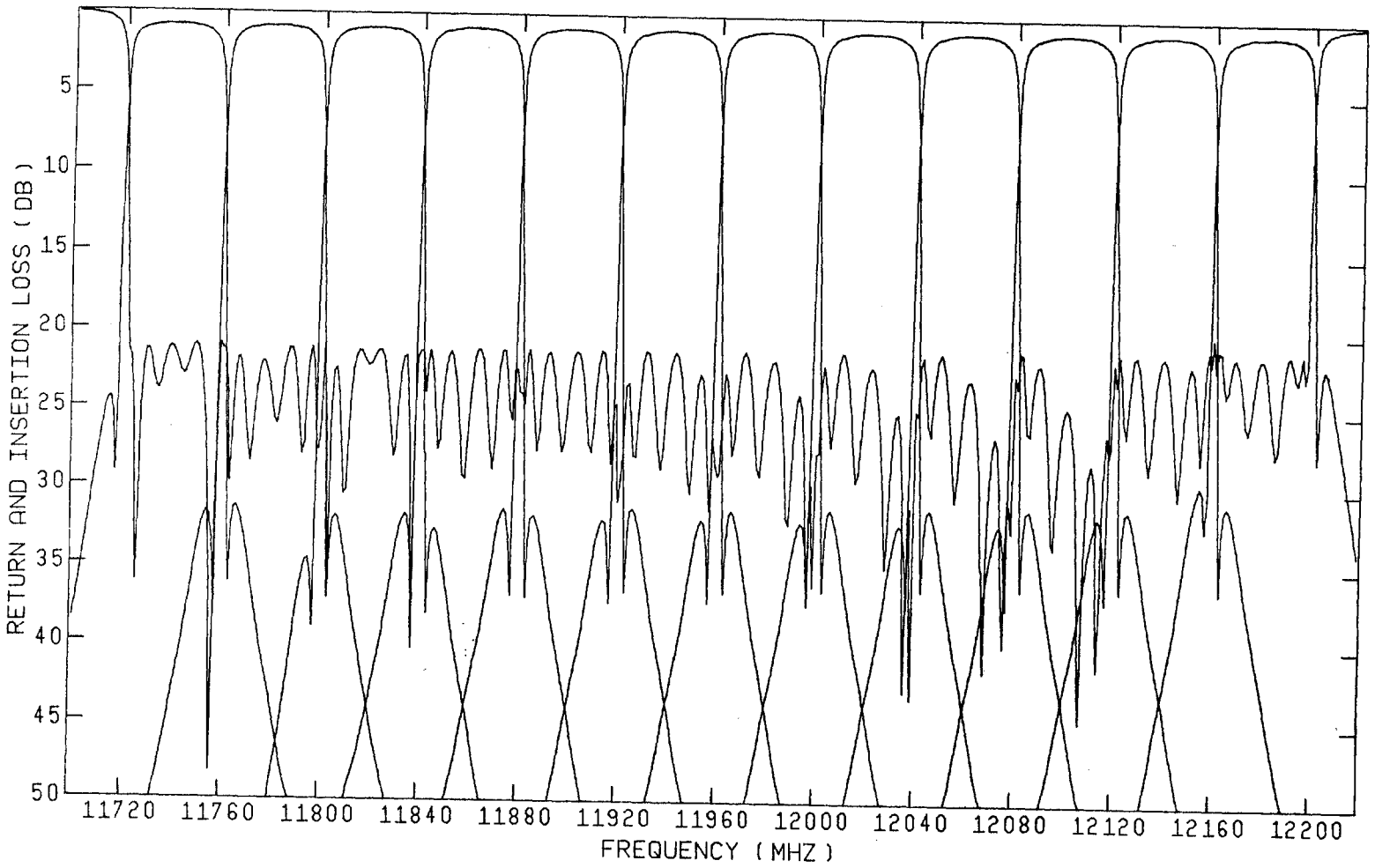

Fig. 4.17 Responses of the 12-channel multiplexer with optimized spacings, input-output transformer ratios, cavity resonances and coupling parameters using minimax optimization.

$\omega_0 \pm 14$ MHz 1.41 dB

$\omega_0 \pm 16$ MHz 1.77 dB

$\omega_0 \pm 18$ MHz 2.79 dB

Fig. 4.2 corresponds to the specifications of this example. 15 variables for each channel, namely six intercavity couplings, six cavity resonant frequencies, input and output transformer ratios and waveguide spacings, were considered. In selection of frequency points, 15 passband points were used for each channel. Both return loss and insertion loss specifications were considered at each point. Moreover, two crossover frequencies, namely, 12000 MHz and 12040 MHz for return loss only were selected. Consequently, we have a total of 92 error functions and 45 variables. The return loss and insertion loss responses for the multiplexer at the starting point and at the solution are shown in Figs. 4.18 and 4.19. The CPU time on the Cyber 170/730 system was about 15 minutes. It is clear from the computational time that the modified minimax algorithm is not as fast as the original algorithm since this problem can be solved in about 8 minutes using the network sensitivities. However, as discussed in Chapter 2, the modified algorithm relieves the user from providing network sensitivities, which in many applications are tremendously complicated or even impossible to evaluate.

4.4.3 16-Channel Multiplexer

As the number of channels for the multiplexer increases, the dimensionality of the problem in terms of the number of parameters and functions to be dealt with increases. This requires the use of increasingly powerful computing facilities. To overcome the dimensionality problem, the design of a continguous band multiplexer structure with an arbitrarily large number of channels and design

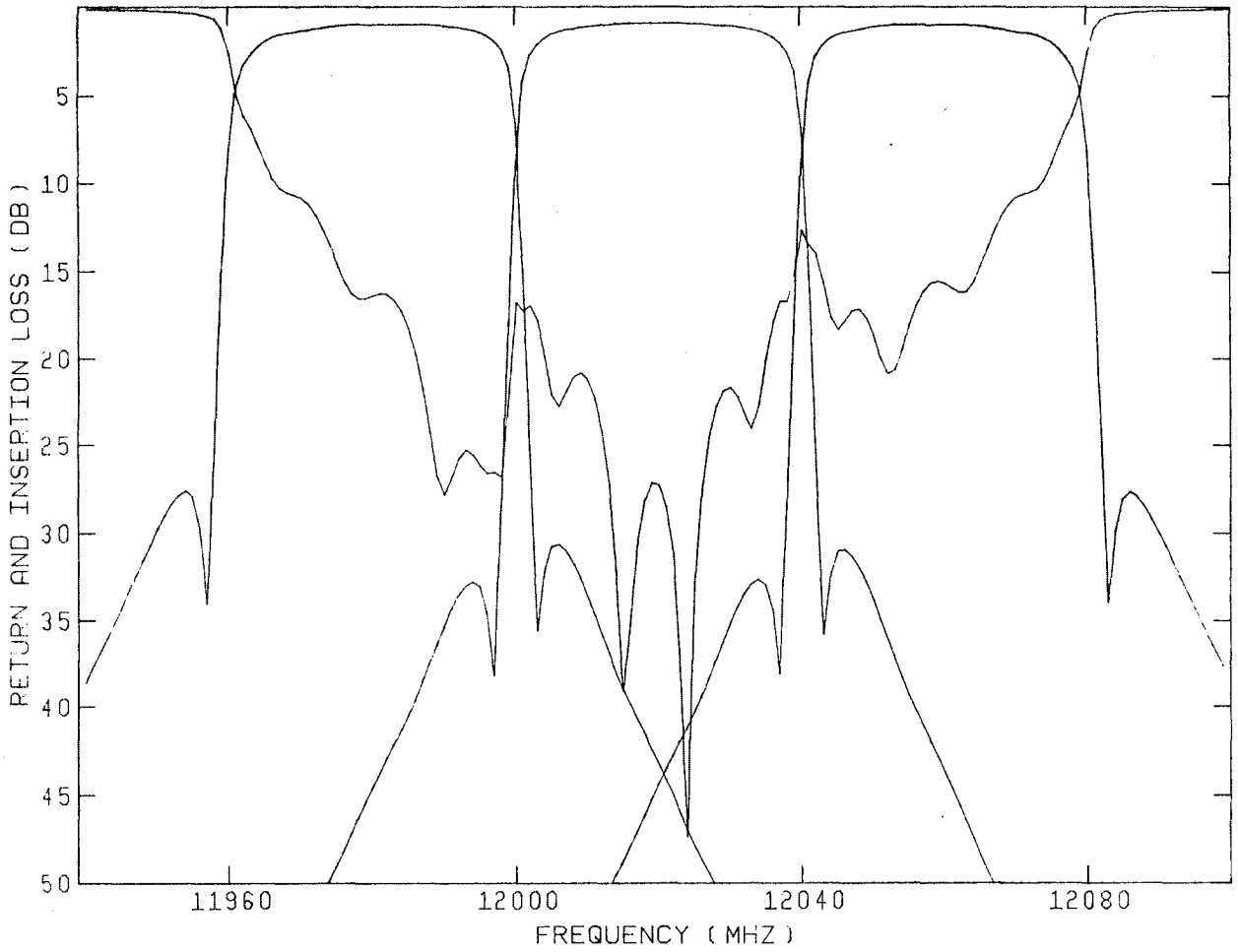

Fig. 4.18 Responses of the 3-channel multiplexer at the starting point.

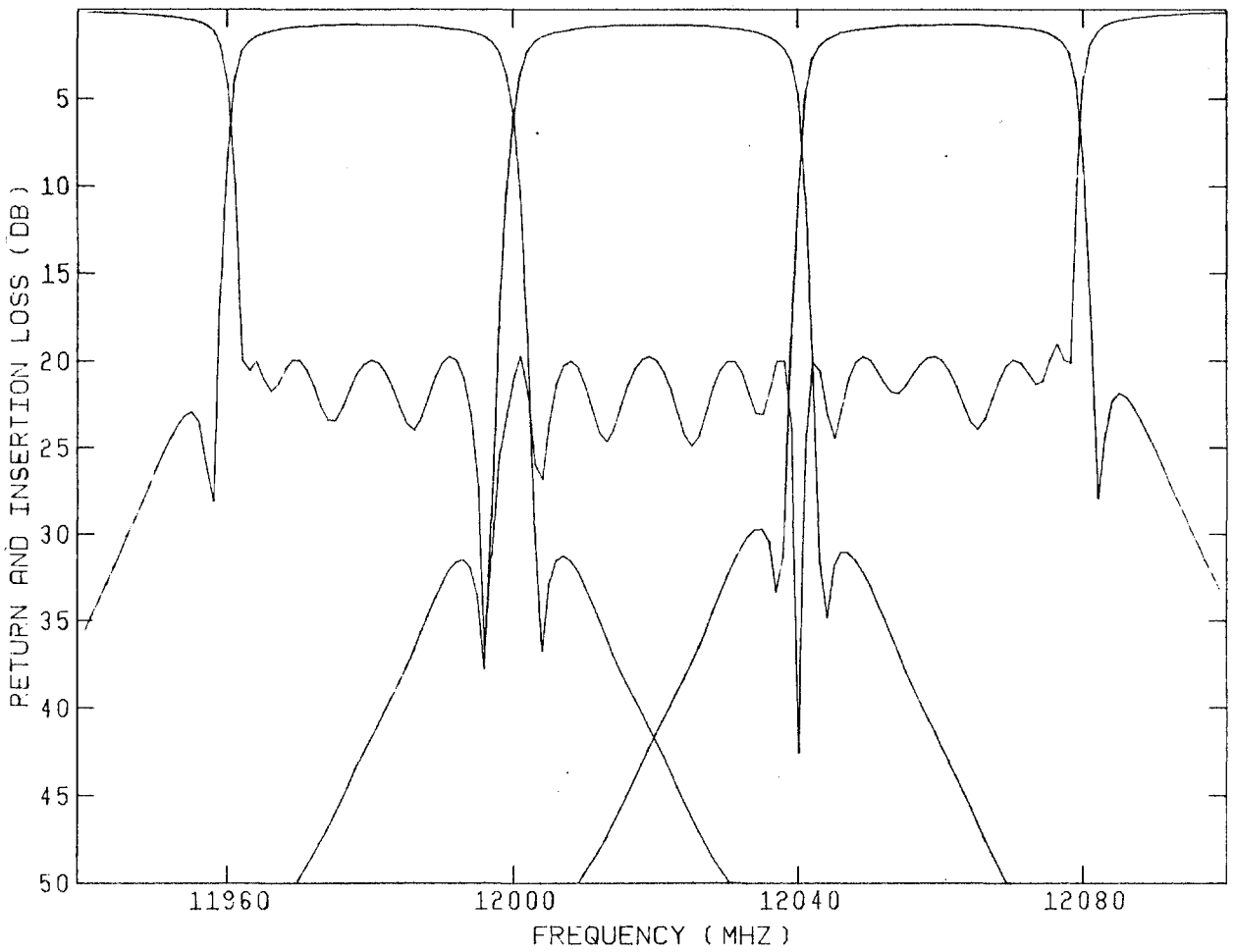

Fig. 4.19 Responses of the 3-channel multiplexer at the solution.

parameters has been formulated as a sequence of appropriately defined smaller optimization problems (Bandler, Chen, Daijavad, Kellermann, Renault and Zhang 1986). The smaller problems correspond to growing a multiplexer by adding one or more channels at a time to the structure.

Suppose we want to design an N-channel multiplexer. To achieve this goal we could perform a sequence of $N-1$ optimizations. In each of these optimizations we add a new channel to the existing k-channel multiplexer. The resulting $(k+1)$ channel structure is then optimized with optimization variables taken from channels k and $k+1$ and specifications imposed on responses in channels $k-1$, k and $k+1$. Sample frequencies are selected from the frequency range covering channels $k-1$, k and $k+1$.

A 16-channel multiplexer was designed starting with a 12-channel optimal design of Fig. 4.17. The procedure described above was used, i.e., 4 optimization problems were solved by adding one channel at a time. The responses for the 16-channel multiplexer obtained after the last optimization are shown in Fig. 4.20.

4.5 CONCLUDING REMARKS

In this chapter we applied the sensitivity formulas and the method of analysis developed previously to design one of the most important microwave devices in communication satellite applications, namely, the manifold type contiguous band multiplexer. Models for individual components of the multiplexer with nonideal effects such as dissipation, dispersion and junction susceptances were discussed in detail. Using a fast and robust gradient-based minimax algorithm, we formulated appropriate optimization problems in which engineering specifications on responses such as common port return loss and channel insertion losses are to be satisfied.

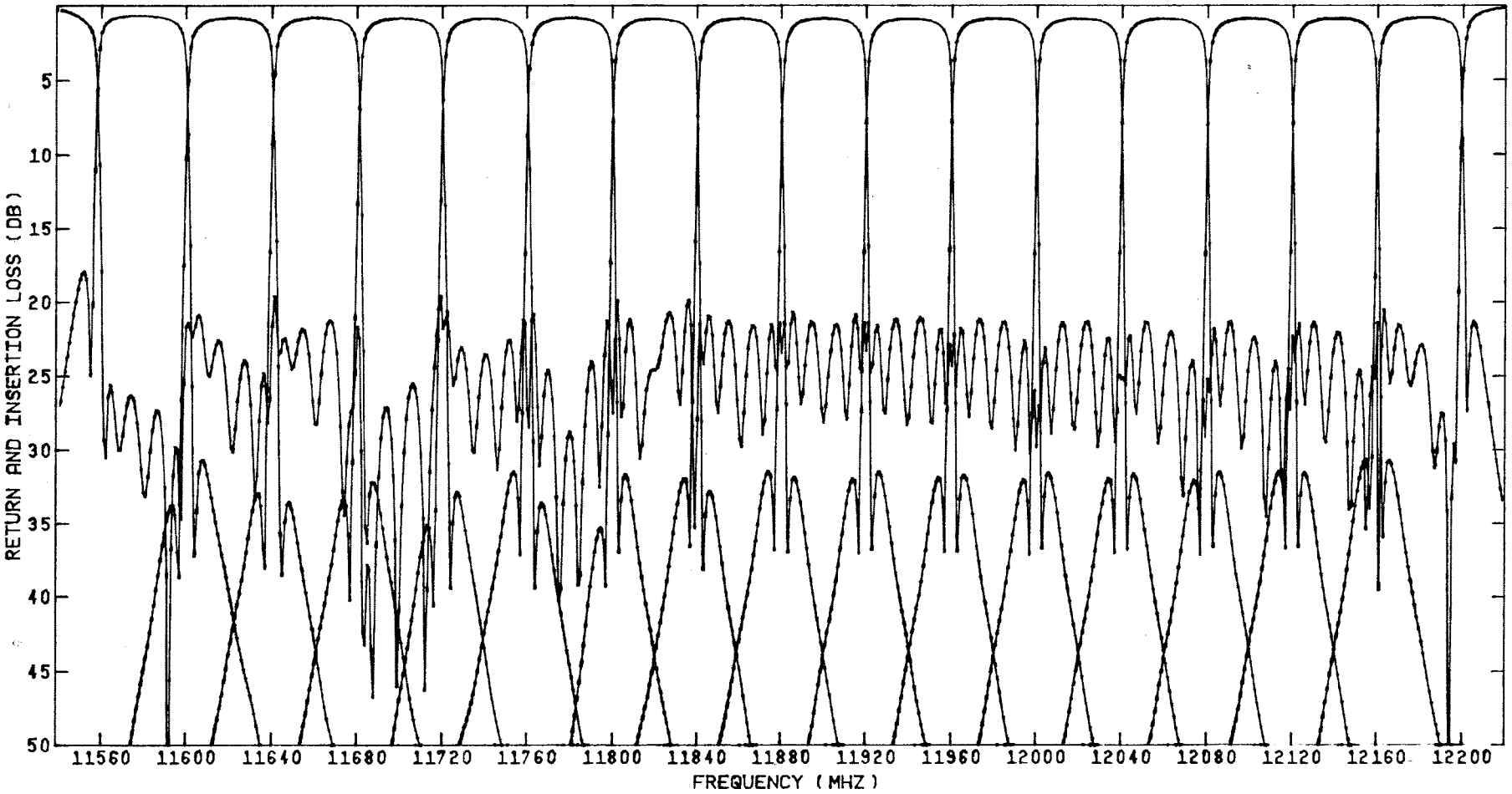

Fig. 4.20 Responses of a nonideal 16-channel multiplexer obtained from the optimal 12-channel structure by growing one channel at a time.

A flexible computer program was developed which utilizes the models described in Chapter 4 and the sensitivity analysis of Chapter 3. The calculation of responses and sensitivities were described in detail.

Some of the largest nonlinear optimization problems ever demonstrated in microwave circuit design for a reasonable computational time have been presented in this chapter to design 3-, 12-, and 16-channel multiplexers.

5

MICROWAVE DEVICE MODELLING

5.1 INTRODUCTION

The problem of approximating a measured response by a network or system response has been formulated as an optimization problem with respect to the equivalent circuit parameters of a proposed model. The traditional approach in modelling is almost entirely directed at achieving the best possible match between measured and calculated responses. When the presence of nonideal effects causes an imperfect match between measured and modelled responses or when the equivalent circuit parameters are not unique with respect to the responses selected, the traditional modelling approach has serious shortcomings. In such cases, a family of solutions for circuit model parameters exist which produce reasonable and similar matches between measured and calculated responses.

In this chapter, we briefly review the concepts in modelling including the formulation utilized in popular microwave software systems. The advanced technique of model evolution through automatic modification of circuit topology presented by Cutteridge and Y.S. Zhang (1984) is also reviewed. We then present a new formulation for modelling using the concept of multi-circuit measurements (Bandler, Chen and Daijavad 1986b). The objective of this new technique is to achieve self-consistent models for passive and active devices using an approach that automatically checks the validity of the model parameters obtained from optimization. If successful, the method provides confidence in the validity of the model parameters, otherwise it proves their incorrectness. The use of the ℓ_1 norm, based on its theoretical properties

which were discussed in Chapter 2, is an integral part of the approach. The use of an efficient gradient-based ℓ_1 algorithm, e.g., the Hald and Madsen algorithm (1985) in conjunction with the gradient approximations described in Chapter 2, makes it possible to employ a state-of-the-art optimization algorithm with any simulation package capable simply of providing responses.

The new modelling technique has been tested on two microwave devices that, because of their application in satellite communications, are of significant interest at the present time. These devices are multi-coupled cavity filters which were described in Chapter 4, and GaAs FET's used in wideband amplifiers.

We conclude this chapter by discussing the application of efficient modelling techniques in developing algorithms for postproduction tuning. We provide an example to illustrate the use of modelling in establishing the relationship between physical parameters of a device and its circuit equivalent model parameters.

5.2 REVIEW OF CONCEPTS IN MODELLING

5.2.1 The Approximation Problem

The traditional approximation problem is stated as follows

$$\underset{\mathbf{x}}{\text{minimize}} \; \|\mathbf{f}\| \tag{5.1}$$

where a typical component of $\mathbf{f}$, namely f_i evaluated at the frequency point ω_i, is given by

$$f_i \triangleq w_i(F_i^c(\mathbf{x}) - F_i^m), \qquad i = 1, 2, \ldots, k \; . \tag{5.2}$$

F_i^m is a measured response at ω_i and F_i^c is the response of an appropriate network which depends nonlinearly on a vector of model parameters $\mathbf{x} \triangleq [x_1 \;\; x_2 \;\; \ldots \;\; x_n]^T$ and w_i denotes a nonnegative weighting factor. $\|\mathbf{f}\|$ denotes the general ℓ_p norm given by

$$\|\mathbf{f}\| = \left(\sum_{i=1}^{k} |f_i^p| \right)^{1/p} . \tag{5.3}$$

The least-squares norm or ℓ_2 is obtained with p = 2. As p→∞ (5.1) becomes the minimax problem. Using the ℓ_1 norm, (5.1) becomes

$$\underset{\mathbf{x}}{\text{minimize}} \|\mathbf{f}\| \triangleq \sum_{i=1}^{k} |f_i| . \tag{5.4}$$

5.2.2 Typical Software for Modelling

Widely used microwave design and modelling programs, e.g., SUPER-COMPACT (1986) and TOUCHSTONE (1985) as well as most in-house software systems utilize the popular S-parameters in device modelling. For an n-port network equivalent, moduli or phases (alternatively, real or imaginary parts) of all or some of the n^2 S-parameters are used as F_i's (calculated F_i^c and measured F_i^m) in (5.2) to evaluate the error function f_i's. Least squares optimization (p = 2 in (5.3)) is used in almost all existing software. The popularity of ℓ_2 is largely due to two factors. One is the smoothing property of ℓ_2 in handling small measurement errors with, say, a normal distribution. These errors which usually result from the limits on the accuracy of the measurement equipment are difficult to overcome. The second reason for applying the least squares optimization is that efficient ℓ_2 optimization techniques have long been known.

The use of the ℓ_1 norm in modelling is becoming popular due to the recent developments in ℓ_1 optimization techniques. As discussed in Chapter 2, the use of ℓ_1 as compared to the other norms ℓ_p with p>1 has the distinctive property that some large components of **f** are ignored, i.e., at the solution there may well be a few f_i's which are much larger than the others. This means that, with the components of **f** as

defined by (5.2), a few large measurement errors can be tolerated by the ℓ_1 norm better than any other norm. However, we do not need to assume that such large errors exist. Later in this chapter we use a new formulation for modelling in which some components of **f** are designed to have large values at the solution, justifying the use of ℓ_1 with or without possible measurement errors.

5.2.3 Advanced Techniques in Modelling

Along with the new multi-circuit technique which will be introduced and discussed in detail in this chapter, another powerful and advanced method in linear modelling of microwave devices is the model evolution technique described by Cutteridge and Y.S. Zhang (1984) as applied to high-frequency bipolar transistors, and by Baden Fuller and Parker (1985) as applied to microstrip spiral inductors. In this technique, based on a heuristic algorithm, a computer program modifies the circuit topology in an iterative fashion to obtain the best topology as well as the parameter values for which the equivalent circuit responses match a set of S-parameter measurements.

The scheme adopted for model evolution comprises three distinct procedures, namely, (i) removal of elements and nodes within the existing topology which can lead to greatly simplified circuits without any loss of performance, (ii) addition of elements without increasing the number of nodes, and (iii) addition of new topographic nodes together with new elements to the existing model.

As an example, Cutteridge and Y.S. Zhang (1984) used the S-parameter measurements at 12 frequencies between 0.1 GHz and 1.0 GHz to model an npn transistor in the common-emitter configuration. Starting with the initial model of

Fig. 5.1a, the circuit was modified in several stages with the model at an intermediate stage and the final model shown in Figs. 5.1b and 5.1c, respectively.

The major difficulty in the construction of programs that achieve topological modification of a network entirely automatically, is the strategy for element and node addition. The number of possibilities for the addition of a single element increases enormously with increasing complexity of the network, and the number of possibilities for simultaneous addition of two or more elements increases even more rapidly. A realistic high-level strategy for topological modification must be employed to keep the overall computing time reasonable. At the present time, such strategies are heuristic and usually highly limited.

5.3 A NEW APPROACH IN MODELLING USING MULTIPLE SETS OF MEASUREMENTS

5.3.1 Introductory Remarks

The use of multiple sets of measurements for a circuit was originally thought of by Bandler, Chen and Daijavad (1986b) as a way of increasing the "identifiability" of the network. The idea is to overcome the problem of non-uniqueness of parameters that exists when only one set of multi-frequency measurements at a certain number of ports (or nodes) are used for identification. By a new set of measurements we mean multi-frequency measurements on one or more responses after making a physical adjustment on the device. Such an adjustment results in the deliberate perturbation of one or a few circuit parameters, therefore, to have multiple sets of measurements, multiple circuits differing from each other in one or a few parameters are created. In the above context, the term multi-circuit identification may also be used.

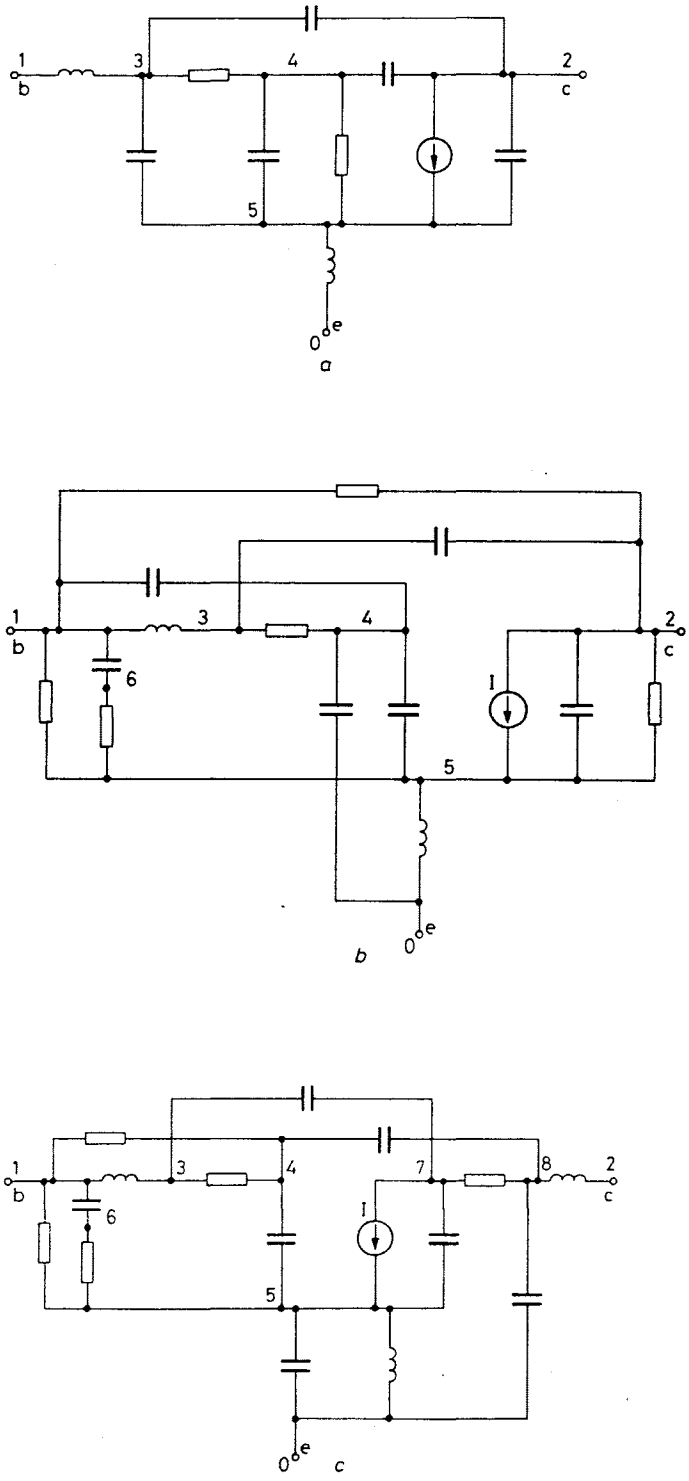

Fig. 5.1 Modelling of an npn transistor. The initial model, the model at an intermediate stage and the final model are shown in a, b and c, respectively. (Reproduced from Cutteridge and Zhang 1984).

In this section, we first use a simple example to illustrate the usefulness of multi-circuit measurements in identifying the parameters uniquely. We formulate an appropriate optimization problem and also discuss its limitations. Finally, we develop a model verification method and formulate a second optimization problem which exploits multi-circuit measurements and the properties of the ℓ_1 optimization in device modelling.

5.3.2 Unique Identification of Parameters Using Multi-Circuit Measurements

Consider the simple RC passive circuit of Fig. 5.2. The parameters $\mathbf{x} = [R_1 \;\; R_2 \;\; C]^T$ are to be identified. If we have measurements only on V_2 given by

$$V_2 = \frac{sCR_1R_2}{1 + sC(R_1+R_2)}, \tag{5.5}$$

it is clear by inspection that $\mathbf{x}$ cannot be uniquely determined regardless of the number of frequency points and the choice of frequencies used. This is because R_1 and R_2 are observed in exactly the same way by V_2. Formally, the non-uniqueness is proved using the concepts discussed in the subject of fault diagnosis of analog circuits (Bandler and Salama 1985a) in the following way. Given a complex-valued vector of responses $\mathbf{h}(\mathbf{x},s_i)$, $i = 1,2,\ldots,n_\omega$ (from which real-valued vector $\mathbf{F}^c(\mathbf{x},\omega)$ is obtained), the measure of identifiability of $\mathbf{x}$ is determined by testing the rank of the $n_\omega \times n$ Jacobian matrix

$$\mathbf{J} \triangleq [\nabla_x \mathbf{h}^T(\mathbf{x})]^T. \tag{5.6}$$

If the rank of matrix $\mathbf{J}$ denoted by ρ is less than n, $\mathbf{x}$ is not uniquely identifiable from $\mathbf{h}$. For the RC circuit example, we have

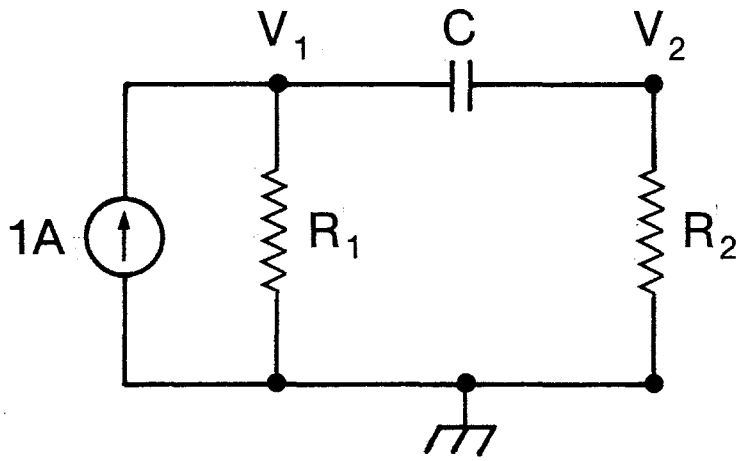

Fig. 5.2 Simple RC network.

$$\mathbf{J} = \begin{bmatrix} \dfrac{s_1 C R_2(1+s_1 C R_2)}{[1+s_1 C(R_1+R_2)]^2} & \dfrac{s_1 C R_1(1+s_1 C R_1)}{[1+s_1 C(R_1+R_2)]^2} & \dfrac{s_1 R_1 R_2}{[1+s_1 C(R_1+R_2)]^2} \\ \vdots & \vdots & \vdots \\ \dfrac{s_{n_\omega} C R_2(1+s_{n_\omega} C R_2)}{[1+s_{n_\omega} C(R_1+R_2)]^2} & \dfrac{s_{n_\omega} C R_1(1+s_{n_\omega} C R_1)}{[1+s_{n_\omega} C(R_1+R_2)]^2} & \dfrac{s_{n_\omega} R_1 R_2}{[1+s_{n_\omega} C(R_1+R_2)]^2} \end{bmatrix} . \quad (5.7)$$

Denoting the three columns of $\mathbf{J}$ by $\mathbf{J}_1$, $\mathbf{J}_2$, and $\mathbf{J}_3$, we have

$$\mathbf{J}_1 - \left(\frac{R_2}{R_1}\right)^2 \mathbf{J}_2 + \frac{C(R_2-R_1)}{R_1^2} \mathbf{J}_3 = \mathbf{0} , \quad (5.8)$$

i.e., $\mathbf{J}$ cannot have a rank greater than 2. Therefore, $\mathbf{x}$ is not unique with respect to V_2.

Now, suppose that a second circuit is created when R_2 is adjusted by an unknown amount. Using a superscript to identify the circuit (1 or 2), we have

$$V_2^1 = \frac{s C^1 R_1^1 R_2^1}{1 + s C^1 (R_1^1 + R_2^1)} \quad (5.9a)$$

and

$$V_2^2 = \frac{s C^1 R_1^1 R_2^2}{1 + s C^1 (R_1^1 + R_2^2)} , \quad (5.9b)$$

noting that $R_1{}^2$ and C^2 are not present since only R_2 has changed.

Taking only two frequencies s_1 and s_2, the expanded parameter vector $\mathbf{x} = [R_1{}^1 \;\; R_2{}^1 \;\; C^1 \;\; R_2{}^2]^T$ is uniquely identifiable because the Jacobian $\mathbf{J}$ given by

$$\mathbf{J} = \begin{bmatrix} \dfrac{s_1 C^1 R_2^1 (1+s_1 C^1 R_2^1)}{[1+s_1 C^1 (R_1^1+R_2^1)]^2} & \dfrac{s_1 C^1 R_1^1 (1+s_1 C^1 R_1^1)}{[1+s_1 C^1 (R_1^1+R_2^1)]^2} & \dfrac{s_1 R_1^1 R_2^1}{[1+s_1 C^1 (R_1^1+R_2^1)]^2} & 0 \\ \dfrac{s_2 C^1 R_2^1 (1+s_2 C^1 R_2^1)}{[1+s_2 C^1 (R_1^1+R_2^1)]^2} & \dfrac{s_2 C^1 R_1^1 (1+s_2 C^1 R_1^1)}{[1+s_2 C^1 (R_1^1+R_2^1)]^2} & \dfrac{s_1 R_1^1 R_2^1}{[1+s_2 C^1 (R_1^1+R_2^1)]^2} & 0 \\ \dfrac{s_1 C^1 R_2^2 (1+s_2 C^1 R_2^2)}{[1+s_1 C^1 (R_1^1+R_2^2)]^2} & 0 & \dfrac{s_1 R_1^1 R_2^2}{[1+s_1 C^1 (R_1^1+R_2^2)]^2} & \dfrac{s_1 C^1 R_1^1 (1+s_1 C^1 R_1^1)}{[1+s_1 C^1 (R_1^1+R_2^2)]^2} \\ \dfrac{s_2 C^1 R_2^2 (1+s_2 C^1 R_2^2)}{[1+s_2 C^1 (R_1^1+R_2^2)]^2} & 0 & \dfrac{s_2 R_1^1 R_2^2}{[1+s_2 C^1 (R_1^1+R_2^2)]^2} & \dfrac{s_2 C^1 R_1^1 (1+s_2 C^1 R_1^1)}{[1+s_2 C^1 (R_1^1+R_2^2)]^2} \end{bmatrix}, \tag{5.10}$$

is of rank 4 if $s_1 \neq s_2$.

To summarize the approach, it can be stated that although the use of unknown perturbations adds to the number of unknown parameters, the addition of new measurements could increase the rank of $\mathbf{J}$ by an amount greater than the increase in n, therefore increasing the chance of uniquely identifying the parameters. The originality of the technique lies in the fact that neither additional ports (nodes) nor additional frequencies are required. The additional measurements on the perturbed system can be performed at the ports (nodes) or frequencies which are subsets of the ports (nodes) or frequencies employed for the unperturbed system.

Based on the above ideas and for n_c circuits, we formulate an ℓ_1 optimization problem as follows:

$$\underset{\mathbf{x}}{\text{minimize}} \sum_{t=1}^{n_c} \sum_{i=1}^{k_t} |f_i^t| , \tag{5.11}$$

where

$$f_i^t \triangleq w_i^t [F_i^c(\mathbf{x}^t) - (F_i^m)^t] \tag{5.12}$$

and

$$\mathbf{x} = \begin{bmatrix} \mathbf{x}^1 \\ \mathbf{x}_a^2 \\ \cdot \\ \cdot \\ \cdot \\ \mathbf{x}_a^{n_c} \end{bmatrix} , \tag{5.13}$$

with superscript and index t identifying the t-th circuit. $\mathbf{x}_a{}^t$ represents the vector of additional parameters introduced after the (t–1)th adjustment. It has only one or a few elements compared to n elements in $\mathbf{x}^t$ which contains all circuit parameters after the change, i.e., including the ones which have not changed. k_t is an index whose value depends on t, therefore a different number of frequencies may be used for different circuits.

5.3.3 An Implementation of the Multi-Circuit Modelling Technique

In this section we describe an implementation of the multi-circuit modelling technique to perform the optimization problem given in (5.11) with variables defined in (5.13). The emphasis is on the way in which the problem is set up such that different circuits are processed individually while the optimization works on all circuits simultaneously.

Assume that a gradient-based ℓ_1 optimization package is available which requires user-defined functions and gradients. Also, assume that a dedicated module with a fixed circuit topology is provided by the user which calculates all S-parameters (or other relevant responses) of the network, at a given frequency and for one set of network parameters. This module also calculates the sensitivities of S-parameters

with respect to all parameters of the circuit at the frequency of operation and at the given set of parameter values.

Now suppose that after measuring the S-parameters of a device at K_1 frequencies, we make an adjustment to the device and measure the S-parameters at K_2 frequencies. In general, the second set of frequencies share some common points with the first set. We can keep making adjustments to the device a total of $n_c - 1$ times, so that a total of n_c circuits (including the initial circuit before any adjustment) exist. After each adjustment, the S-parameters are measured and recorded. For the t-th circuit, there are K_t frequencies at which S-parameters are measured. Note that after each adjustment we may or may not recover the initial setting before making another adjustment.

The first step in the implementation is pre-processing of the available measurements to select responses and frequencies used for each circuit in the optimization. For the t-th circuit, any or all of the K_t frequencies may be chosen. For each S-parameter it is possible to select its magnitude or phase (real part or imaginary part) or both. After this step, we have K_t' frequencies and k_t measurements for the t-th circuit, where measurements correspond to different responses and different frequencies. As an example, suppose that S-parameters of a two-port network after one adjustment are measured at 5 frequencies. We have $K_2 = 5$. If the real and imaginary parts of S_{21} and S_{12} for the first and fifth points and the real and imaginary parts of all S-parameters for the third point are selected for the optimization, we have $K_2' = 3$ and $k_2 = 16$. It is clear that when the responses of the t-th circuit are calculated based on its model ($F_i^c(\mathbf{x}^t)$ in (5.12), where $i = 1, \ldots, k_t$), the user-defined module for simulation and sensitivity analysis of the network which calculates all

complex S-parameters at one frequency is called only K_t' times. For instance, in the above hypothetical example, the module is called 3 times for t = 2.

Based on the selection of responses at frequency i', $i' = 1, \ldots, K_t'$ for circuit t, we form a true-false code which simply shows whether a particular response was selected or not at i'. This true-false code will be used to form exactly k_t error functions corresponding to circuit t in the optimization.

As is emphasized in the term $F_i^c(\mathbf{x}^t)$, we have to ensure that the responses for each circuit are evaluated at its corresponding set of parameters. We propose setting up an index matrix as part of the implementation. Assume that there are n variable parameters in the circuit equivalent for the device (topology is preselected and fixed). These are the parameters which can change as a result of a physical adjustment. Based on the knowledge of the likely parameters that change after each adjustment, we set up an index matrix **B** with the following rules.

1) $\mathbf{B} = [b_{t,j}]$ is an $n_c \times n$ matrix.

2) We have $b_{1,j} = j$, $j = 1, \ldots, n$.

3) $b_{t,j}$ is an integer which identifies the position of the jth element of $\mathbf{x}^t$ ($\mathbf{x}^t$ has n elements) in the overall **x** vector of (5.13).

An example will clarify the above set up. Suppose that there are 5 variable parameters in the equivalent circuit. After the first adjustment, it is expected that the first and the third variable change. A second adjustment is made such that the 5th variable changes. If we make the second adjustment after recovering the initial setting, matrix **B** is given by

$$\mathbf{B} = \begin{bmatrix} 1 & 2 & 3 & 4 & 5 \\ 6 & 2 & 7 & 4 & 5 \\ 1 & 2 & 3 & 4 & 8 \end{bmatrix}. \tag{5.14}$$

On the other hand, if the second adjustment is performed without recovering the initial setting, we have

$$\mathbf{B} = \begin{bmatrix} 1 & 2 & 3 & 4 & 5 \\ 6 & 2 & 7 & 4 & 5 \\ 6 & 2 & 7 & 4 & 8 \end{bmatrix} . \tag{5.15}$$

In either case, $\mathbf{x}^1$ has 5 elements, $\mathbf{x}_a^2$ has two elements, $\mathbf{x}_a^3$ has one element and the overall $\mathbf{x}$ vector has eight elements. However, different circuits are achieved using (5.14) or (5.15) and therefore the index matrix plays an important role.

Using the elements of $\mathbf{B}$, the total number of variables and the number of elements in $\mathbf{x}_a^t$, $t = 2,\ldots, n_c$, are automatically obtained. We have

$$N_t = \max_j \{b_{t,j}\}, \tag{5.16}$$

where N_t denotes the total number of variables after the $(t-1)$th adjustment. Clearly, N_{n_c} is equal to the size of vector $\mathbf{x}$ in (5.13). The size of $\mathbf{x}_a^t$ denoted by a_t is calculated as

$$a_t = N_t - N_{t-1} . \tag{5.17}$$

Having defined matrix $\mathbf{B}$, we can recover the $\mathbf{x}^t$ vector for each circuit from the overall $\mathbf{x}$ in a straightforward manner. The jth element of $\mathbf{x}^t$ is given by

$$x_j^t = x_{\text{index}}, \qquad j = 1, \ldots, n, \tag{5.18a}$$

where

$$\text{index} = b_{t,j} . \tag{5.18b}$$

For instance, from (5.14), we get

$$\mathbf{x}^2 = \begin{bmatrix} x_6 \\ x_2 \\ x_7 \\ x_4 \\ x_5 \end{bmatrix} \quad \text{and} \quad \mathbf{x}^3 = \begin{bmatrix} x_1 \\ x_2 \\ x_3 \\ x_4 \\ x_8 \end{bmatrix} . \tag{5.19}$$

At this point, we can develop a simple algorithm corresponding to one iteration of the ℓ_1 optimization problem defined in (5.11). Given the $\mathbf{x}$ vector (initial guess for the first iteration and determined by the optimization routine in the subsequent iterations), we want to calculate all functions and gradients.

Step 1 For $t = 1, 2, \ldots, n_c$, execute Steps 2 to 6.

Step 2 Obtain $\mathbf{x}^t$ from $\mathbf{x}$ using (5.18).

Step 3 For $i' = 1, 2, \ldots, K_t'$, execute Steps 4 to 6.

Step 4 Call the user-defined module which calculates all S-parameters and n derivatives of each S-parameter at one frequency (i'th frequency of the t-th circuit), and at the parameter values in $\mathbf{x}^t$.

Step 5 Check the true-false code for each possible response at the i'th frequency and for each true answer, form one error function f_i^t.

Comment Based on each true answer, one f_i^t in (5.12) is formed and the index i which is initially zero is incremented by one. In this way, at $i' = K_t'$, i automatically reaches k_t.

Step 6 For $j = 1, 2, \ldots, n$, execute the following

$$\frac{\partial f_i^t}{\partial x_{index}} \leftarrow \frac{\partial f_i^t}{\partial x_j^t}$$

Comment For each f_i^t formed in Step 5, there are n derivatives which are readily calculated using the derivatives obtained from the user-defined module (derivatives of $F_i^c(\mathbf{x}^t)$) and weighting factor w_i^t. These n derivatives correspond to n elements of the $\mathbf{x}$ matrix which are positioned according to the index $b_{t,j}$. It is assumed that $\partial f_i^t/\partial \mathbf{x}$ has been initialized to zero, therefore, the derivatives of f_i^t with respect to the remaining elements of $\mathbf{x}$ (i.e., except the ones given by x_{index}) are zero.

5.3.4 Model Verification Using Multi-Circuit Measurements

Although the optimization problem formulated in (5.11) with the variables given in (5.13) enhances the unique identification of parameters, its limitations should be considered carefully. The limitations are related to the way in which model parameters $\mathbf{x}$ are controlled by physical adjustments on the device.

Parameters $\mathbf{x}$ are generally controlled by some physical parameters $\boldsymbol{\phi} \triangleq [\phi_1 \ \phi_2 \ \ldots \ \phi_\ell]^T$. For instance, in active device modelling intrinsic network parameters are controlled by bias voltages or currents, or in waveguide filters the penetration of a screw may control a particular element of the network model. The actual functional relationship between $\boldsymbol{\phi}$ and $\mathbf{x}$ may not be known, however, we often know which element or elements of $\mathbf{x}$ are affected by an adjustment on an element of $\boldsymbol{\phi}$. The success of the optimization problem (5.11) is dependent on this knowledge, i.e., after each physical adjustment, the correct candidates should be present in $\mathbf{x}_a$. To ensure this, we should overestimate the number of model parameters which are likely to change after adjusting an element of $\boldsymbol{\phi}$. On the other hand, we would like to have as few elements as possible in each $\mathbf{x}_a$ vector, so that the increase in the number of variables can be overcompensated for by the increase in rank of matrix $\mathbf{J}$ resulting from the addition of new measurements.

In practice, by overestimating the number of elements in $\mathbf{x}_a$ or by making physical adjustments which indeed affect many model parameters, (a change in bias voltage may affect all intrinsic parameters of a transistor model) the optimization problem of (5.11) may not be better- conditioned than the traditional single circuit optimization. This means that the chance for unique identification of parameters may not increase. However, multi-circuit measurements could still be used as an alter-

native to selecting different or more frequency points as may be done in the single circuit approach.

We now formulate another optimization problem which either verifies the model parameters obtained or proves their inconsistency with respect to physical adjustments. The information about which elements of $\mathbf{x}$ are affected by adjusting an element of $\boldsymbol{\phi}$, although used to judge the consistency of results, is not required a priori. Therefore, the formulation is applicable to all practical cases.

Suppose that we make an easy-to-achieve adjustment on an element of $\boldsymbol{\phi}$ such that one or a few components of $\mathbf{x}$ are changed in a dominant fashion and the rest remain constant or change slightly. Consider the following ℓ_1 optimization problem

$$\underset{\mathbf{x}}{\text{minimize}} \sum_{t=1}^{2} \sum_{i=1}^{k_t} \left| f_i^t \right| + \sum_{j=1}^{n} \beta_j \left| x_j^1 - x_j^2 \right| , \tag{5.20}$$

where β_j represents an appropriate weighting factor and $\mathbf{x}$ is a vector which contains circuit parameters of both the original and perturbed networks, i.e.,

$$\mathbf{x} = \begin{bmatrix} \mathbf{x}^1 \\ \mathbf{x}^2 \end{bmatrix} . \tag{5.21}$$

Notice that, despite its appearance, (5.20) can be rewritten easily in the standard ℓ_1 optimization form, which is minimizing $\Sigma |\cdot|$, by taking the individual functions from either the nonlinear part f_i^t,or the linear part $x_j^1 - x_j^2$.

The above formulation has the following properties:

1) Considering only the first part of the objective function, the formulation is equivalent to performing two optimizations, i.e., matching the calculated response of the original circuit model with its corresponding measurements and repeating the procedure for the perturbed circuit.

2) By adding the second part to the objective function, we take advantage of the knowledge that only one or a few model parameters should change dominantly by perturbing a component of $\boldsymbol{\phi}$. Therefore, we penalize the objective function for any difference between $\mathbf{x}^1$ and $\mathbf{x}^2$. However, since the ℓ_1 norm is used, one or a few large changes from $\mathbf{x}^1$ to $\mathbf{x}^2$ are still allowed. Discussions on the use of the ℓ_1 norm in Chapter 2 should be referred to.

The confidence in the validity of the equivalent circuit parameters increases if a) an optimization using the objective function of (5.20) results in a reasonable match between calculated and measured responses for both circuits 1 and 2 (original and perturbed) and b) the examination of the solution vector $\mathbf{x}$ reveals changes from $\mathbf{x}^1$ to $\mathbf{x}^2$ which are consistent with the adjustment to $\boldsymbol{\phi}$, i.e., only the expected components have changed significantly. We can build upon our confidence even more by generalizing the technique to more adjustments to $\boldsymbol{\phi}$, i.e., formulating the optimization problem as

$$\underset{\mathbf{x}}{\text{minimize}} \sum_{t=1}^{n_c} \sum_{i=1}^{k_t} \left| f_i^t \right| + \sum_{t=2}^{n_c} \sum_{j=1}^{n} \beta_j^t \left| x_j^1 - x_j^t \right| , \tag{5.22}$$

where n_c circuits and their corresponding sets of responses, measurements and parameters are considered and the first circuit is the reference model before any adjustment to $\boldsymbol{\phi}$. In this case, $\mathbf{x}$ is given by

$$\mathbf{x} = \begin{bmatrix} \mathbf{x}^1 \\ \mathbf{x}^2 \\ \cdot \\ \cdot \\ \cdot \\ \mathbf{x}^{n_c} \end{bmatrix} . \tag{5.23}$$

By observing inconsistencies in changes of $\mathbf{x}$ with the actual change in $\boldsymbol{\phi}$, the new technique exposes the existence of nonideal effects not taken into account in the model. Having confidence in the parameters as well as observing a good match between measured and modelled responses means that the parameters and the model are valid, even if different responses or different frequency ranges are used.

The implementation of optimization problem (5.22) with variables given in (5.23) is similar to the implementation of Section 5.3.3. The structure of $\mathbf{x}$ is simpler in this case and the elements of the index matrix $\mathbf{B}$ are automatically given by

$$b_{t,j} = (t-1) \times n + j, \qquad t = 1, ..., n_c, \quad j = 1, ..., n . \tag{5.24}$$

5.4 MODELLING OF MULTI-COUPLED CAVITY FILTERS

In Chapter 4 we discussed the multi-coupled cavity filters in the context of multiplexer design. The impedance matrix description of the filters and dissipation and dispersion effects were presented in detail. Modelling of the filters, i.e., determining the coupling values by processing the measured responses such as input and output return loss, insertion loss and group delay, is of significance in both filter and multiplexer tuning. We will further comment on the tuning problem in Section 5.6.

5.4.1 6th Order Filter Example

A 6th order multi-coupled cavity filter centered at 11785.5 MHz with a 56.2 MHz bandwidth is considered. Measurements on input and output return loss, insertion loss and group delay of an optimally tuned filter and the same filter after a deliberate adjustment on the screw which dominantly controls coupling M_{12}, were provided by ComDev (1985). Although the passband return loss changes significantly, we anticipate that such a physical adjustment affects only model parameters

M_{12}, M_{11} and M_{22} (the last two correspond to cavity resonant frequencies) in a dominant fashion, possibly with slight changes in other parameters.

Using the new technique described in this chapter, we simultaneously processed measurements on passband return loss (input reflection coefficient with a weighting of 1), and stopband insertion loss (with a weighting of 0.05) of both filters, i.e., the original and perturbed models. The ℓ_1 algorithm with exact gradients was used. The evaluation of sensitivities is discussed in detail by Bandler, Chen and Daijavad (1986a). The model parameters identified for the two filters are summarized in Table 5.1. Figs. 5.3 and 5.4 illustrate the measured and modelled responses of the original filter and the filter after adjustment, respectively. An examination of the results in Table 5.1 and Figs. 5.3-5.4 shows that not only an excellent match between measured and modelled responses has been achieved, but also the changes in parameters are completely consistent with the actual physical adjustment. Therefore, by means of only one optimization, we have built confidence in the validity of the equivalent circuit parameters. The problem involved 84 nonlinear functions (42×2 responses for original and perturbed filters) and 12 linear functions (change in parameters of two circuit equivalents) and 24 variables. The solution was achieved in 72 seconds of CPU time on the VAX 11/780 system.

5.4.2 8th Order Filter Example

In this example, we used the new modelling technique to reject a certain set of parameters obtained for an 8th-order multi-cavity filter by proving their inconsistent behaviour with respect to physical adjustments. We then improved the

TABLE 5.1

RESULTS FOR THE 6TH ORDER FILTER EXAMPLE

Coupling	Original Filter	Perturbed Filter	Change in Parameter
M_{11}	-0.0473	-0.1472	-0.0999*
M_{22}	-0.0204	-0.0696	-0.0492*
M_{33}	-0.0305	-0.0230	0.0075
M_{44}	0.0005	0.0066	0.0061
M_{55}	-0.0026	0.0014	0.0040
M_{66}	0.0177	-0.0047	-0.0224
M_{12}	0.8489	0.7119	-0.1370*
M_{23}	0.6064	0.5969	-0.0095
M_{34}	0.5106	0.5101	-0.0005
M_{45}	0.7709	0.7709	0.0000
M_{56}	0.7898	0.7806	-0.0092
M_{36}	-0.2783	-0.2850	-0.0067

* significant change in parameter value.

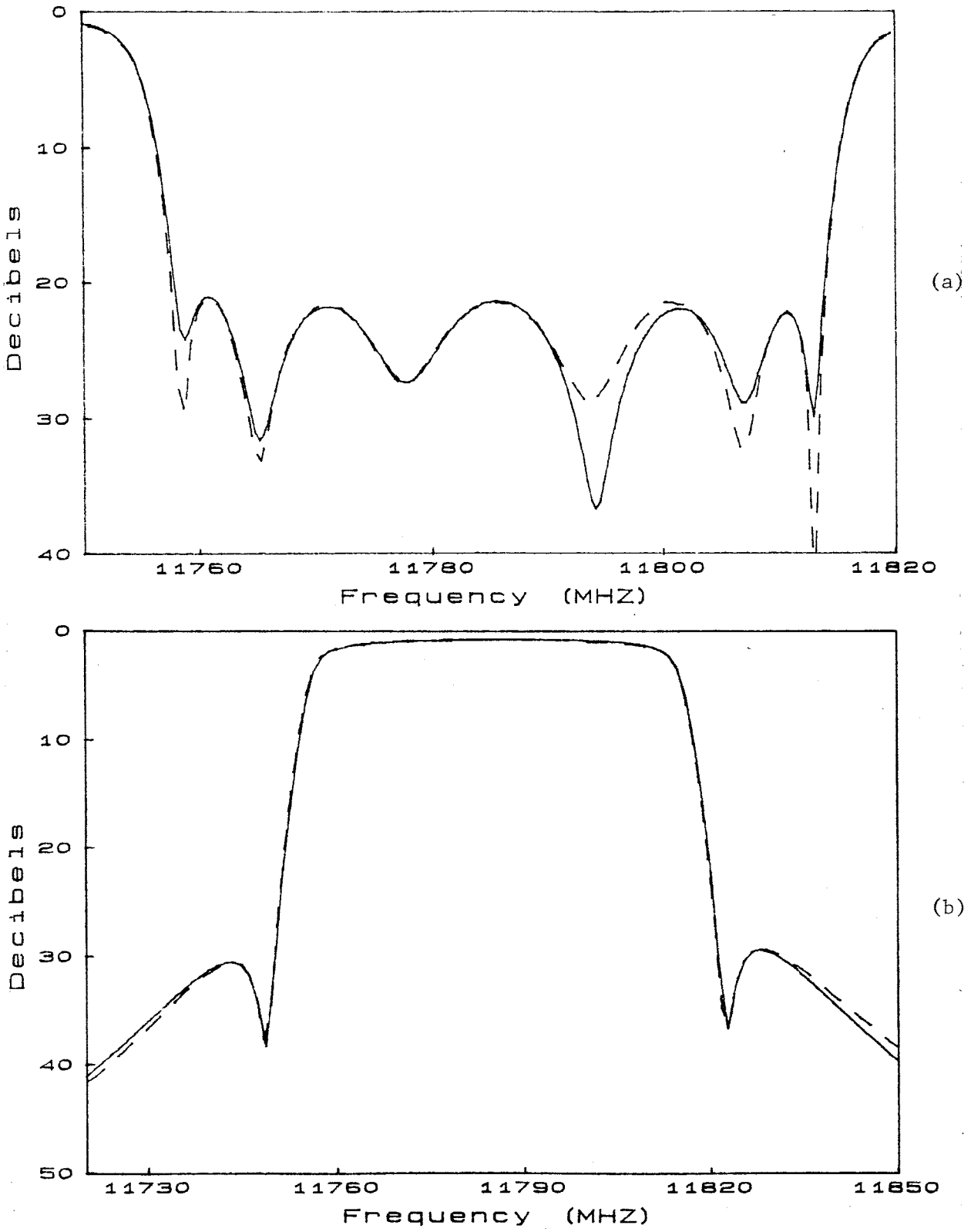

Fig. 5.3 Input return loss (a) and insertion loss (b) responses of the 6th order filter before adjusting the screw. The solid line represents the modelled response and the dashed line shows measurement data.

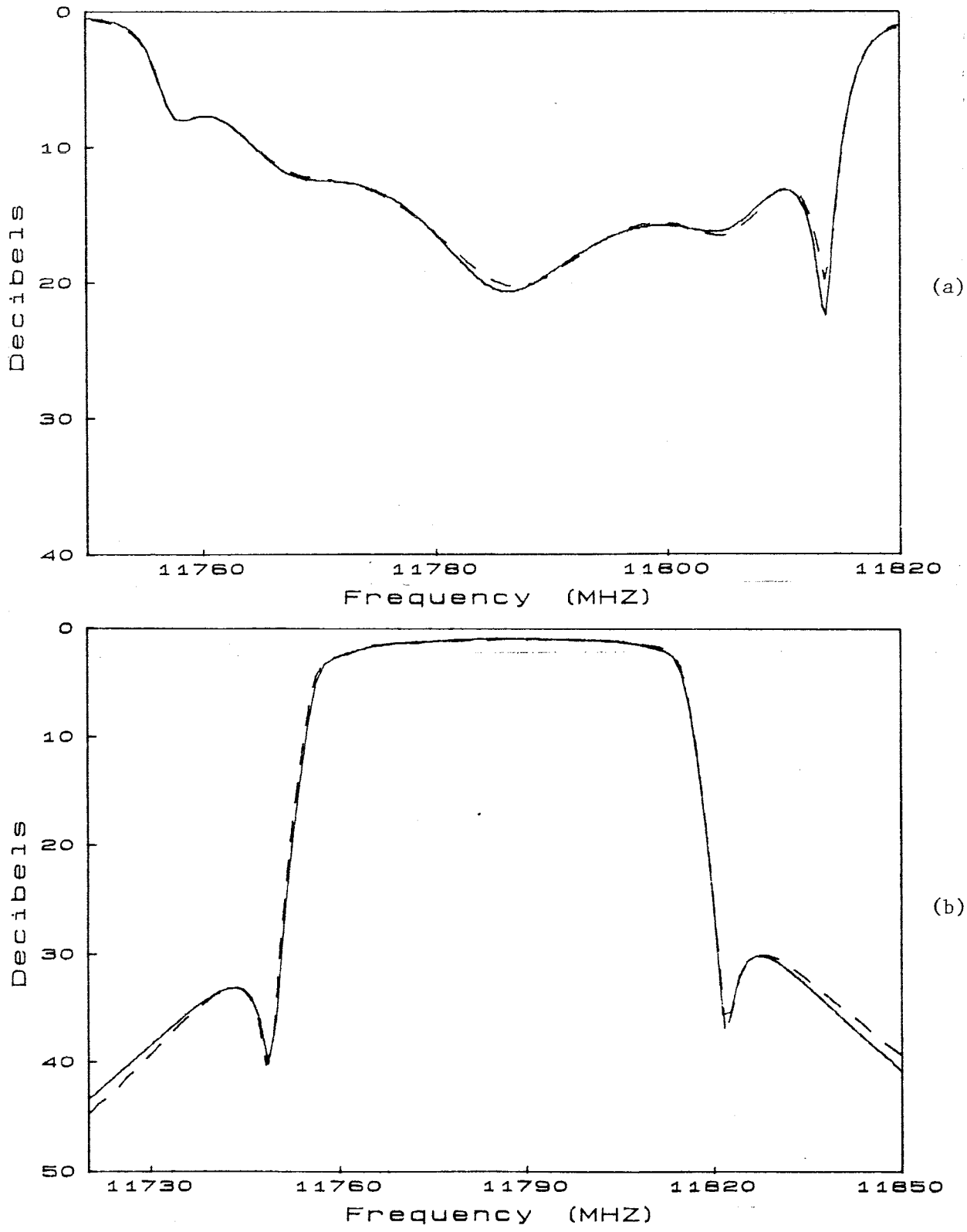

Fig. 5.4 Input return loss (a) and insertion loss (b) responses of the 6th order filter after adjusting the screw. The solid line represents the modelled response and the dashed line shows measurement data.

model by including an ideally zero stray coupling in the model and obtained parameters which not only produce a good match between measured and modelled responses, but also behave consistently when perturbed by a physical adjustment.

The 8th-order filter is centered at 11902.5 MHz with a 60 MHz bandwidth. Return loss and insertion loss measurements of an optimally tuned filter and the same filter after an adjustment on the iris which dominantly controls coupling M_{23}, were provided by ComDev (1985). Based on the physical structure of the filter, screw couplings M_{12}, M_{34}, M_{56} and M_{78}, the iris couplings M_{23}, M_{14}, M_{45}, M_{67} and M_{58}, as well as all cavity resonant frequencies and input-output couplings (transformer ratios) are anticipated as possible non-zero parameters to be identified.

In the first attempt, the stray coupling M_{36} was ignored and passband measurements on input and output return loss and stopband isolation for both filters were used to identify the parameters of the filters. The parameters are summarized in Table 5.2. An examination of the results shows no apparent trend for the change in parameters, i.e., it would have been impossible to guess the source of perturbation (adjustment on the iris controlling M_{23}) from these results. This is the kind of inconsistency that would not have been discovered if only the original circuit had been considered.

In a second attempt, we included the stray coupling M_{36} in the circuit model and processed exactly the same measurements as before. Table 5.2 also contains the identified parameters of the two filters for this case. A comparison of the original and perturbed filter parameters reveals that the significant change in couplings M_{12}, M_{23} and M_{34} and cavity resonant frequencies M_{22} and M_{33} is absolutely consistent with the actual adjustment on the iris, i.e., by inspecting the

TABLE 5.2

RESULTS FOR THE 8TH ORDER FILTER EXAMPLE

	M_{36} ignored		M_{36} present	
Coupling	Original	Perturbed	Original	Perturbed
M_{11}	-0.0306	-0.1122	-0.0260	-0.0529
M_{22}	0.0026	-0.0243	0.0354	0.6503*
M_{33}	-0.0176	-0.0339	-0.0674	-0.6113*
M_{44}	-0.0105	-0.0579	-0.0078	-0.0151
M_{55}	-0.0273	-0.0009	-0.0214	0.0506
M_{66}	-0.0256	0.0457	-0.0179	-0.0027
M_{77}	-0.0502	0.0679	-0.0424	-0.0278
M_{88}	-0.0423	0.0594	-0.0426	-0.0272
M_{12}	0.7789	0.7462	0.3879	0.2876*
M_{23}	0.8061	0.8376	0.9990	0.8160*
M_{34}	0.4460	0.4205	0.0270	-0.1250*
M_{45}	0.5335	0.5343	0.4791	0.5105
M_{56}	0.5131	0.5373	0.5006	0.5026
M_{67}	0.7260	0.7469	0.6495	0.6451
M_{78}	0.8330	0.8476	0.8447	0.8463
M_{14}	0.3470	-0.3582	-0.7648	-0.7959
M_{58}	-0.1995	-0.1892	-0.1000	-0.0953
M_{36}	-	-	0.1314	0.1459

input and output couplings: $n_1^2 = n_2^2 = 1.067$

* significant change in parameter value.

change in parameters, it is possible to deduce which iris has been adjusted. The measured and modelled input return loss and insertion loss responses of the two filters are illustrated in Figs. 5.5 and 5.6. It is interesting to mention that the match between measured and modelled responses in the first attempt where M_{36} was ignored and inconsistent parameters were found, is almost as good as the match in Figs. 5.5 and 5.6. This justifies the essence of the new modelling technique which attempts to identify the most consistent set of parameters among many that produce a reasonable match between measured and calculated responses.

5.5 FET MODELLING

5.5.1 A Brief Introduction

Demand has been increasing for low-noise receivers and driver amplifiers for commercial satellite communications, especially at X-band frequencies. The frequency range from 10.7 to 12.7 GHz covers the international, domestic, and direct broadcast communication bands. The GaAs MMIC (monolithic microwave integrated circuits) approach offers the potential for lower-cost amplification modules and a significant reduction in component size compared to hybrid MIC modules. MMIC fabrication also provides performance uniformity, reduced phase variation, and potentially higher reliability. Hung et al. (1985) have described design considerations, fabrication process, and performance for the newly developed MMIC amplifier modules operating in the X-band.

Design of these MMIC's begins with the development of an equivalent circuit model for the FET device. Fig. 5.7 shows the equivalent circuit of a carrier-mounted FET. This circuit equivalent (Curtice and Camisa 1984) or slightly different circuits used by other researchers are small-signal models. For large-signal analysis

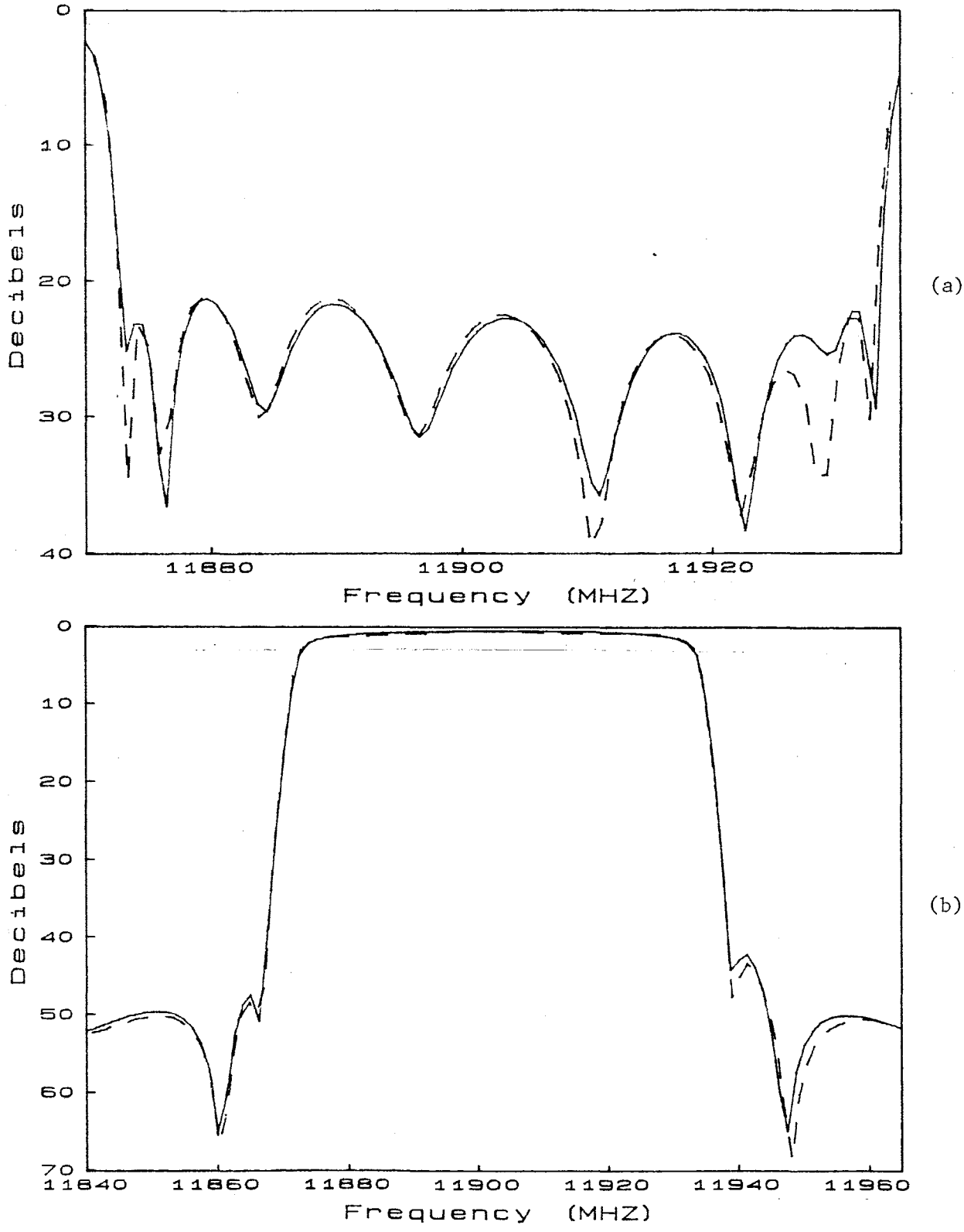

Fig. 5.5 Input return loss (a) and insertion loss (b) responses of the 8th order filter before adjusting the iris. The solid line represents the modelled response and the dashed line shows measurement data.

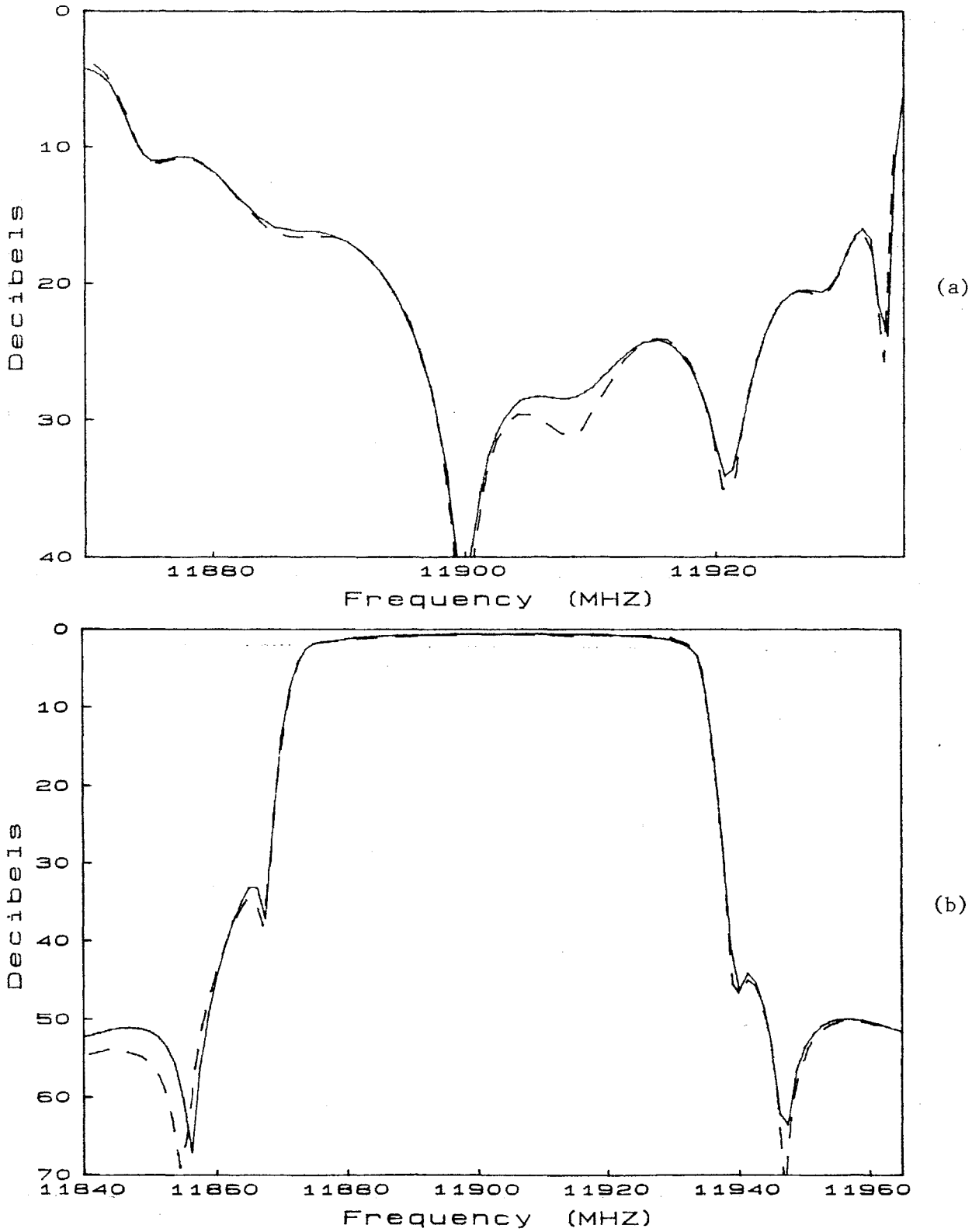

Fig. 5.6 Input return loss (a) and insertion loss (b) responses of the 8th order filter after adjusting the iris. The solid line represents the modelled response and the dashed line shows measurement data.

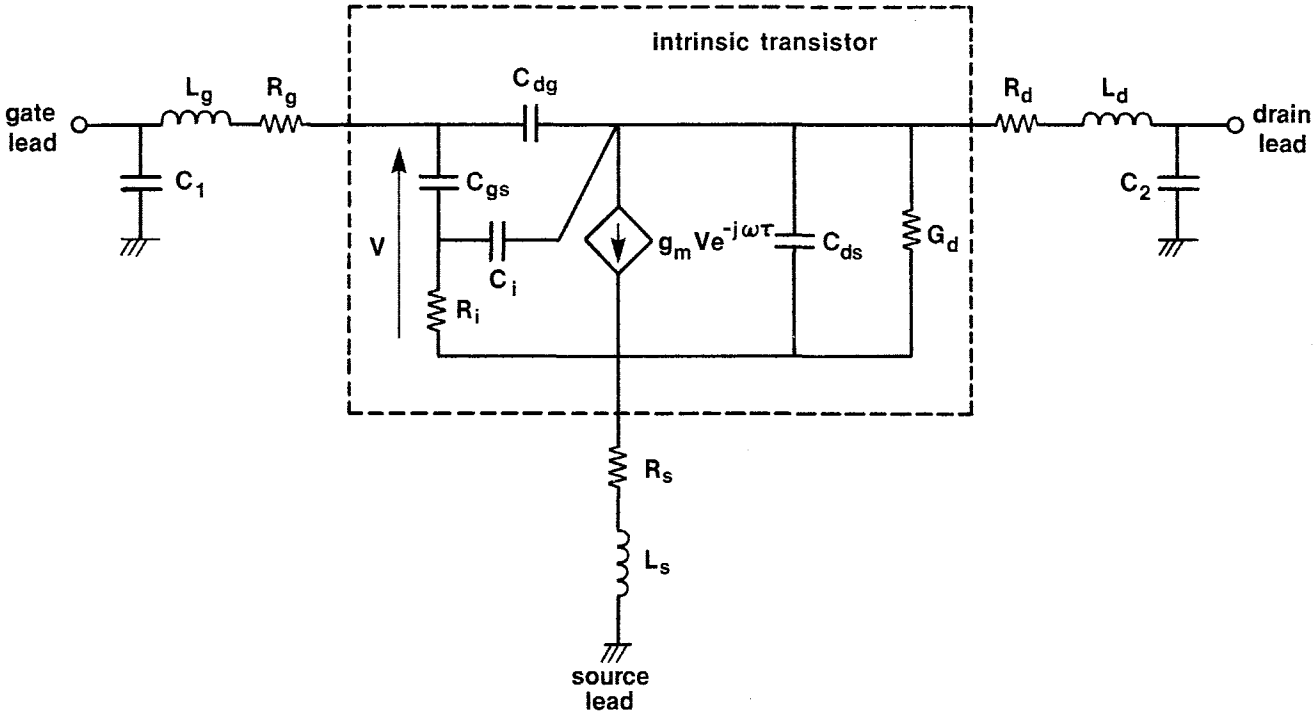

Fig. 5.7 Equivalent circuit of a carrier-mounted FET.

of GaAs FET amplifiers, a nonlinear circuit equivalent is used and time-domain analysis is performed. Nonlinear models are subjects of interest in high power FET's (see for example, Curtice and Ettenberg 1985; Materka and Kacprzak 1985), however, their analysis is out of the scope of this thesis. To appreciate the physical dimensions for a π-FET configuration, Fig. 5.8 illustrates the cross section of the FET structure.

In this section, we apply the new modelling technique described previously to determine the parameters of the equivalent circuit 5.7 from S-parameter measurements. Unique identification of parameters for the FET equivalent circuit is of prime interest to researchers at the present time, since most of the available software runs into diffculties in doing so.

5.5.2 NEC700 Example

Device NEC700, for which measurement data is supplied with TOUCHSTONE, was considered. Using S-parameter data, single-circuit modelling with the ℓ_1 objective was performed. The goal of this experiment was to prepare for the more complicated multi-circuit case by testing some common formulas and assumptions. The equivalent circuit of Fig. 5.7 at normal operating bias (including the carrier) with 16 possible variables was used. An ℓ_1 optimization with exact gradients, which are evaluated using the formulas derived in Chapter 3 was performed. Measurement data was taken from 4 to 20 GHz. Table 5.3 summarizes the identified parameters and Figs. 5.9a, 5.9b and 5.9c illustrate the measured and modelled responses.

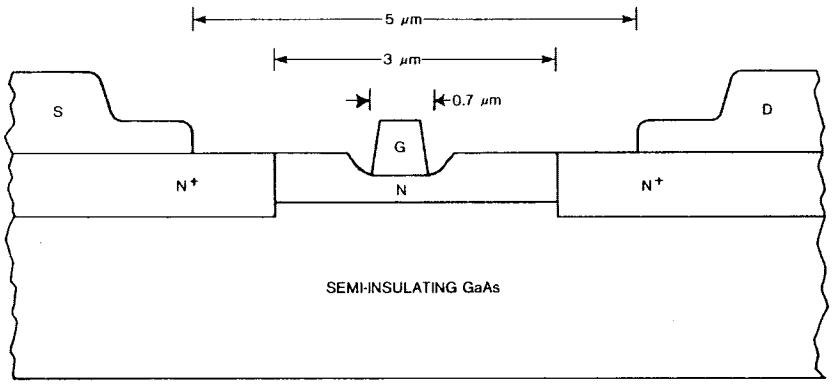

Fig. 5.8 Cross section of a n-FET structure (Reproduced from Hung et al. 1985).

TABLE 5.3

RESULTS FOR THE NEC700 FET EXAMPLE

Parameter		Value
C_1	(pF)	0.0448
C_2	(pF)	0.0058
C_{dg}	(pF)	0.0289
C_{gs}	(pF)	0.2867
C_{ds}	(pF)	0.0822
C_i	(pF)	0.0100
R_g	(Ω)	3.5000
R_d	(Ω)	2.0000
R_s	(Ω)	3.6270
R_i	(Ω)	7.3178
$G_d{}^{-1}$	(kΩ)	0.2064
L_g	(nH)	0.0585
L_d	(nH)	0.0496
L_s	(nH)	0.0379
g_m	(S)	0.0572
τ	(ps)	3.1711

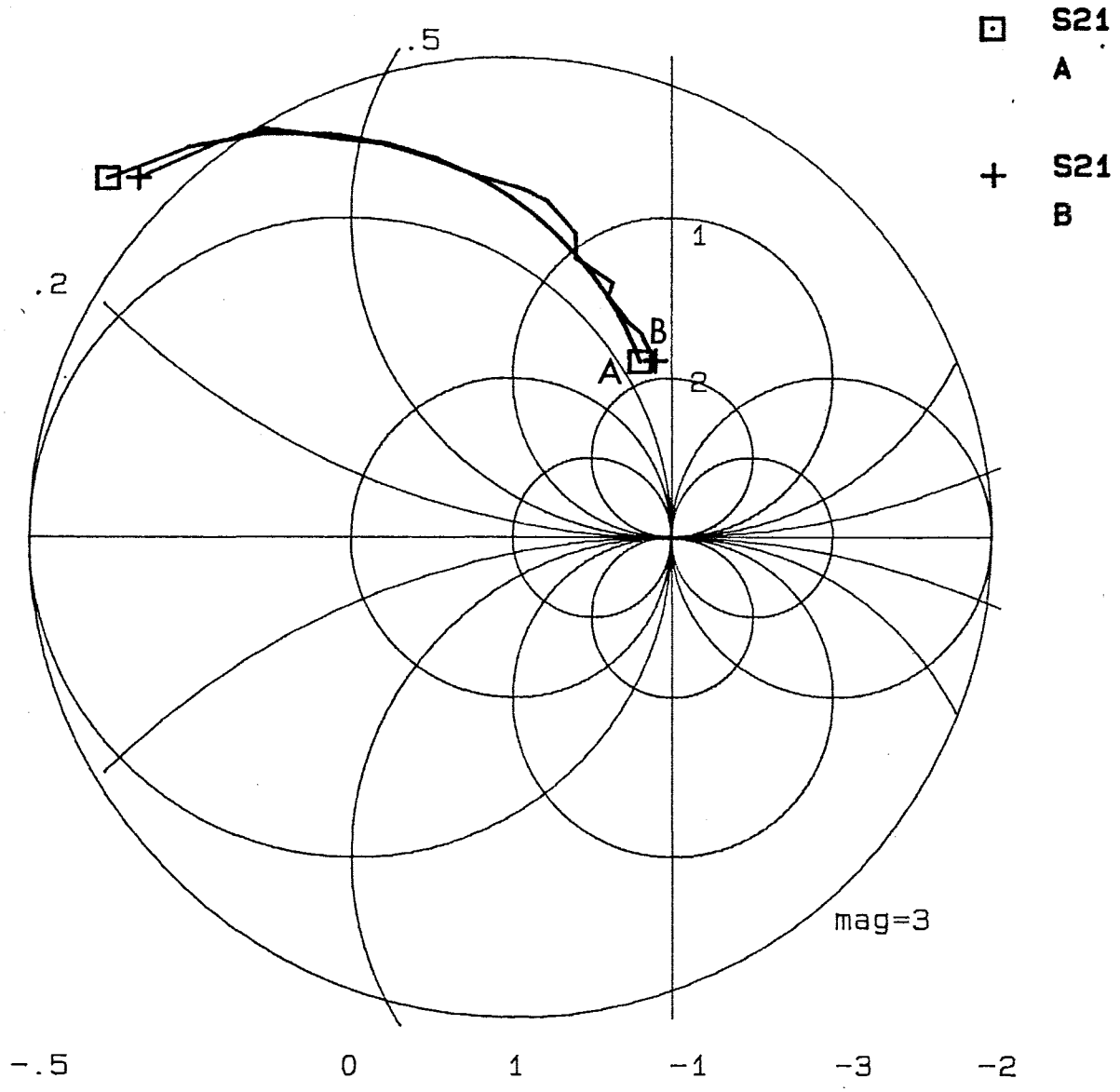

Fig. 5.9a Smith Chart display of S_{21} in modelling of NEC700. The frequency range is from 4 to 20 GHz. Points A and B mark the high frequency end of modelled and measured responses, respectively.

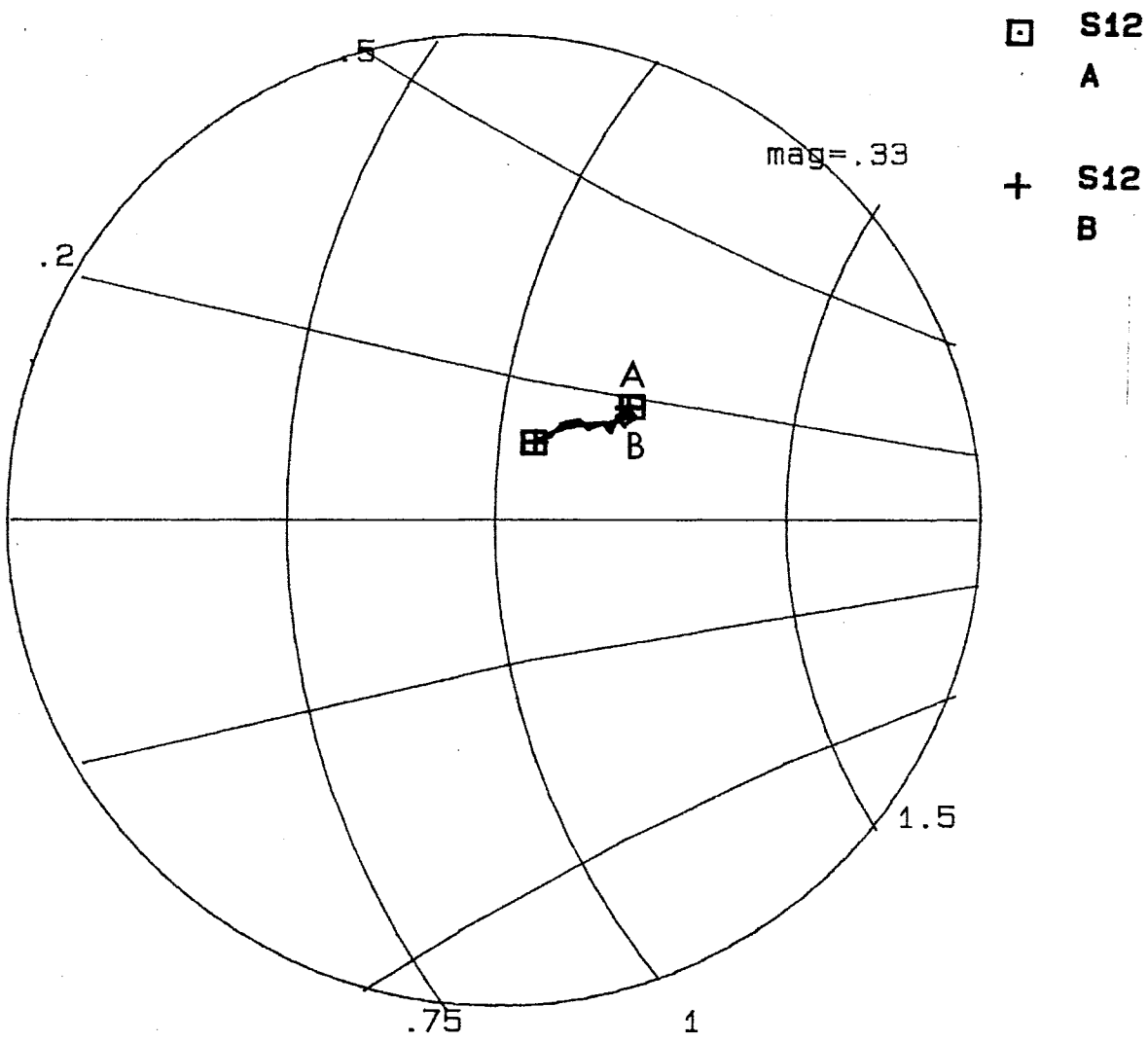

Fig. 5.9b Smith Chart display of S_{12} in modelling of NEC700. The frequency range is from 4 to 20 GHz. Points A and B mark the high frequency end of modelled and measured responses, respectively.

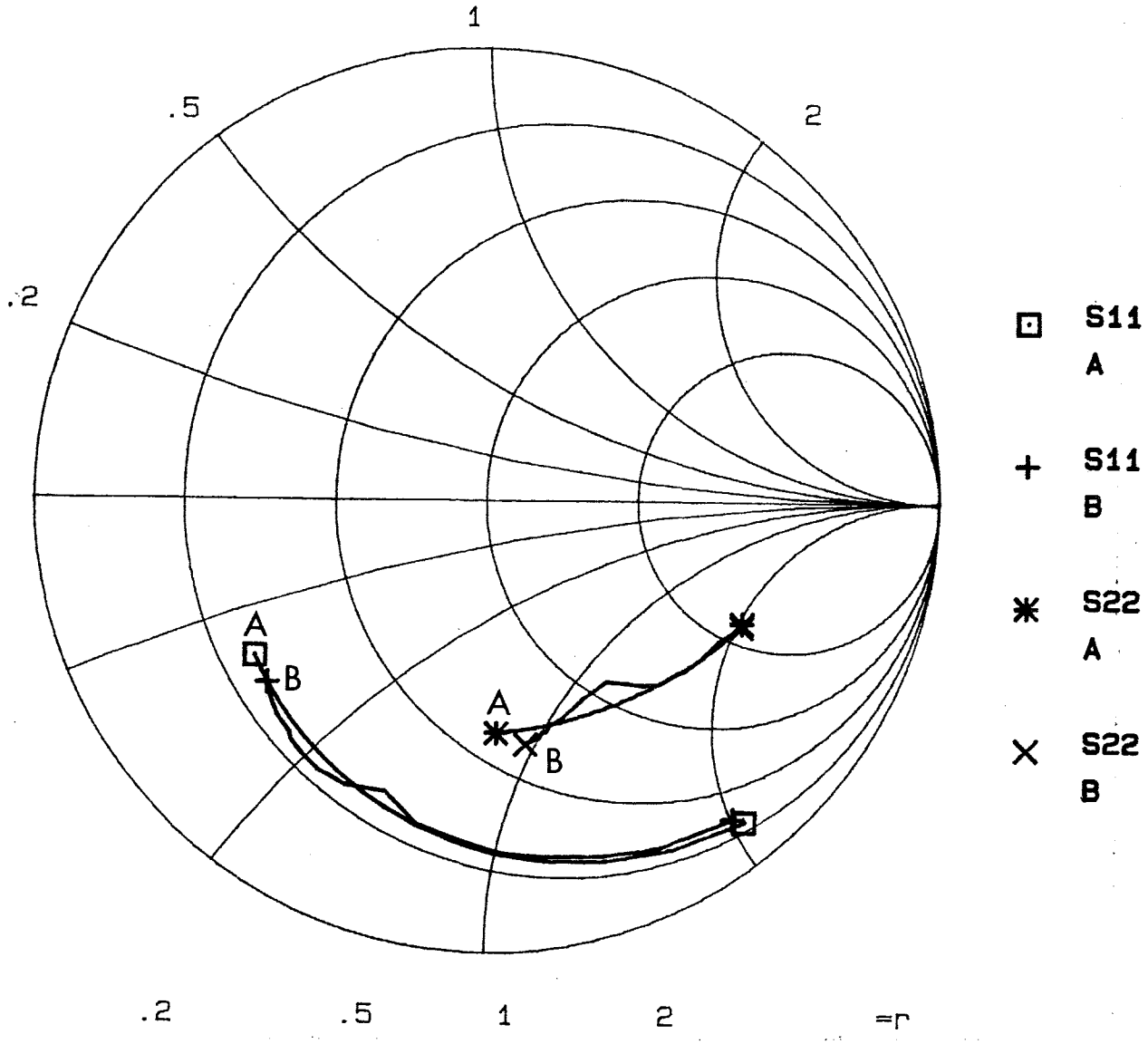

Fig. 5.9c Smith Chart display of S_{11} and S_{22} in modelling of NEC700. The frequency range is from 4 to 20 GHz. Points A and B mark the high frequency end of modelled and measured responses, respectively.

5.5.3 B1824-20C Example

Using S-parameter data for the device B1824-20C from 4 to 18 GHz, Curtice and Camisa (1984) have achieved a very good model for the FET chip. They have used the traditional least squares optimization of responses utilizing SUPER-COMPACT. Their success is due to the fact that they have reduced the number of possible variables in Fig. 5.7 from 16 to 8 by using dc and zero-bias measurements. We created two sets of artificial S-parameter measurements with TOUCHSTONE: one set using the parameters reported by Curtice and Camisa (operating bias $V_{ds} = 8.0$ V, $V_{gs} = -2.0$ V and $I_{ds} = 128.0$ mA) and the other by changing the values of C_1, C_2, L_g and L_d to simulate the effect of taking different reference planes for the carriers. Both sets of data are shown in Fig. 5.10, where the S-parameters of the two circuits are plotted on a Smith Chart.

Using the technique described in this chapter, we processed the measurements on the two circuits simultaneously by minimizing the function defined in (5.20). The objective of this experiment is to show that even if the equivalent circuit parameters were not known, as is the case using real measurements, the consistency of the results would be proved only if the intrinsic parameters of the FET remain unchanged between the two circuits. This was indeed the case for the experiment performed. Although the maximum number of possible variables, namely 32 (16 for each circuit), were allowed for in the optimization, the intrinsic parameters were found to be the same between the two circuits and, as expected, C_1, C_2, L_g and L_d changed from circuit 1 to 2. Table 5.4 summarizes the parameter values obtained. The problem involved 128 nonlinear functions (real and imaginary parts of 4 S-parameters, at 8 frequencies, for two circuits), 16 linear functions and 32 variables. The CPU time on the VAX 11/780 system was 79 seconds.

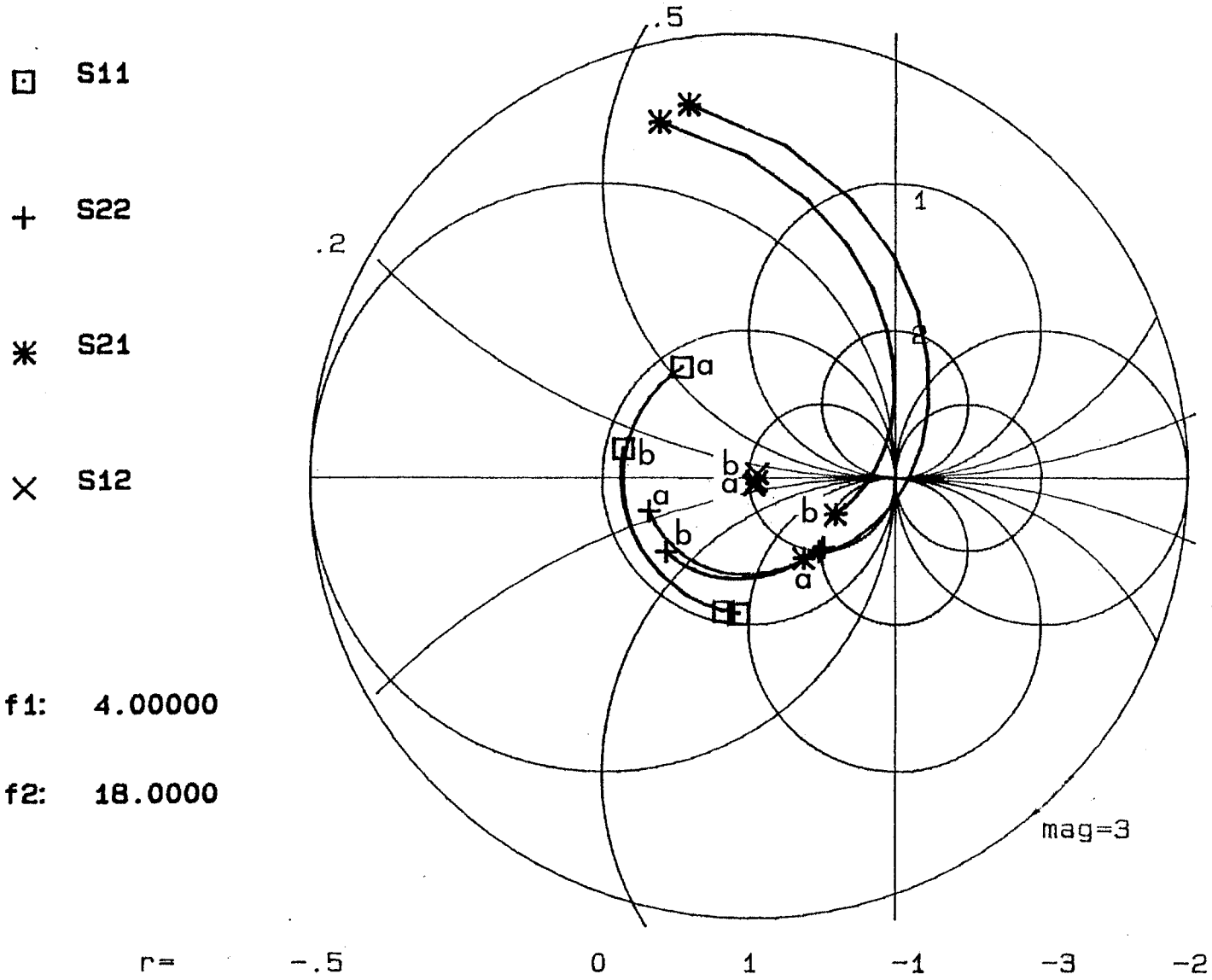

Fig. 5.10 Smith Chart display of S_{11}, S_{22}, S_{12} and S_{21} for the carrier mounted FET device B1824-20C, before and after adjustment parameters. Points a and b mark the high frequency end of original and perturbed network responses, respectively.

TABLE 5.4

RESULTS FOR THE GaAs FET B1824-20C EXAMPLE

Parameter		Original Circuit	Perturbed Circuit
C_1	(pF)	0.0440	0.0200*
C_2	(pF)	0.0389	0.0200*
C_{dg}	(pF)	0.0416	0.0416
C_{gs}	(pF)	0.6869	0.6869
C_{ds}	(pF)	0.1900	0.1900
C_i	(pF)	0.0100	0.0100
R_g	(Ω)	0.5490	0.5490
R_d	(Ω)	1.3670	1.3670
R_s	(Ω)	1.0480	1.0480
R_i	(Ω)	1.0842	1.0842
G_d^{-1}	(kΩ)	0.3761	0.3763
L_g	(nH)	0.3158	0.1500*
L_d	(nH)	0.2515	0.1499*
L_s	(nH)	0.0105	0.0105
g_m	(S)	0.0423	0.0423
τ	(ps)	7.4035	7.4035

* significant change in parameter value.

5.6 TUNING BASED ON EFFICIENT MODELLING

5.6.1 Fundamental Concepts

In this section, we discuss the possibility of using an efficient modelling technique in conjunction with algorithms developed for postproduction tuning of microwave devices. In particular, we have in mind the tuning of such devices for which the physical parameters used in tuning (e.g., physical dimensions, screw penetration, etc.) are different in nature from the model parameters of the equivalent circuit.

Bandler and Salama (1985b) have discussed the use of a functional approach to microwave postproduction tuning. In their approach, the physical parameters used for tuning are the circuit model parameters themselves (actually, a subset with the smallest possible number of parameters) with uncertainties due to tolerances associated with them. Without attempting to determine parameters of the manufactured circuit, i.e., finding the network element values, the functional tuning algorithms carry out a sequence of tunable parameter adjustments until the performance specifications for the device are met.

Based on the notation used earlier in this chapter for model and physical parameters, i.e., $\mathbf{x}$ and $\boldsymbol{\phi}$, respectively, in Bandler and Salama's approach $\boldsymbol{\phi}$ is a subset of $\mathbf{x}$ with unknown values throughout the tuning process.

Now, consider the tuning of a device for which the physical parameters are completely different in nature from the model parameters. For instance, the physical parameter is the size of an iris or the amount of a screw penetration in a cavity and the model parameter is a coupling value in coupled cavity filters. As a special case, the physical parameters could be the controllable nominal values of unknown circuit model parameters. An analytical relationship between $\boldsymbol{\phi}$ and $\mathbf{x}$ may not exist or may

be very difficult to achieve in a global sense. Although it is possible to carry out a functional tuning directly using $\boldsymbol{\phi}$, i.e., adjusting $\boldsymbol{\phi}$ until specifications on responses are met without considering any circuit equivalents, the approach could be extremely inefficient and time-consuming if we start with a highly detuned device. This is due to the highly nonlinear relationship between circuit responses and physical parameters. A more efficient tuning algorithm for such devices can be developed if efficient and reliable modelling is possible.

The nonlinear relationship between circuit reponses and $\boldsymbol{\phi}$ can be broken down to a nonlinear relationship between responses and $\mathbf{x}$ and a mildly nonlinear relationship between $\mathbf{x}$ and $\boldsymbol{\phi}$. Since the responses are analytically calculated from $\mathbf{x}$, and conversely $\mathbf{x}$ can be found from the responses using a reliable modelling technique, the tuning is simplified to a less nonlinear problem which is effectively from $\boldsymbol{\phi}$ to $\mathbf{x}$ instead of from $\boldsymbol{\phi}$ to responses.

Apart from identifying $\mathbf{x}$ from responses at each stage of the tuning process, modelling is also used to establish a local relationship between $\mathbf{x}$ and $\boldsymbol{\phi}$ at the start of the tuning process. This relationship which predicts the change in $\mathbf{x}$ as a result of the change in $\boldsymbol{\phi}$ is updated in the tuning process. The modelling technique described in this chapter was used to establish a relationship between physical and model parameters of a multi-coupled cavity filter. The results verified that the relationship between $\mathbf{x}$ and $\boldsymbol{\phi}$ is indeed mildly nonlinear (in fact, it is almost linear) and therefore, a tuning algorithm involving the intermediate model parameters is more efficient than a direct functional tuning algorithm for such filters.

5.6.2 Example in Establishing the Relationship Between Physical and Model Parameters

Consider a 6th order multi-coupled cavity filter centered at 11783 MHz with a 56 MHz bandwidth. The estimated unloaded Q-factor for the filter is 7600. From the physical structure of the filter, we have screw couplings M_{12}, M_{34} and M_{56}, and iris couplings M_{23}, M_{45} and M_{36}. We want to establish the relationship between the position of the screws (their penetrations in the cavities) which are physically adjustable, and the coupling values which are the model parameters in this case. To achieve this, a filter was manually tuned to achieve a reference optimum response. Starting from this reference tuned filter, the screw which is supposed to control coupling M_{12} was adjusted four times; twice in the clockwise direction (screw penetrates more in the cavity) with 90 degree and 180 degree turns as compared to the reference, and twice in the anticlockwise direction, again with 90 and 180 degree turns. After each adjustment, filter responses (input-output return loss, insertion loss and group delay) were measured and recorded. Using the modelling technique of this chapter, the measurements were processed (passband input return loss and stopband insertion loss) to identify filter parameters (coupling values) in each case.

Figure 5.11 illustrates the variation of coupling values (model parameters) as the position of the screw changes (adjustment on the physical parameter). Clearly, the coupling value M_{12} increases almost linearly as the screw penetrates more in the cavity while the other couplings remain almost constant (slight changes). The behaviour is highly desirable as far as the tuning is concerned. The experiment was repeated with the screws controlling M_{34} and M_{56}. The reference filter (angle zero for the screw) was the same optimally tuned filter as used in the M_{12} case. The plots of model parameters versus change in physical parameters are shown in Figs. 5.12 and

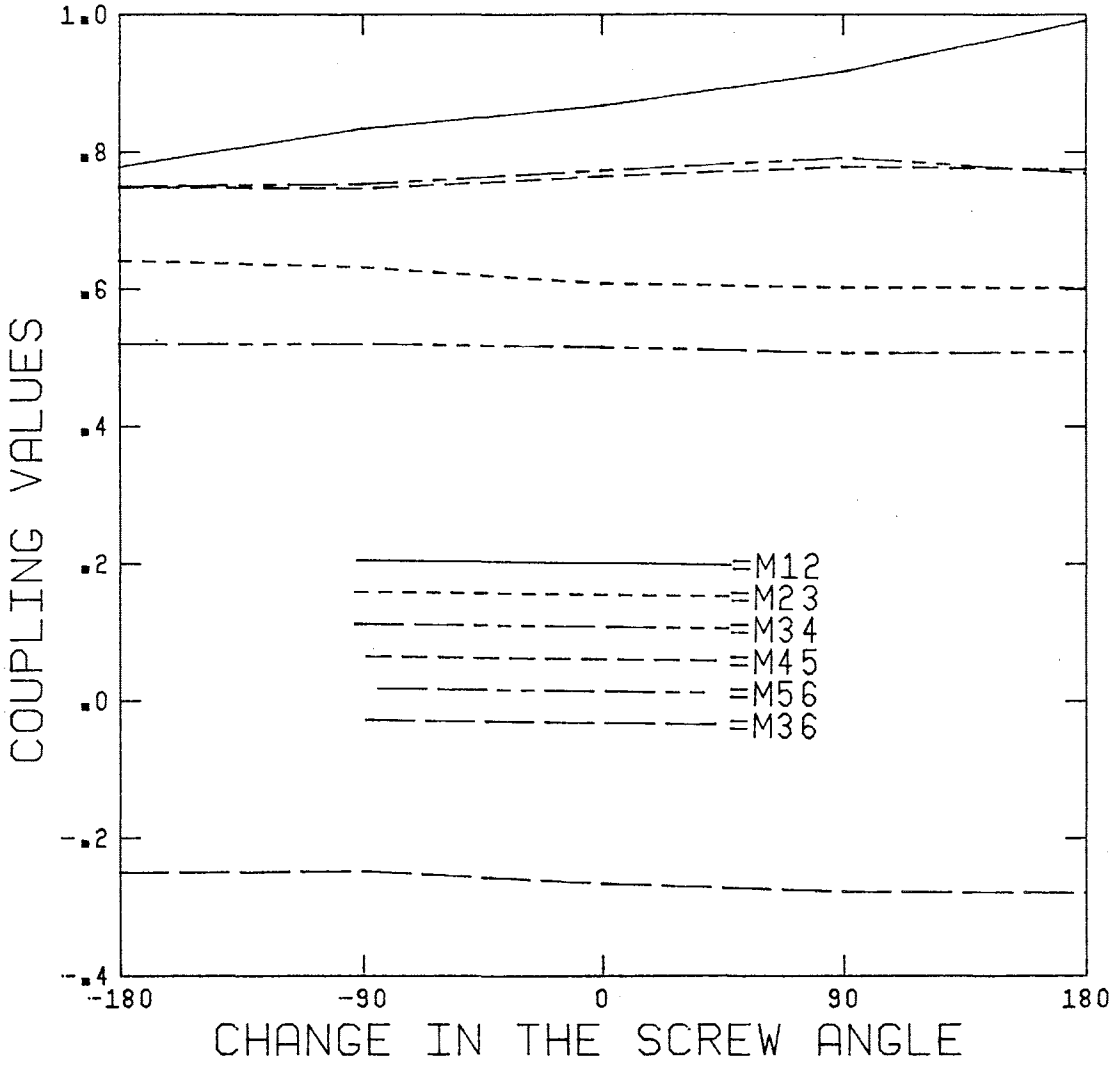

Fig. 5.11 The variation of coupling values in a 6th order filter as the position of the screw which dominantly controls M_{12} changes.

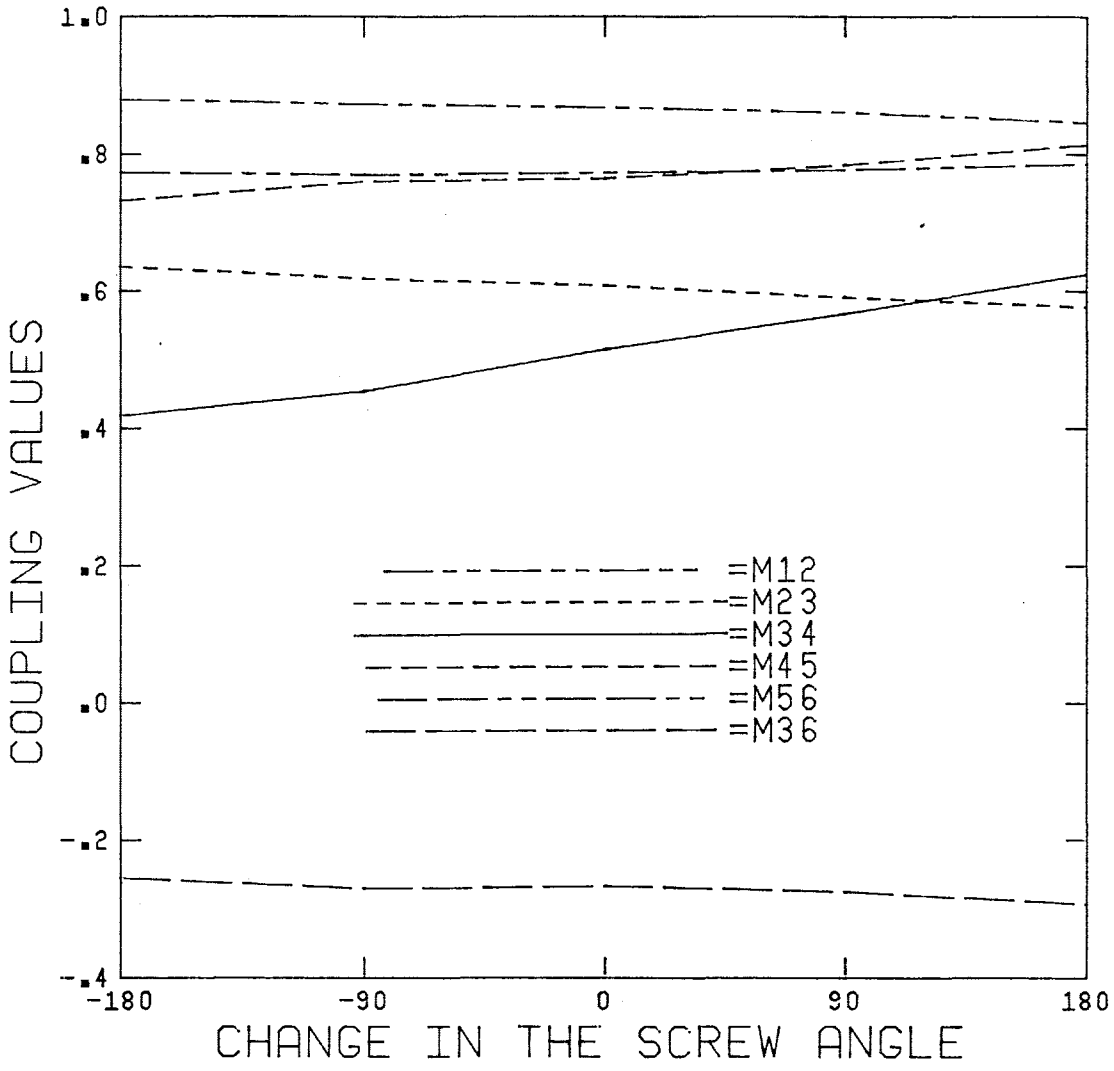

Fig. 5.12 The variation of coupling values in a 6th order filter as the position of the screw which dominantly controls M_{34} changes.

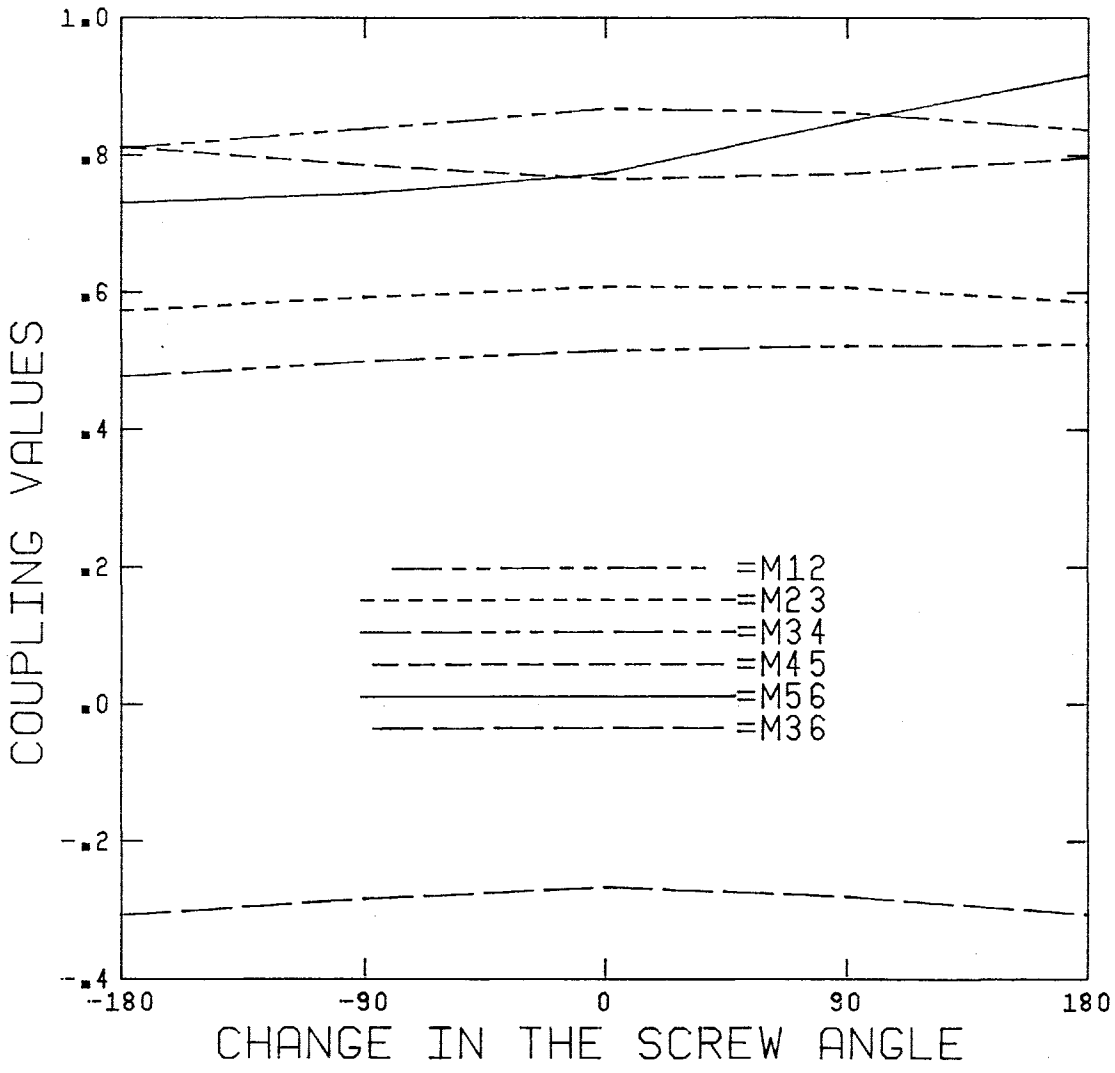

Fig. 5.13 The variation of coupling values in a 6th order filter as the position of the screw which dominantly controls M_{56} changes.

5.13, which correspond to the M_{34} and M_{56} screws, respectively. Again, we have almost linear or almost constant lines in both plots.

The measurements used in this experiment were all provided by ComDev (1986).

5.7 CONCLUDING REMARKS

In this chapter, we discussed the traditional formulation for modelling and presented a new formulation exploiting multi-circuit measurements. The way in which the multi-circuit measurements may contribute to the unique identification of parameters has been described mathematically with the help of a simple example. An optimization problem which is directly aimed at overcoming the non-uniqueness of parameters was formulated and its implementation was described in detail. A second formulation which is aimed at the automatic verification of model parameters by checking the consistency of their behaviour with respect to physical adjustments on the device, was proposed.

Promising results in modelling of narrowband multi-coupled cavity filters and wideband GaAs FET's were obtained which justify the use of our multi-circuit approach and formulation. The author strongly believes that the use of multiple sets of measurements and a formulation which ties modelling (performed by the computer) to the actual physical adjustments on the device will enhance further developments in modelling and tuning of microwave devices. The use of modelling in establishing the relationship between physical and model parameters has been illustrated.

6

CONCLUSIONS

This thesis has considered the application of recent minimax and ℓ_1 optimization techniques in the design and modelling of microwave circuits. The difference between design and modelling problems is the way in which performance specifications are given. In the design of microwave circuits in the frequency domain, there are upper and lower engineering specifications over different frequency bands of interest which a manufactured design must meet. In the modelling problem, an equivalent circuit must be obtained such that the circuit responses match the measurements on a device as closely as possible. The measurements play the role of specifications in modelling.

Both design and modelling problems are formulated as optimization problems with the objective being the norm of the error functions resulting from specifications on performance functions of interest. The minimax norm for design and the ℓ_1 norm for modelling have been used in this thesis. Fast and efficient algorithms for minimax and ℓ_1 optimization originated by Hald and Madsen, which may be the best of their class currently available, are utilized.

The use of gradient-based optimization algorithms requires efficient sensitivity analysis. The approach presented in Chapter 3 deals with the sensitivities in a straightforward manner. It is applicable to a large class of linear circuit structures in the frequency domain. The approaches for sensitivity evaluations in cascaded and branched cascaded networks were developed with microwave applications in mind.

Optimal design of multiplexing networks has directly emerged from the theoretical foundations of Chapters 2 and 3. The size and complexity of this problem, with the design examples involving up to 60 nonlinear variables and as many as 100 nonlinear error functions, necessitates the use of fast and reliable optimization techniques, which in turn require the gradients to be supplied. To maintain the engineering relevance of the work, nonideal effects in the multiplexer structure were considered. Close cooperation with industry has resulted in a realistic implementation of the theoretical results. This implementation has had an impact in terms of achieving major reductions in CPU times required for practical designs.

The multiplexer design example, apart from being a problem of current interest in microwave research and practice, gives enormous credibility to the use of optimization techniques in large engineering problems in general, and microwave problems in particular. In recent years, many commercially available software systems have been developed in the microwave area. It will not be very long before the flexibility, user-friendly features and graphical capabilities of these systems, combined with powerful optimization techniques which have been employed in this thesis, form an indispensable tool used by all microwave engineers.

Based on the theoretical properties of the ℓ_1 norm applied to multi-circuit measurements, a new modelling technique was presented in Chapter 5. Two optimization problems were formulated with the aim of achieving unique equivalent circuit parameters which remain valid and consistent as the experimental environment changes, e.g., as a result of making physical adjustments to the device. By relating the concept of modelling to actual physical adjustments, the relationships between model and physical parameters are established and a framework for developing new postproduction tuning algorithms is created. Industrial cooperation

in testing the new modelling technique has affected the theoretical work extensively. The model verification method presented in Chapter 5 was developed only after some limitations of the experimental environment became evident as the real data was processed.

For microwave devices such as amplifiers realized using MMIC's (monolithic microwave integrated circuits), modelling is used to predict device scattering parameters at millimeter wave frequencies where they cannot be measured with current commercial equipment. By applying the new modelling technique to GaAs FET's, it is felt that this thesis can contribute to the subject which has been of tremendous interest to microwave engineers in the past few years.

One of the most recent methods for efficient gradient approximations, applicable to both minimax and ℓ_1 optimizations, was reviewed in Chapter 2. It is predicted that this technique will realize its full potential in solving those microwave problems which involve nonlinear devices or complicated field equations, in the near future.

A number of problems related to the topics in this thesis are worth further research and development.

(a) In Chapter 5, an advanced technique in model evolution, i.e., automatic modification of network topology was discussed. The technique is sequential in the sense that different network topologies are tried one after another. Apart from further theoretical work in developing strategies and criteria for the automatic modification, it would be very useful to combine the modification techniqe with the simultaneous processing of multiple circuits which was introduced in this thesis. The idea is to process simplified models such as low frequency models of a microwave device

simultaneously with its more complicated models at normal operating frequencies, with constraints on consistency of the parameters.

(b) As was discussed in Chapter 5, an efficient modelling technique has applications in developing new postproduction tuning algorithms. In such algorithms, the functional relationship between the model parameters and physically adjustable or designable elements of a device are approximated automatically and adaptively. The involvement of model parameters which usually have mildly nonlinear dependence on physical parameters, and the fact that the nonlinear relationship between responses and model parameters is under control by using a reliable modelling technique gives us an incentive to develop new tuning algorithms. These algorithms will enhance large volume production of complicated microwave components.

(c) It would be of great practical value to investigate an implementation of the modelling technique described which exploits the latest developments in hardware-software systems reported by industry. The most recent advances include the introduction of systems capable of simultaneoulsy processing and displaying measurement data obtained from a network analyzer, and the simulation and/or optimization results computed using compatible personal computers.

(d) Modelling of power FET's under large-signal conditions where the equivalent circuit is nonlinear is a topic of significant current interest. It would be useful to study the feasibility of extending or modifying the current

modelling formulations to nonlinear systems where time domain analysis becomes more appropriate.

(e) In the multiplexer structure of Chapter 4, some nonideal effects such as dissipation, dispersion and junction susceptances were discussed. These nonideal effects were modelled using empirical formulas obtained through experience or experiments. The problem of modelling some of the nonideal effects present in the multiplexer structure using measurements on the device is worth further study and will result in multiplexer designs which will require less effort in postproduction tuning.

(f) From a theoretical point of view, it is worth further research to study the implications of the sensitivity formulas obtained for lossless reciprocal 2-port networks of Chapter 3 in sensitivity analysis of lossless reciprocal n-ports.

APPENDIX A

SECOND-ORDER SENSITIVITY FORMULA

FOR TERMINATED TWO-PORTS

Here we present the derivation of the second-order sensitivity formula for the port voltages of a terminated two-port, as given by (3.26).

Using (3.25), the first-order sensitivity with respect to ω is given by

$$(\mathbf{V}_p)_\omega = \mathbf{H}\,(\mathbf{z}_\omega\,\mathbf{I}_p - \mathbf{z}\,\mathbf{T}_\omega\,\mathbf{V}_p)\,. \tag{A.1}$$

Differentiating (A.1) with respect to ϕ, we get

$$(\mathbf{V}_p)_{\phi\omega} = \mathbf{H}[\mathbf{z}_{\phi\omega}\,\mathbf{I}_p + \mathbf{z}_\omega(\mathbf{I}_p)_\phi - \mathbf{z}_\phi\,\mathbf{T}_\omega\,\mathbf{V}_p - \mathbf{z}\,\mathbf{T}_{\phi\omega}\,\mathbf{V}_p - \mathbf{z}\,\mathbf{T}_\omega(\mathbf{V}_p)_\phi]$$

$$+\,\mathbf{H}_\phi(\mathbf{z}_\omega\,\mathbf{I}_p - \mathbf{z}\,\mathbf{T}_\omega\,\mathbf{V}_p)\,. \tag{A.2}$$

Using the definition of $\mathbf{H}$ in (3.24), we have

$$\mathbf{H}_\phi(\mathbf{z}_\omega\,\mathbf{I}_p - \mathbf{z}\,\mathbf{T}_\omega\,\mathbf{V}_p) = -\mathbf{H}(\mathbf{H}^{-1})_\phi\,\mathbf{H}(\mathbf{z}_\omega\,\mathbf{I}_p - \mathbf{z}\,\mathbf{T}_\omega\,\mathbf{V}_p)$$

$$= -\mathbf{H}\,(\mathbf{z}_\phi\,\mathbf{T} + \mathbf{z}\,\mathbf{T}_\phi)\,(\mathbf{V}_p)_\omega\,. \tag{A.3}$$

The sensitivity of the port current vector is obtained using (3.22) as

$$(\mathbf{I}_p)_\phi = -[\,\mathbf{T}_\phi\,\mathbf{V}_p + \mathbf{T}(\mathbf{V}_p)_\phi]\,. \tag{A.4}$$

Finally, substituting (A.3) and (A.4) in (A.2) and collecting terms, we get

$$(\mathbf{V}_p)_{\phi\omega} = -\mathbf{H}\{\mathbf{z}_\omega[\mathbf{T}_\phi\,\mathbf{V}_p + \mathbf{T}(\mathbf{V}_p)_\phi] + \mathbf{z}_\phi[\mathbf{T}_\omega\,\mathbf{V}_p + \mathbf{T}(\mathbf{V}_p)_\omega]$$

$$+\,\mathbf{z}[\mathbf{T}_\phi(\mathbf{V}_p)_\omega + \mathbf{T}_\omega(\mathbf{V}_p)_\phi + \mathbf{T}_{\phi\omega}\,\mathbf{V}_p] - \mathbf{z}_{\phi\omega}\,\mathbf{I}_p\}\,. \tag{A.5}$$

REFERENCES

A.E. Atia (1974), "Computer-aided design of waveguide multiplexers", IEEE Trans. Microwave Theory Tech., vol. MTT-22, pp. 332-336.

A.E. Atia and A.E. Williams (1971), "New types of waveguide bandpass filters for satellite transponders", COMSAT Technical Review, vol. 1, pp. 21-43.

A.E. Atia and A.E. Williams (1972), "Narrow-bandpass waveguide filters", IEEE Trans. Microwave Theory Tech., vol. MTT-20, pp. 258-265.

A.J. Baden Fuller and A.M. Parker (1985), "Equivalent circuit of microstrip spiral inductor circuit generation by computer", Electronics Letters, vol. 21, pp. 279-280.

J.W. Bandler and C. Charalambous (1974), "Nonlinear programming using minimax techniques", J. Optimization Theory and Applications, vol. 13, pp. 607-619.

J.W. Bandler, S.H. Chen and S. Daijavad (1984a), "Proof and extension of general sensitivity formulas for lossless two-ports", Electronics Letters, vol. 20, pp. 481-482.

J.W. Bandler, S.H. Chen and S. Daijavad (1984b), "Novel approach to multicoupled-cavity filter sensitivity and group delay computation", Electronics Letters, vol. 20, pp. 580-582.

J.W. Bandler, S.H. Chen and S. Daijavad (1985a), "Exact sensitivity analysis and optimization for multi-cavity microwave communication filters", Proc. IEEE Int. Symp. Circuits and Systems (Kyoto, Japan), pp. 1587-1590.

J.W. Bandler, S.H. Chen and S. Daijavad (1985b), "Simple derivation of a general sensitivity formula for lossless two-ports", Proc. IEEE, vol. 73, pp. 165-166.

J.W. Bandler, S.H. Chen and S. Daijavad (1986a), "Exact sensitivity analysis for optimization of multi-coupled cavity filters", Int. J. Circuit Theory and Applic., vol. 14, pp. 63-77.

J.W. Bandler, S.H. Chen and S. Daijavad (1986b), "Microwave device modelling using efficient ℓ_1 optimization: a novel approach", IEEE Trans. Microwave Theory Tech., vol. MTT-34.

J.W. Bandler, S.H. Chen, S. Daijavad and W. Kellermann (1984), "Optimal design of multi-cavity filters and contiguous-band multiplexers", Proc. 14th European Microwave Conf. (Liege, Belgium), pp. 863-868.

J.W. Bandler, S.H. Chen, S. Daijavad, W. Kellermann, M. Renault and Q.J. Zhang (1986), "Large scale minimax optimization of microwave multiplexers", Proc. 16th European Microwave Conf. (Dublin, Ireland).

J.W. Bandler, S.H. Chen, S. Daijavad and K. Madsen (1986), "Efficient gradient approximations for nonlinear optimization of circuits and systems", Proc. IEEE Int. Symp. Circuits and Systems (San Jose, CA), pp. 964-967.

J.W. Bandler, S. Daijavad and Q.J. Zhang (1985a), "Novel approach to multiplexer simulation and sensitivity analysis", Electronics Letters, vol. 21, pp. 408-409.

J.W. Bandler, S. Daijavad and Q.J. Zhang (1985b), "Computer aided design of branched cascaded networks", Proc. IEEE Int. Symp. Circuits and Systems (Kyoto, Japan), pp. 1579-1582.

J.W. Bandler, S. Daijavad and Q.J. Zhang (1986), "Exact simulation and sensitivity analysis of multiplexing networks", IEEE Trans. Microwave Theory Tech., vol. MTT-34, pp. 93-102.

J.W. Bandler, W. Kellermann and K. Madsen (1985a), "A superlinearly convergent minimax algorithm for microwave circuit design", IEEE Trans. Microwave Theory Tech., vol. MTT-33, pp. 1519-1530.

J.W. Bandler, W. Kellermann and K. Madsen (1985b), "A superlinearly convergent algorithm for nonlinear ℓ_1 optimization with circuit applications", Proc. IEEE Int. Symp. Circuits and Systems (Kyoto, Japan), pp. 977-980.

J.W. Bandler, W. Kellermann and K. Madsen (1985c), "An algorithm for nonlinear ℓ_1 optimization for design and diagnosis of networks", Department of Electrical and Computer Engineering, McMaster University, Hamilton, Canada, Report SOS-85-14.

J.W. Bandler and M.R.M. Rizk (1979), "Optimization of Electrical Circuits", Mathematical Programming Study on Engineering Optimization, vol. 11, pp. 1-64.

J.W. Bandler and M.R.M. Rizk (1981), "Analysis and sensitivity evaluation of 2p-port cascaded networks", IEEE Trans. Microwave Theory Tech., vol. MTT-29, pp. 719-723.

J.W. Bandler, M.R.M. Rizk and H.L. Abdel-Malek (1978), "New results in network simulation, sensitivity and tolerance analysis for cascaded structures", IEEE Trans. Microwave Theory Tech., vol. MTT-26, pp. 963-972.

J.W. Bandler, M.R.M. Rizk and H. Tromp (1976), "Efficient calculation of exact group delay sensitivities", IEEE Trans. Microwave Theory Tech., vol. MTT-24, pp. 188-194.

J.W. Bandler and A.E. Salama (1985a), "Fault diagnosis of analog circuits", Proc. IEEE, vol. 73, pp. 1279-1325.

J.W. Bandler and A.E. Salama (1985b), "Functional approach to microwave post-production tuning", IEEE Trans. Microwave Theory Tech., vol. MTT-33, pp. 302-310.

J.W. Bandler and W.M. Zuberek (1982), "MMLC – a Fortran package for minimization with general constraints", Department of Electrical and Computer Engineering, McMaster University, Hamilton, Canada, Report SOS-82-5.

R.H. Bartels and A.R. Conn (1981), "An approach to nonlinear ℓ_1 data fitting", University of Waterloo, Computer Science Department, Report CS-81-17.

F.H. Branin, Jr. (1973), "Network sensitivity and noise analysis simplified", IEEE Trans. Circuit Theory, vol. CT-20, pp. 285-288.

R.K. Brayton, G.D. Hachtel and A.L. Sangiovanni-Vincentelli (1981), "A survey of optimization techniques for integrated-circuit design", Proc. IEEE, vol. 69, pp. 1334-1362.

C.G. Broyden (1965), "A class of methods for solving nonlinear simultaneous equations", Math of Computation, vol. 19, pp. 577-593.

R.J. Cameron (1982), "Dual-mode realisations for assymetric filter characteristics", ESA Journal, vol. 6, pp. 339-356.

C. Charalambous (1973), "Nonlinear least pth approximation and nonlinear programming with applications in the design of networks and systems", Ph.D. Thesis, McMaster University, Hamilton, Canada.

M.H. Chen (1983), "A 12-channel contiguous band multiplexer at KU-band", 1983 IEEE Int. Microwave Symp. Digest (Boston, MA), pp. 77-79.

M.H. Chen (1985), "Current state-of-the-art technology on contiguous-band multiplexer", Proc. IEEE Int. Symp. Circuits and Systems (Kyoto, Japan), pp. 1583-1586.

M.H. Chen, F. Assal and C. Mahle (1976), "A contiguous band multiplexer", COMSAT Technical Review, vol. 6, pp. 285-306.

L.O. Chua and P.M. Lin (1975), Computer-Aided Analysis of Electronic Circuits: Algorithms and Computational Techniques. Englewood Cliffs, N.J.: Prentice-Hall.

ComDev Ltd. (1983), 155 Sheldon Drive, Cambridge, Ontario, Canada N1R 7H6, private communications.

ComDev Ltd. (1985), 155 Sheldon Drive, Cambridge, Ontario, Canada N1R 7H6, private communications.

ComDev Ltd. (1986), 155 Sheldon Drive, Cambridge, Ontario, Canada N1R 7H6, private communications.

W.R. Curtice and R.L. Camisa (1984), "Self-consistent GaAs FET models for amplifier design and device diagnostics", IEEE Trans. Microwave Theory Tech., vol. MTT-32, pp. 1573-1578.

W.R. Curtice and M. Ettenberg (1985), "A nonlinear GaAs FET model for use in the design of output circuits for power amplifiers", IEEE Trans. Microwave Theory Tech., vol. MTT-33, pp. 1383-1394.

O.P.D. Cutteridge and Y.S. Zhang (1984), "Computer-aided linear modelling of high-frequency bipolar transistors", IEE Proc., vol. 131, part G, pp. 252-260.

S.W. Director and R.A. Rohrer (1969), "Generized adjoint network and network sensitivities", IEEE Trans. Circuit Theory, vol. CT-16, pp. 318-323.

S.W. Director (1971), "LU factorization in network sensitivity calculations", IEEE Trans. Circuit Theory, vol. CT-18, pp. 184-185.

R.G. Egri, A.E. Williams and A.E. Atia (1983), "A contiguous-band multiplexer design", 1983 IEEE Int. Microwave Symp. Digest (Boston, MA), pp. 86-88.

R.A. El-Attar, M. Vidyasagar and S.R.K. Dutta (1979), "An algorithm for ℓ_1-norm minimization with application to nonlinear ℓ_1-approximation", SIAM J. Numerical Analysis, vol. 16, pp. 70-86.

J. Hald and K. Madsen (1981), "Combined LP and quasi-Newton methods for minimax optimization", Mathematical Programming, vol. 20, pp. 49-62.

J. Hald and K. Madsen (1985), "Combined LP and quasi-Newton methods for nonlinear ℓ_1 optimization", SIAM J. Numerical Analysis, vol. 22, pp. 68-80.

S.P. Han (1981), "Variable metric methods for minimizing a class of nondifferentiable functions", Mathematical Programming, vol. 20, pp. 1-13.

R. Hettich (1976), "A Newton method for nonlinear Chebyshev approximation", in Approximation Theory, R. Schaback and K. Scherer, Eds., Lecture Notes in Mathematics, 556, Springer Berlin, pp. 222-236.

S.C. Holme (1984), "A 12GHz 12 channel multiplexer for satellite applications", 1984 IEEE Int. Microwave Symp. Digest (San Fransisco, CA), pp. 295-296.

H.-L. Hung, E. Enobakhare, J. Abita, P. McNally, C. Mahle and H. Huang (1985), "GaAs FET MMIC low-noise amplifiers for satellite communications", RCA Review, vol. 46, pp. 431-440.

W. Kellermann (1986), "Advances in optimization of circuits and systems using recent minimax and ℓ_1 algorithms", Ph.D. Thesis, McMaster University, Hamilton, Canada.

C.M. Kudsia (1982), "Manifestations and limits of dual-mode filter configurations for communications satellite multiplexers", AIAA 9th Communications Satellite Systems Conf. (San Diego, CA), pp. 294-303.

K. Madsen (1975), "Minimax solution of nonlinear equations without calculating derivatives", Mathematical Programming Study 3, pp. 110-126.

K. Madsen And H. Schjaer-Jacobsen (1976), "Singularities in minimax optimization of networks", IEEE Trans. Circuits and Systems, vol. CAS-23, pp. 456-460.

K. Madsen, H. Schjaer-Jacobsen and J. Voldby (1975), "Automated minimax design of networks", IEEE Trans. Circuits and Systems, vol. CAS-22, pp. 791-796.

N. Marcuvitz (1951), Waveguide Handbook, MIT Rad. Lab. Ser., vol. 10. New York: McGraw-Hill.

A. Materka and T. Kacprzak (1985), "Computer calculations of large-signal GaAs FET amplifier characteristics", IEEE Trans. Microwave Theory Tech., vol. MTT-33, pp. 129-135.

G.L. Matthaei, L. Young and E.M.T. Jones (1964), Microwave Filters, Impedance Matching Networks and Coupling Structures. New York: McGraw-Hill.

T. Nomoto (1984), "Channel multiplexers for broadcasting satellite transponders in the 12GHz band", Trans. IECE Japan, J67-B, 8, pp. 916-923.

H.J. Orchard, G.C. Temes and T. Cataltepe (1983), "General sensitivity formulas for lossless two-ports", Electronics Letters, vol. 19, pp. 576-578.

H.J. Orchard, G.C. Temes and T. Cataltepe (1985), "Sensitivity formulas for terminated lossless two-ports", IEEE Trans. Circuits and Systems, vol. CAS-32, pp. 459-466.

M.R. Osborne and G.A. Watson (1971), "On an algorithm for discrete nonlinear ℓ_1 optimization", Computer J., vol. 12, pp. 63-68.

M.J.D. Powell (1970), "A Fortran subroutine for unconstrained minimization, requiring first derivatives of the objective functions", AERE Harwell, Oxfordshire, England, Report AERE-R.6469, pp. 20-27.

M.J.D. Powell (1978), "The convergence of variable metric method for nonlinearly constrained optimization calculations", in Nonlinear Programming, O.L. Mangasarian, R.R. Meyer and S.M. Robinson, Eds. New York: Academic Press, pp. 27-63.

M.R.M. Rizk (1979), "Advances in simulation and optimization of electrical networks", Ph.D. Thesis, McMaster University, Hamilton, Canada.

SUPER-COMPACT (1986), Communications Consulting Corp., Upper Saddle River, NJ.

R. Tong, J. Dorey, P. Mabson, W.C. Tang, E. Klein-Lebbink and C.M. Kudsia (1982), "An 11 GHz contiguous band output multiplexing network for Intelsat VI spacecraft", 1982 IEEE Int. Microwave Symp. Digest (Dallas, TX), pp. 405-407.

R. Tong and C.M. Kudsia (1984), "Enhanced performance and increased EIRP in communications satellites using contiguous multiplexers", AIAA 10th Communications Satellite Systems Conf. (Orlando, FL), pp. 532-541.

R. Tong and D. Smith (1984), "A 12-channel contiguous band multiplexer for satellite application", 1984 IEEE Int. Microwave Symp. Digest (San Francisco, CA), pp. 297-298.

TOUCHSTONE (1985), EEsof. Inc., Westlake Village, CA.

G.A. Watson (1979), "The minimax solution of an overdetermined system of nonlinear equations", J. IMA, vol. 23, pp. 167-180.

A.E. Williams (1970), "A four-cavity elliptic waveguide filter", IEEE Trans. Microwave Theory Tech., vol. MTT-18, pp. 1109-1114.

W.M. Zuberek (1984), "Numerical approximation of gradients for circuit optimization", Proc. 27th Midwest Symp. Circuits and Systems (Morgantown, WV), pp. 200-203.

AUTHOR INDEX

SUBJECT INDEX